Jongyun Moon

Hydrogen Sensor Application of Anodic Titanium Oxide Nanostructures

Turku Centre *for* Computer Science

TUCS Dissertations
No 207, March 2016

Hydrogen Sensor Application of Anodic Titanium Oxide Nanostructures

Jongyun Moon

To be presented, with the permission of the Faculty Mathematics and Natural Sciences of the University of Turku, for public criticism in the Auditorium XXI of Agora on March 11, 2016 at 12:00.

University of Turku

Department of Information Technology

20014 Turun Yliopisto

Finland

2016

Supervised by

Ph.D. Risto Punkkinen
Department of Information Technology
University of Turku
Turku, Finland

Professor Ph.D Aulis Tuominen
Department of Information Technology
University of Turku
Turku, Finland

Reviewed by

Professor Ph.D. Andrej Plecenik
Department of Experimental Physics
Comenius University in Bratislava
Bratislava, Slovak Republic

Research professor Ph.D. Krisztian Kordas
Department of Electrical Engineering
University of Oulu
Oulu, Finland

Opponent

Professor Ph.D. János Mizsei
Department of Electron Devices
Budapest University of Technology and Economics
Budapest, Hungary

ISBN 978-952-12-3358-6
ISSN 1239-1883

The originality of this thesis has been checked in accordance with the University of Turku quality assurance system using the Turnitin OriginalityCheck service.

Abstract

Hydrogen (H_2) fuel cells have been considered a promising renewable energy source. The recent growth of H_2 economy has required highly sensitive, micro-sized and cost-effective H_2 sensor for monitoring concentrations and alerting to leakages due to the flammability and explosiveness of H_2 Titanium dioxide (TiO_2) made by electrochemical anodic oxidation has shown great potential as a H_2 sensing material. The aim of this thesis is to develop highly sensitive H_2 sensor using anodized TiO_2. The sensor enables mass production and integration with microelectronics by preparing the oxide layer on suitable substrate.

Morphology, elemental composition, crystal phase, electrical properties and H_2 sensing properties of TiO_2 nanostructures prepared on Ti foil, Si and SiO_2/Si substrates were characterized. Initially, vertically oriented TiO_2 nanotubes as the sensing material were obtained by anodizing Ti foil. The morphological properties of tubes could be tailored by varying the applied voltages of the anodization. The transparent oxide layer creates an interference color phenomena with white light illumination on the oxide surface. This coloration effect can be used to predict the morphological properties of the TiO_2 nanostructures. The crystal phase transition from amorphous to anatase or rutile, or the mixture of anatase and rutile was observed with varying heat treatment temperatures. However, the H_2 sensing properties of TiO_2 nanotubes at room temperature were insufficient.

H_2 sensors using TiO_2 nanostructures formed on Si and SiO_2/Si substrates were demonstrated. In both cases, a Ti layer deposited on the substrates by a DC magnetron sputtering method was successfully anodized. A mesoporous TiO_2 layer obtained on Si by anodization in an aqueous electrolyte at 5°C showed diode behavior, which was influenced by the work function difference of Pt metal electrodes and the oxide layer. The sensor enabled the detection of H_2 (20-1000 ppm) at low operating temperatures (50–140°C) in ambient air. A Pd decorated tubular TiO_2 layer was prepared on metal electrodes patterned SiO_2/Si wafer by anodization in an organic electrolyte at 5°C. The sensor showed significantly enhanced H_2 sensing properties, and detected hydrogen in the range of a few ppm with fast response/recovery time. The metal electrodes placed under the oxide layer also enhanced the mechanical tolerance of the sensor.

The concept of TiO_2 nanostructures on alternative substrates could be a prospect for microelectronic applications and mass production of gas sensors. The gas sensor properties can be further improved by modifying material morphologies and decorating it with catalytic materials.

Tiivistelmä

Vety (H_2) polttokennojen lähteenä on osoittautunut hyväksi uusiutuvaksi energia-lähteeksi. Kasvava vetytalous vaatii herkkiä, pienikokoisia ja edullisia antureita monitoroimaan vetypitoisuuksia ja varoittamaan mahdollisista vuodoista, sillä vety on palava ja sopivina seoksina räjähtävä kaasu. Tämän väitöskirjatyön tavoitteena on ollut kehittää herkkä vetyilmaisin, joka perustuu anodisoimalla valmistettuun titaanidioksidiin (TiO_2). TiO_2 on osoittautunut hyväksi materiaaliksi vedyn ilmaisuun. Jos anturi pystytään valmistamaan sopivalle alustalle, niin silloin olisi mahdollisuus anturien massavalmistukseen ja integrointiin mikroelektroniikkaan.

TiO_2-nanorakenteita valmistettiin Ti-kalvolle, piille ja piidioksidille ja niiden rakenteelliset ja sähköiset ominaisuudet sekä vetyherkkyys karakterisoitiin. Vedylle herkkä nanoputkimainen TiO_2-rakenne saatiin anodisoimalla Ti-kalvoa. Syntynyt nanoputkirakenne riippui mm. anodisointijännitteestä. Interferenssin vaikutuksesta läpinäkyvä oksidikerros näkyi värikkäänä, kun sitä valaistiin valkoisella valolla. Värin perusteella voitiin päätellä TiO_2-nanorakenteen paksuus. Syntyjään kiderakenne on amorfinen, mutta se voidaan muuttaa lämpökäsittelyllä anataasiksi, rutiiliksi tai niiden seokseksi. Tyypillinen anturin toimintalämpötila on (200–300) °C. Ongelmallista on kuitenkin saada anturit toimimaan jo huoneenlämmössä.

Valmistimme H_2-antureita Si- ja SiO_2/Si-pohjille. Molemmissa tapauksissa Ti sputteroitiin ensin alustalle ja anodisoitiin sitten 5 °C:ssa. Ensimmäisessä tapauksessa (mesorakenteisessa) TiO_2:ssa Pt-elektrodin ja oksidikerroksen välille muodostunut Schottky-diodi aiheutti virran diodimaisen käyttäytymisen. Muodostettu ilmaisin kykeni mittaamaan (20 – 1000) ppm:n vetypitoisuuksia ilmassa (50 – 140) °C:n lämpötiloissa. Jälkimmäisessä valmistettiin nanoputkimainen TiO_2-rakenne termisesti oksidoidun piin päälle anodisoimalla Ti-kerros orgaanisessa elektrolyytissä 5 °C:ssa. Tässä rakenteessa metallielektrodit olivat TiO_2-kerroksen alla. Kun rakenteen pinnalle lisättiin hieman palladiumia, saavutettiin huomattavasti parempi herkkyys ja nopeampi reagointiaika kuin mesorakenteella (1 – 2000) ppm:n vetypitoisuuksissa.

Kerrosmainen TiO_2-rakenne eristävän substraatin päällä mahdollistaa anturien massavalmistuksen ja ehkäpä yhdistämisen mikroelektroniikkaan. Anturin ominaisuuksia voidaan parantaa rakenteellisilla muutoksilla ja katalyyttisillä lisäaineilla.

Acknowledgements

Like most international students, I made a scary move in 2008. Being in Finland I may have missed many opportunities over the years, but now I can see that I have gained a lot more than possibly lost. Hereby, I am thankfully express my gratitude to the people who have guided me and enabled me to get this far.

I would like to thank to my first supervisor, Professor Aulis Tuominen, who gave me the opportunity to start my life in Finland and who has given me many opportunities to enjoy various interesting experiences here. If it wasn't you, I wouldn't be here today. I would also like to thank my second supervisor, Dr. Risto Punkkinen. Your hard work and your wonderful attitude toward science have directed me to this stage. You have shown me what a scientist should be. I extend my appreciations to the pre-examiners of my thesis, Professor Andrej Plecenik and Professor Krisztian Kordas. My thesis was much improved by your criticism and advice. I also humbly thank Professor János Mizsei for being opponent. I am honored that these great scientists have given their time and attention to my work.

During my studies I have also had the privilege to work with numerous great scientists and engineers from other organizations, such as Dr. Marianna Kemell, who encouraged me and gave valuable comments for my work. I am also grateful to Mr. Ermei Mäkilä, at Sensorex Oy and Gasera Oy and Dr. Lippo Lassila for their collaboration. I am thankful to CIMO and the Fortum foundation for financial support.

During this long journey, I have met many wonderful people who have supported my life and work in Finland. I firstly have to say thank to Dr. Arho Suominen, who has a wonderful open mind and has helped me from the very beginning of my PhD until now. I am also grateful to Dr. Hannu-Pekka Hedman. With the benefit your intelligence, I was able to carry out my work wonderfully. I also owe many thanks to Pia Lehmussaari for supporting me and being a good friend. I am grateful to my former colleagues; Dr. Sami Hyrynsalmi, Anne-Marie Tuikka, Ilkka Toukko, Henrik Lagercrantz, Dr. Wukui Zheng, from the Electronic productization research group. You guys were awesome to work with and I am still missing the time we spent together.

My life has been full of joy with my dear friends, who shared my concerns and encouraged me. Hereby, I would like to say thank to Dr. Aous

Abdulmajeed (my best buddy on this planet), Emmanule Mbole (the oldest friend, the sincerest friend, my English teacher, Driss El Bikou, Erick Oanda, Sara Helena, Dr. Masahiko Kobayashi, Prince Dadson, Dr. Taiseer Sulaiman, Dr. Andi Mwegerano, Toni Hannula, Satu Leppänen, Tarek Omran, Khalil Shahramian, , Guillaume Clement, Sujung Kim, Uli Meyer, Kyung-Yeol Chun, Dr. KowanJa Jee and Hyesook Lee. I thank Dr. Timothy Wilson for proof reading of my thesis. In addition, I am deeply thankful to Arttu Punkkinen and Matleena Punkkinen for their hard work in checking my papers. And special thanks to Hamed Hassain for being my mentor like elder brother and wonderful food for many years in Delhi Darbar, and Maria Byskata, Laura Salonen and Hyunhee Song for the preparation of my dissertation event.

I am greatly indebted to Professor In-Jung Lee for taking me under his wing. I could have gotten lost if I hadn't met you during my wanderings. I am thankful to my supervisors and mentors during my master's degree, Professor Hong Kim for giving me great advice as my supervisor and Professor Ki Chang Jung for giving me the first opportunity to build my research career. In the beginning of my research career, it was wonderful to work with Professor Jeonghun Kim and Dr. Jonghyuk Song. I also deeply appreciate Sangjin Nam and Dong-un Lee for being my mentors.
I send my warm regards to Hong Ja Jung who always had belief in me. I am grateful to my friends in Korea including Junwon Choi for being the third son of my family, and Kunhong, Wonsub, Myunghan, ByungKi for their support, in spite of our distance.

Finally, I express my deepest gratitude to my family. My parents, Okchae Moon 문옥채 and Jumsoon Paek 백점순, who have supported, believed in me and loved me from my birth. No word can describe how thankful I am. My sister, Hyangjung 향정, my brother Jongjin 종진, I could only have come this far because I believe in you two, thank you so much.
It is impossible to predict how God will guide me in the future. The only thing I am sure of is that I will do my best whatever I face in the future. I know that this moment is not an end but a new beginning.

List of original publications

This thesis is based on the following original publications, which are referred in the text by the Roman numerals I-IV

I. **Jongyun Moon**, Marianna Kemell, Byungki Park, Arho Suominen, Ermei Mäkilä, Risto Punkkinen, Hannu-Pekka Hedman, Hong Kim, Lippo V Lassila, Aulis Tuominen, The correlation between the interference colour and growth procedure of anodic titanium dioxide nanotube arrays, 2014, Coloration Technology, 130, 1, 1-7.

II. **Jongyun Moon**, Ilkka Tuokko, Arho Suominen, Aulis Tuominen, Dongseok Oh, Byungki. Park, Hong Kim, Hydrogen sensing performance of TiO_2 nanotubes at room temperature, 2010, Electronics Conference (BEC)12th Biennial Baltic, 73-76.

III. **Jongyun Moon**, Hannu-Pekka Hedman, Marianna Kemell, Arho Suominen, Ermei Mäkilä, Hong Kim, Aulis Tuominen, Risto Punkkinen, A study of monitoring hydrogen using mesoporous TiO_2 synthesized by anodization, 2013, Sensors and Actuators B: Chemical, 189, 246-250.

IV. **Jongyun Moon**, Hannu-Pekka Hedman, Marianna Kemell, Aulis Tuominen, Risto Punkkinen, Hydrogen sensor of Pd decorated tubular TiO_2 film prepared by anodization with patterned electrodes on SiO_2/Si substrate, 2016, Sensors and Actuators B: Chemical, 222, 190-197

Author's Contribution

The author has been responsible for sample preparation and writing of publications I, II, III and IV. In particular, the author contributed spectrophotometer analysis for publication I, field scanning microscopy analysis for publication III and IV, and gas sensor measurements for publication II, III and IV.

Abbreviations

Al	Aluminum
Al_2O_3	Aluminum oxide
a*	Saturation
b*	Degree of lightness
CMOS	Complementary metal oxide semiconductor
EDS	Energy-dispersive X-ray spectroscopy
FESEM	Field emission Scanning electron microscope
H_2	Hydrogen
HFC	Hydrogen fuel cells
H_2SO_4	Sulfuric acid
HF	Hydrofluoric acid
IC	Integrated circuit
In_2O_3	Indium oxide
KF	Potassium fluoride
L*	Hue
LPG	Liquefied petroleum gas
MEMS	Micro electro mechanical systems
N_2	Nitrogen
NH_4F	Ammonium fluoride
NaF	Sodium fluoride
1D	One dimensional
O_2	Oxygen
PVD	Physical vapor deposition
PV	Photovoltaic
Pd	Palladium
Pt	Platinum
Si	Silicon
SiO_2	Silicon oxide
SnO_2	Tin oxide
Ti	Titanium
TiO_2	Titanium dioxide
TCD	Total color difference
WO_3	Tungsten oxide
XRD	X-ray Diffraction
ZnO	Zinc oxide

Contents

Chapter 1

Background

Increasing emissions of air pollutants and global climate change caused by consuming fossil fuels have been a concern for several decades. This is not only resulting in environmental problems, but also ecological imbalance. Hence, society aims at reducing greenhouse gas emission and finding alternative energy sources. Renewable energy sources, such as hydropower, wind power, photovoltaic (PV) and hydrogen fuel cells (HFC), are favored to reduce the use of fossil fuels, and especially wind power and PV show fast growth rates [1]. However, these technologies still need further development because these energy sources are not yet flexible enough to be carried or stored.

The importance of hydrogen has increased since hydrogen has been started to be considered as an alternative renewable energy resource as well as its wide utilization in various other applications, such as, petroleum processing, fertilizer production, and fuel cells [2]. Hydrogen is a clean, efficient and abundant resource in nature. Moreover, hydrogen can not only provide a solution for dwindling fossil fuel resources, but also encourages its development as an energy carrier. Therefore, with the increasing importance of hydrogen fuel, it has been defined as one of the six alternative fuels for automobile industries by the U.S. Department of Energy which has worked to build a hydrogen infrastructure [3]. Nevertheless, hydrogen is limited in its use because of its chemical/physical properties, as it is a colorless, odorless, and tasteless and flammable gas. Hydrogen in air is flammable and explosive in the concentration of 4–75 vol. %. Therefore, a hydrogen sensor is a prerequisite to alert in the case of the accumulation of hydrogen in different atmospheric conditions and to prevent the risk of the explosion.

Many different types of hydrogen sensors have been available on the market. Much effort has been made to improve gas sensing properties, which are sensitivity, selectivity, and response/recovery time. As the hydrogen industry evolves, more specific hydrogen sensing properties are required in respect with the applications. Thus, the desired characteristics

of hydrogen sensors have been discussed comprehensively throughout several reviews [2,4] and their summary is presented in Table 1.

Table 1: Sensor requirements for hydrogen sensor research & development.

Parameter	Value
Measurement Range	0.1% – 10% (Safety) 1 – 100% (Fuel cells)
Operating temperature	–30 – 80°C (Safety) 70 – 150°C (Fuel cells)
Response time	< 1s
Gas environment	Ambient air 10% – 98% RH
Lifetime	10 years
Interference	Resistant (e.g., hydrocarbons)
Reliability (Sufficient accuracy and sensitivity)	Uncertainty < 5 – 10% of signal
Pressure	80-110 kPa

Metal oxide semiconductors, such as SnO_2, ZnO, and TiO_2, have been widely used as gas sensing materials due to some advantages, such as low cost, high sensitivity and feasibility of mass production. The working mechanism of metal oxide semiconductor gas sensors is based on changes of the sensor resistance including electrical resistance of the sensing materials and contact resistance when a target gas is introduced in the detecting atmosphere.

Among the various metal oxide materials, TiO_2 prepared by anodic oxidation has received much attention. Since the discovery of a porous oxide surface formed in fluoride containing electrolyte by Zwilling [5], numerous studies have attempted the modification of this material and have been able to show potential for usage in various applications, such as photovoltaic, photo-catalyst and gas sensors. Eventually, a TiO_2 nanotube array prepared by anodic oxidation was reported by Grimes and co-workers in 2001 [6]. Interestingly, anodically prepared TiO_2 nanotubes have shown great hydrogen detection properties compared to other TiO_2 nanostructures. However, the technologies using anodically prepared TiO_2 layer are still difficult to be commercialized due to the following reasons. First of all, it is expensive to produce the final product using novel material due to manufacturing and characterizing processes using nanotechnologies. Secondly, its structural characteristics are not optimistic comparing to existing materials, such as SnO_2 powder. In other words, when the material is a solid thin layer prepared on a substrate, its usage is more limited compared to powder type of TiO_2 nanostructures. Finally, gas sensors using

an anodic TiO_2 layer are not yet on a stage of mass production for microelectronic applications.

Therefore, this study is focused on the development of a hydrogen gas sensor using anodic TiO_2 nanostructures, which currently need further improvement of material manufacturing efficiency and gas sensing abilities.

Chapter 2

Literature review

2.1 Definition of chemical sensors

A gas sensor is defined by the International Union of Pure and Applied Chemistry (IUPAC) as follows: “a chemical sensor is a device that transforms chemical information, ranging from the concentration of a specific sample component to total composition analysis, into an analytically useful signal. The chemical information, mentioned above, may originate from a chemical reaction of the analyte or from a physical property of the system investigated” [7]. Chemical sensors are made of a receptor (a chemical recognition system) and a transducer. The receptor is typically a material, such as a thin layer, which reacts to gas molecules selectively. Such chemical reactions take place by adsorption, ion exchange or liquid-liquid extraction at the interface between gas molecules and receptor surface. The transducer measures the chemical information obtained from the receptor and converts it into a useful analytical or digital signal.

2.2 Classification of hydrogen sensors

The physical or chemical reaction of hydrogen with the element comprising the sensor produces changes in various properties, such as temperature, refractive index, mass and electrical properties. According to the working principle of the sensor, hydrogen sensors have been classified and summarized as listed below.

Table 2: Classification of hydrogen sensors by operating principles [4].

Working principle	Type of sensor	Signal source
Catalytic: Heat effects caused by combustible gases with oxygen on catalytic surface	Pellistor	Electrical resistance change resulting from temperature changes of an activated bead, based on exothermic reaction
	Thermoelectric	Based on the Seebeck effect[1] (thermoelectric effect) caused by oxidation of hydrogen
Thermal conductivity: The measured temperature changes from a hot body	Pellistor like sensor	Detecting the temperature changes between 'hot' and 'cold' element
Electrochemical: Detection of charge transport change or electrical properties caused by electrical reaction at sensing electrodes.	Amperometric	Detecting current changes resulted from chemical reaction
	Potentiometric	The potential difference between a sensing electrode and reference electrode
Resistance based	Semiconducting metal–oxide sensor	Change of electrical resistance by reaction of hydrogen with adsorbed oxygen
	Metallic resistor	Electrical resistivity caused by adsorption of hydrogen from the ambient atmosphere (Resistance of PdH_2 > Pd)
Work function based Measures the electron volts that are the minimum energy to remove an electron from solid surface.	Metal–semiconductor (Schottky) diode	Changes of work function of sensing materials (Pt, Pd) via hydrogen diffusion
	Metal–insulator–semiconductor transistor	Field effect transistor that converts the change of work function of a catalytic metal gate into an electrical signal according to hydrogen concentration
Mechanical		Changes of physical properties of sensing metals by hydrogen adsorption that causes expansion of the metal lattice.
Optical Measures changes of optical properties of sensing materials	Micro-mirror optical fibre sensor	Changes in the reflectivity of the sensing layer (Pd)
	Surface plasmon resonance	Change of resonant wavelength or angle of the incident light source.
Acoustic Measures changes in the acoustic wave properties of piezoelectric materials	Quartz crystal microbalance	Resonance frequency caused by a thin quartz disk that is sensitive to hydrogen adsorption
	Evanescent based sensor	Reaction of evanescent[2] materials with hydrogen causes a change in its refractive index, which can be detected as change of transmittance

[1] The Seebeck effect is to convert the temperature difference of two different metals into electricity. This phenomena is caused by metals, which respond to temperature, current loops and magnetic fields.

[2] An evanescent field, which is a magnetic field, can form at the boundary between a medium, for example, at the core of optical fiber. The evanescent field is weakened exponentially with distance from the core.

2.3 Characterization of gas sensing properties

The gas sensing properties of metal oxide gas sensors can often be characterized by several factors, such as, sensitivity, response time, recovery time, optimal operating temperature and detection limit. In metal oxide gas sensors, sensitivity (S, response) mostly indicates the ratio of the resistance measured in background gas (eg. air and N_2) and the resistance measured in a mixed atmosphere with a target gas. This can usually be defined in several different forms, assuming that the resistance of the sensor is the measuring signal; (i) $S=R_a/R_g$, (ii) $S=R_g/R_a$, (iii) $S=(R_a-R_g)/R_g$ and (iv) $S=(R_g-R_a)/R_a$, where R_a is the resistance of the sensor in background atmosphere and R_g is the resistance of the sensor in target gas. In this study, the sensitivity was determined by using (iii) formula.

Response time was estimated as the time when the sensor reached 90% of the steady-state value of the resistance to H_2 and recovery time was estimated as the time when the sensor recovered to 90% of the initial resistance. In practice, the obtained response and recovery time from gas sensing measurements are mostly longer than the actual sensor's reaction time due to the delay time caused for the replacement of gases in the testing environment. Therefore, a sensor with good gas sensing properties has high sensitivity, a short reaction time, a low operating temperature and a long life time (high tolerance).

2.4 Historical background of metal oxide gas sensors

The first gas sensor application with semiconductors was reported by Brattain and Bardeen in 1953 [8]. Later on, metal oxide gas sensors were commercialized by Taguchi, the so-called Taguchi sensor, and it is still on the market [9]. The Taguchi sensor consists of a heater embedded in an aluminum ceramic tube, and sensing material, SnO_2, mounted on the tube by two gold electrodes, as seen in Figure 1.

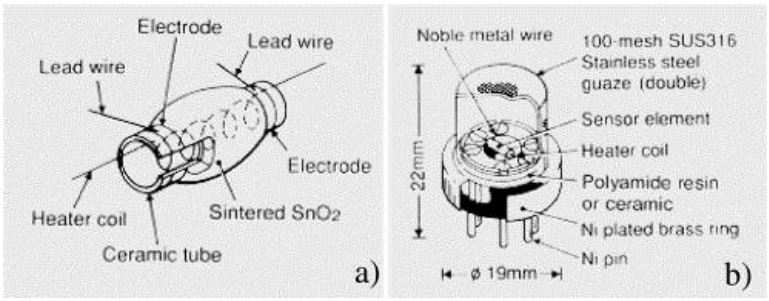

Figure 1: Schematic of the Taguchi-type sensor (a) Sensor Element and (b) Packaged Sensor [9].

For decades, the screen printing technique has been commercially favored to produce smaller sensors than that by Taguchi. It brought the advantages of a mass production of sensor arrays that consist of a metal oxide sensing layer deposited on a ceramic substrate through batch processing. However, gas sensors made by screen printing still require further improvement for power consumption, mounting technology and selectivity. These requirements have led the research interest to miniaturization, which requires highly sensitive control of thin layer deposition for micro-sized sensor module processes [10]. Consequently, metal oxide gas sensor technology integrated with microelectro-mechanical system (MEMS) which reduces sensor size, power consumption and production cost has emerged. Suehle et al. [11] reported a metal oxide gas sensor on a micro hotplate based on a complementary metal oxide semiconductor (CMOS) process in 1993 as one of the first micromachined gas sensor models. As power consumption and mass production in gas sensor modules are the main interest in the present research field toward integrated circuit (IC) technology, CMOS technology was a success as it accomplished a significant reduction in total power consumption. Moreover, CMOS technologies enable self-containing sensing modules including all sensors, fabrication process, interface on a chip as well as possible wireless interface [12].

2.5 Hydrogen gas sensors using metal oxide semiconductors

The existing gas sensor technologies, including catalytic, thermal conductivity and metal oxide sensors, have been developed with MEMS [10,13,14]. Essentially, for metal oxide semiconductor technologies, the main interest has been on nano-sized material structures. A number of studies have shown that the gas sensing performance of micro-sized gas

sensors can be improved by controlling the morphological structures of the deposited oxide layer and by doping with noble metals, such as Pd [15]. These advanced materials can be deposited on silicon or Al_2O_3 based substrates and embedded in a micro-sensor module. In this chapter, the most widely studied metal oxide materials for hydrogen sensing applications are introduced.

2.5.1 Tin oxide (SnO_2)

Tin dioxide (SnO_2) is one of the first and most studied gas sensing materials with ZnO. SnO_2 exists in a crystalline structure of rutile and has a wide band gap (3.6 eV at 300K). SnO_2 nanostructures have been synthesized by the sol-gel method [16], the hydrothermal method [17], chemical vapor deposition [18], thermal evaporation and etc. They have been found to exist as nanorods, nanofibers, nanoribbons, nanobelts and nanowires. Wang et al. [19] made a comparison of gas sensors made of SnO_2 thin film and nanowires as well as other nanostructures. This result obviously showed that one dimensional (1D) nanostructural materials enhanced sensor properties, such as selectivity, response / recovery time, and sensitivity. Table 3 represents the hydrogen sensing properties of various SnO_2 nanostructures.

Table 3: Summary of various hydrogen sensors using SnO_2 nanostructures.

Structure	Synthesis method	Catalyst	Detection limit (ppm)	Operating temperature (°C)	Ref.
Nanowire	Thermal evaporation		10	300	[19]
Nanorods	Thermal evaporation		500	300	[19]
Nanobelt	Thermal evaporation		30000	80	[20]
Nanotubes	Surface sol–gel process		100	450	[21]
Nanowire	Thermal vaporization	Pd	5000	22	[22]
Nanofiber	Electro spinning	Pd	0.02	22	[23]

In general, SnO_2 based sensors require high operation temperatures ranging from 200 to 500°C. To counteract high power consumption, some studies have demonstrated sensors that operate at room temperature. A gas sensor using an In_2O_3-doped SnO_2 thin film synthesized by the sol–gel method was integrated with MEMS [24]. Much effort has been made to improve the sensing performance of SnO_2 by decorating with catalytic

materials, such as Pd. Pd nanoparticle decorated SnO_2 nanowires showed enhanced hydrogen sensing properties at room temperature[22]. However, the slow recovery time (> 20 min) observed in most SnO_2 based sensors is a disadvantage [25].

2.5.2 Zinc Oxide (ZnO)

Zinc oxide (ZnO) is a semiconductor with a wide band gap (3.3 eV) and has widely been used in catalytic, electronic, optoelectronic and photochemical applications. As mentioned above, ZnO is one of the first discovered sensing materials and has been extensively used for gas sensor applications. Various ZnO nanostructures and their preparation methods have been reported [26] and used for hydrogen sensing as shown in Table 4.

Table 4: Summary of various hydrogen sensors using ZnO nanostructures.

Structure	Synthesis method	Catalyst	Detection limit (ppm)	Operating temperature (°C)	Ref.
Thin film	RF sputtering		200	400	[27]
Thin film	RF sputtering		50	350	[28]
Nanorods	Hydrothermal		200	22	[29]
Nanowires	Chemical vapor deposition		100	22	[30]
Nanorods	Sol-gel	Pd	100	22	[31]
Nanorods	Atomic layer deposition		5	22	[32]
Nanorods	Molecular beam epitaxy	Pt	500	22	[33]
Nanotubes	Electrospinning		2.3	200	[34]

However, the sensor performance of ZnO as bulk material is not satisfactory, compared to 1D nanostructural ZnO. For example, Tien and co-workers [33] compared hydrogen sensing properties between Pt coated ZnO thin film and ZnO nanorods, which were prepared by Pulsed Laser Deposition and nucleating ZnO nanorods, respectively. The sensor consisting of nanorods showed higher response to hydrogen than the thin film, because of the high surface to volume ratios. Therefore, aligned 1D structure, such as nanorods and nanowires, are preferred for gas sensor applications. ZnO nanorods or nanowires have been synthesized by the vapor-liquid solid (VLS) growth process, template assisted growth and hydrothermal process. With or without the support of catalytic materials,

such as Pd or Pt, it has recently reported that ZnO nanostructures can detect hydrogen at room temperature. This low operating temperature is one of main demands in semiconductor gas sensors. Lupan and co-workers [29] demonstrated a single ZnO nanorod hydrogen sensor synthesized by a hydrothermal method using an aqueous-based approach in a reactor. The sensor shows a sensitivity of 4% to 200 ppm H_2 and high selectivity to O_2, CH_4, CO, ethanol and Liquefied petroleum gas (LPG), as the sensitivity to these gases were lower than 0.25%.

Due to its material properties, which are the wide energy band gap of 3.37 eV at room temperature and large exciton energy of 60 meV [35], ZnO nanostructures can provide the feasibility to fabricate a flexible and a transparent gas sensor. Rashid et al. [31] demonstrated a flexible hydrogen sensor that consists of Pd decorated ZnO nanorods film prepared by the sol-gel method and deposited on polyimide substrate, showing appreciable hydrogen sensing performance, that is, a sensitivity of ~91% to 1000 ppm H_2 at room temperature. In addition, the sensor shows high mechanical robustness (bending 90°).

2.5.3 Tungsten Oxide (WO_3)

Tungsten oxide (WO_3) has been known a gas sensor material especially sensitive to NO_2 [36]. WO_3 sensors are typically used with Pt or Pd nanoparticles as catalytic material to improve their H_2 sensing performance.

The nanostructures commonly associated with WO_3 are nanowires, nanorods and nanotubes [37]. The most commonly used method to obtain WO_3 nanostructures is physical vapor deposition (PVD) that uses WO_3 materials as a solid target or powder. The PVD process includes sputtering, thermal evaporation, electron-beam deposition, pulsed laser deposition and arc-discharge deposition techniques. For example, a gas sensor using a WO_3 thin film deposited on a Si substrate by thermal evaporation has been demonstrated [38]. The as-deposited WO_3 sensor, which is amorphous, has no response to target gases (H_2, ethanol). The annealing procedure plays an important role in gas sensor performance as shown by the fact that WO_3 annealed at 400°C displayed significantly improved response to 600 – 10000 ppm H_2 compared to WO_3 annealed at 300°C. Increasing the interest of 1D nanostructured materials, An and co-workers [39] reported that WO_3 nanotubes using a TeO_2 nanowire template showed notable performance to 1-50 ppm NO_2. This study indicated that tubular structures show enhanced gas sensing properties compared to nanorod structures due to the higher surface to volume ratio of the WO_3 nanotubes.

Recently, anodic oxidation has been utilized to form nanoporous WO_3 film [40-42]. Despite of increasing interest, only a few studies have reported the

gas sensing properties of anodic WO_3 film. Kukkola et al. [43] demonstrated a gas sensor using mesoporous WO_3 obtained by anodic oxidation in a NaF based electrolyte. After the oxidation process the oxide film was detached from tungsten basis, the oxide film was transplanted to a Si substrate to connect with metal electrodes, which were made for electrical measurements. The sensor showed better sensing properties to H_2 in air and Ar than to CO, NO and O_2. This work suggests some feasibility of anodic WO_3 films to be used in gas sensors. Various hydrogen sensors using WO_3 are presented in Table 5.

Table 5: Summary of various hydrogen sensors using WO_3 nanostructures.

Structure	Synthesis Method	Catalyst	Detection limit (ppm)	Operating Temperature (°C)	Ref.
Thin film	Vacuum sublimation	Pd	250	80-120	[44]
Nanowires	Vacuum sublimation	Pt-Pd	10	25	[45]
Nanowires	Hydrothermal	Pd or Pt	10	150-250	[46]
Thin film	RF sputtering	Pt	30	200	[36]

2.6 Titanium dioxide (TiO_2) for hydrogen sensing applications

Titanium (Ti) was discovered in 1791 by W. Gregor and named menachanite [47]. 4 years later M. H. Klaproth named it as titanium after the Titans in Greek mythology [48]. Titanium dioxide (TiO_2) is a naturally formed oxide of Ti. It was discovered in 1821 and at the beginning of the 20th century the mass production of TiO_2 began and it was frequently used in paints, white pigments, and sun-blocks. The discovery of photo-electrochemical water splitting properties of TiO_2 anode in 1972 made a breakthrough in the research area of solar energy conversion [49]. In 1977, the photocatalysis effect of TiO_2, which made a significant contribution to environmental applications, was first demonstrated by examining the decomposition of cyanide in water [50,51].

TiO_2 is a transition metal oxide and shows n-type semiconductor behavior [52]. Its crystalline phases are known to be rutile (tetragonal), anatase (tetragonal) and brookite (orthorhombic) as seen in Figure 2. In these phases, titanium ions (Ti^{4+}) are bonded with six oxygen ions (O^{2-}). Rutile is the only stable phase while anatase and brookite are metastable at all temperatures. As-prepared TiO_2 has been found to be amorphous in many

cases [53-56] while anatase or rutile can directly be obtained by a hydrothermal method [57]. The crystal phase transition from amorphous to anatase or rutile can be done by heat treatment [58]. In the case of anodically prepared TiO_2 samples, the anatase phase can be obtained at temperatures ranging from 300 to 500°C and the anatase phase transforms to rutile at 500 - 900°C [56].

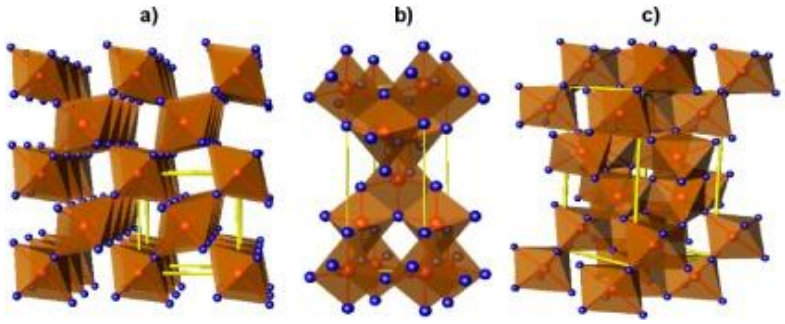

Figure 2: Crystal structures of TiO_2 polymorphs. Red spheres are Ti^{4+}, blue spheres are O^{2-} and yellow lines represent the unit cell. (a) Rutile. (b) Anatase. (c) Brookite. Reprinted with permission from [59]. Copyright © 2013 IOP Publishing Ltd.

During the last decades, scientists have been interested in 1D nanostructures and their modifications. TiO_2 nanostructures have been prepared as porous thin layers, nanotube arrays [6,60], nanotubes [54], nanobelts [61], nanofibers [62], nanorods [63] and nanowires [64]. These nanostructures have been produced using various methods, for example, the hydrothermal [65], sol-gel [53] and anodization methods [66]. These TiO_2 nanostructures react to both oxidizing gases (O_2, NO_2) [67,68] and reducing gases (H_2, CO, NH_3, H_2S) [69-72]. Depending on the target gas, the reaction can be displayed via the increased (oxidizing gas) or decreased (reducing gas) resistance of the material.

For several decades, studies have shown the importance of the structural properties of TiO_2 in determining hydrogen sensing properties. Hydrogen sensing properties consisting of TiO_2 nanostructures made by different methods are summarized in Table 6. The role of structural properties can simply be confirmed by comparing the sensing properties of various nanostructures. According to earlier studies [73-75], compact TiO_2 layers certainly exhibited lower hydrogen sensing properties than nanostructured ones. Jun et al. [74] reported that thermally oxidized TiO_2 at 900°C formed

porous structures and showed better sensitivity in the presence of hydrogen than a compact layer oxidized at 600°C.

Table 6: Summary of various hydrogen sensors using TiO_2 nanostructures.

Structure	Synthesis Method	Catalyst	Detection limit (ppm)	Operating Temperature (°C)	Ref.
Thin film	Anodization	Pt	500	250	[76]
Thin film	Thermal oxidation		10	300	[74]
Nanotubes	Anodization		10	22	[77]
Porous	Anodization		1000	250	[78]
Nanotubes	Anodization	Pd, Pt	10	290	[79]
Nanowire	Thermal evaporation	Pd	500	100	[80]
Mesoporous	Sol-gel	Nb_2O_5	500	450	[81]
Nanohelix	Rotating oblique angle deposition		1.3	250	[82]
Nanopowder	Sol-gel	V_2O_5	1000	200	[83]

TiO_2 nanotube arrays prepared by anodization have received the most significant attention among the other nanostructures for hydrogen sensing applications due to its dramatic sensitivity to hydrogen [77,84]. The morphological role of TiO_2 nanotubes was investigated by comparing several of TiO_2 nanotube sensors which have different pore diameters. It was found that the sensor with the smaller diameter of 22 nm had higher sensitivity than the one with 53 nm and 76 nm. In other words, the smaller diameter of the tube pores increases surface area which enables more hydrogen molecules to adsorb in the oxide surface [84]. Later, it was noticed that a more important factor in determining the sensing properties is the wall thickness of the pores where hydrogen adsorption mainly takes place. Paulose et al. [77] demonstrated hydrogen sensing characterization using TiO_2 nanotubes with different lengths (350 nm – 2000 nm) and similar diameters of pores (30 nm). It was found that the tube length or the thickness of the oxide was not directly relevant to high sensitivity.

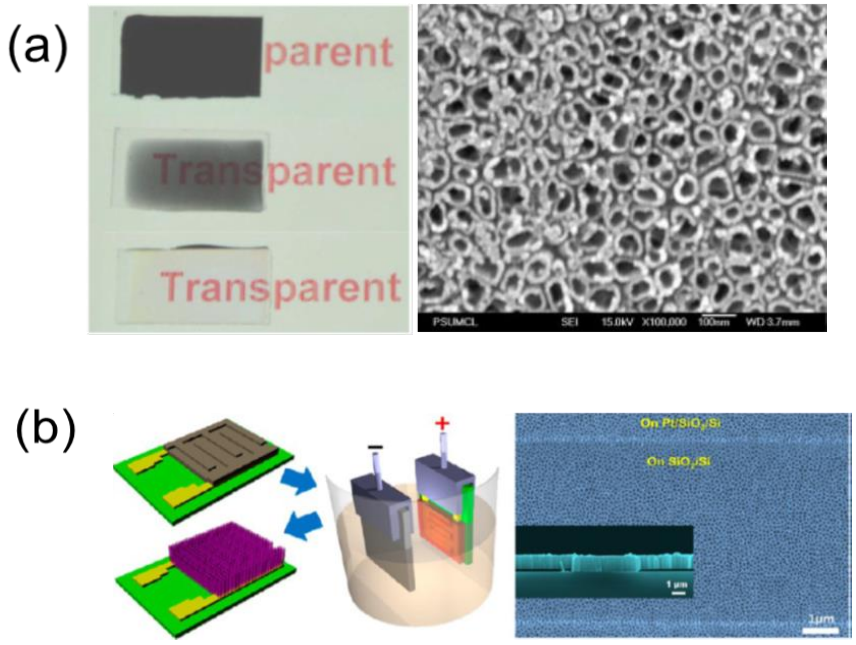

Figure 3: Anodically prepared TiO_2 nanotubes on alternative substrates.
a) Self-organized TiO_2 nanotubes on glass substrate: Stages in the fabrication of nanotubes (Ti deposited sample, sample taken out of the bath in the middle of anodization and sample after heat treatment, respectively). Reprinted with permission from [66]. Copyright 2006 Elsevier B.V,
b) Schematic of sensor to form on a patterned SiO_2/Si substrate (left), FESEM image of TiO_2 nanotube arrays (right), cross sectional image (inset). Reprinted with permission from [85]. Copyright © 2013 American Chemical Society

Despite promising sensing performance, the hydrogen sensor using nanotubes is limited for mass production. Typically, a gas sensor using TiO_2 nanotubes is constructed with the metal electrodes deposited on the oxide layer. The contacts between the measurement device and these metal electrodes are made by external wires using wire-bonding or noble metal paste. However, the metal electrodes deposited on the oxide layer or nanotubular layer may diffuse through the oxide layer and result in electrical short-circuits [86]. Therefore, different approaches for the sensor structures have been considered, such as forming the oxide layer on metal electrodes. However, TiO_2 nanostructures formed on alternative substrates usually showed inferior gas sensing properties. Mor et al. [87] demonstrated a hydrogen gas sensor of TiO_2 nanotubes on glass with

discontinuous Pd. Despite the support of the Pd catalyst, the resistance change of the sensor was significantly smaller than that made from Ti foil [84,87]. Recently, Kim et al. reported TiO_2 nanotube arrays on SiO_2/Si substrate with 5 μm gap–Pt electrodes patterned by photolithography as shown in the schematic of the sensor seen in Figure 3 [85]. By applying a voltage to the Pt electrodes, the Ti layer was completely anodized in ethylene glycol solution with 0.3 wt. % of NH_4F and 3 vol % of water and formed highly ordered tubular structures. Kimura et al. [88] demonstrated a micro-scaled gas sensor of TiO_2 nanotubes by a localized anodization method that used Ti layers deposited on a SiO_2/Si substrate as electrodes. Their result showed that reducing the thickness of oxide and the sensor size as well as thinning the wall thickness of the tubes increased the gas sensing properties. These reviewed works have attempted to prepare an anodic TiO_2 layer and to form particular nanostructures by varying experimental parameters or modifying the sensor geometry. However, despite all of this research, there still remain challenges regarding the mass production of the sensor, improvements of gas sensing abilities, such as selectivity.

2.7 Hydrogen sensing mechanism of metal oxide gas sensors

The sensor signal of metal oxide sensors is based on the resistance changes created in the sensing material. In spite of this simple operation principle, interdisciplinary knowledge including semiconductor physics, surface chemistry, solid-state chemistry, and micro-electronics are required to understand the characteristics of metal oxide gas sensors. Like other metal oxides, such as SnO_2, the gas sensing properties of TiO_2 based sensors can be elucidated by the receptor and the transducer function. The receptor function is the reaction of each crystal of metal oxide to the ambient atmosphere and the target gases [89]. The transducer function represents how the chemical or physical signal of the sensing materials transduces into an output signal. The transducer function can sufficiently be varied by the different microstructures of the metal oxides.

In ambient atmosphere, oxygen molecules are adsorbed on the metal oxide surface and act as electron acceptors. The types of adsorbed oxygen species are governed by the sensor temperature by forming O_2^- ions below 150°C or O^- ions between 150–400°C, which are the typical operating temperatures of metal oxide sensors, and O^{2-} ions are formed above 600°C [90]. The change of electrical properties is resulted from the reaction of the chemisorbed oxygen ions with the target gases. The oxygen molecules adsorb on the oxide surface electrons (e) extracted from conduction band

(E_C), which reach the surface through an electric field. They are then trapped at the surface. This process as described in Figure 4 leads to upward band bending (qV_s=eV_s) and creates a depletion layer or a space charge layer (Λ_{air}). Λ_{air} is dependent on Debye length (L_D), which is a characteristic of the semiconductor material for a particular donor concentration [91-93].

$$L_D = \sqrt{\frac{kT\varepsilon}{q^2 n}} \quad (1)$$

where k, T, q, ε and n represent the Boltzmann constant, absolute temperature, electron charge, permittivity and charge-carrier concentration.

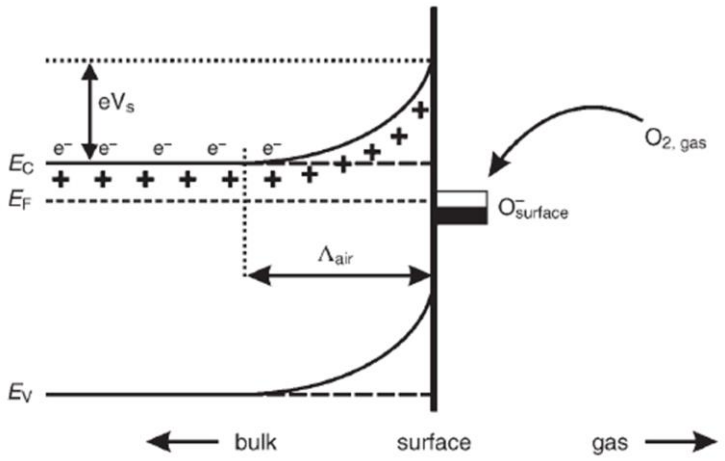

Figure 4: Band bending model in a wide band gap semiconductor after chemisorption of charged species by oxygen adsorption on surface sites. E_C, E_V, and E_F, denote the energy of the conduction band, valence band, and the Fermi level, respectively, while Λ_{air} denotes the thickness of the space-charge layer, and eV_s the potential barrier. The conducting electrons are represented by e- and + represents the donor sites. Reprinted with permission from [94]. Copyright 2011 WILEY-VCH Verlag GmbH & Co. KGaA, Weinheim

It is thought that reducing gases, such as H_2 react with the chemisorbed oxygen ions via forming H_2O. This process releases electrons, which then return to the conduction, leading to the decrease of the upward band bending described in Figure 4 [95]. The impact of the microstructures of

metal oxides is related to the band bending and conduction. The creation of the conduction takes place along percolation paths via a grain boundary or a neck grain boundary in the case of a porous thick layer, and surface in the case of a compact thin film [96]. Thus, depending on the metal oxides structures used for gas sensing applications, different interactions with target gases are induced. The conductance (G) depends on the potential barrier (qV_s=eV_s) between the adjacent grains of the metal oxide, which can be described as

$$G \approx G_0 \exp(-\frac{qV_s}{kT}) \quad (2)$$

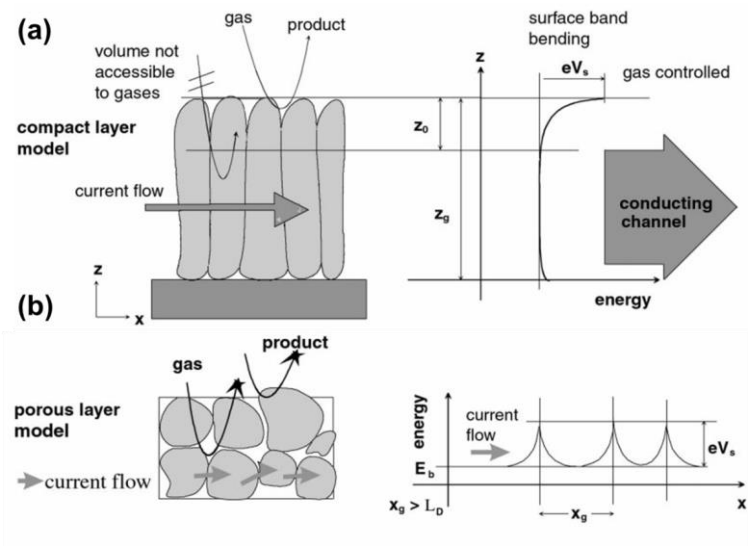

Figure 5: Geometry and band bending diagram of a compact and porous sensing layer. x_g grain size, L_D Debye length, eV_s band bending, z_0 thickness of the depleted surface layer and z_g layer thickness. Reprinted with permission from [10] Copyright © 2001 Elsevier Science B.V.

The microstructural geometry and the band bending of compact and porous structures in the presence of a target gas are described in Figure 5. The reaction of the oxide layer to the target gas takes place only on the metal oxide surface due to the geometry of the compact layer (Figure 5a). This can create a gas-affected layer and a gas-unaffected layer, resulting in two parallel resistances. Thus, the thickness of the oxide plays an important role in influencing the gas sensing properties. In the case of a porous structure, the current flows through interconnected contacts and each grain has a depletion layer (Figure 5b). Thus, porous structures enable the gas

species to access a larger reaction area of the metal oxide. This leads to a gas sensor consisting of a porous metal oxide having higher sensitivity than that consisting of a compact layer.

Anodically prepared TiO_2 layers are essentially porous or tubular structures, which are connected by the necks or walls of pores. In the presence of oxygen, an electron depletion region is formed in the pore wall surface where oxygen chemisorption occurs. The wall thickness of pores is an important factor in influencing the resistance change on the oxide surface. Hence, it is important to control the geometrical parameters, such as pore diameter, wall thickness and the thickness of the oxide layer. The relation of pore wall thickness and band bending is illustrated in Figure 6.

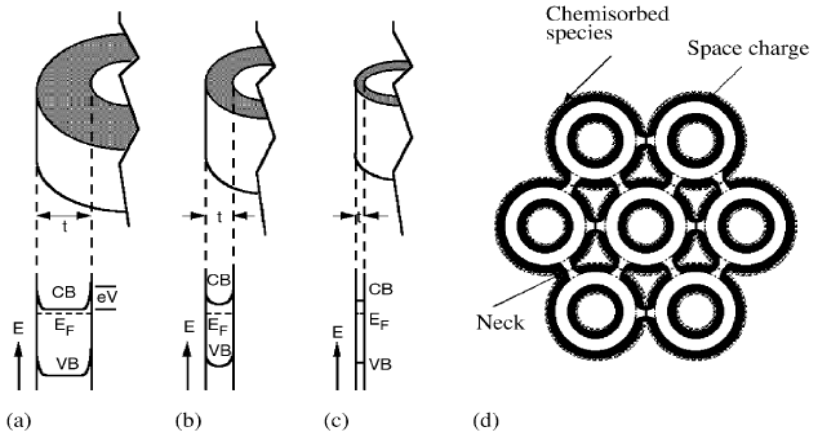

Figure 6: The influence of nanotube wall thickness on band bending due to oxygen chemisorption: (a) when nanotube wall half-thickness (t/2) >> L_D, (b) t/2 ≈ L_D, and (c) t/2 ≤ L_D. (d) schematic illustration of pores, top view. Reprinted with permission from [77] Copyright 2015 IOP Publishing Ltd.

A catalyst is defined as a substance that promotes the speed of a chemical reaction without changing itself. In metal oxide gas sensors, various catalytic materials, such as Pd, Pt and Au, have been used to promote the reaction of the sensor to a target gas. Catalytic effect can be created by a thin layer deposited on an oxide layer or electrodes, which create electrical contacts between the oxide layer and the device in order to measure the resistance. The catalytic effect can be explained by two concepts: electrical and chemical. The electrical concept can be elucidated when the catalytic material attracts electrons from the oxide crystals. This can be observed as increased resistance. Many catalytic materials (PdO, Ag_2O and CuO) are p-

type semiconductors [97]. By loading catalysts on the oxide surface, the work function of the oxide can be significantly increased. Therefore, when the sensor is exposed to a target gas, the catalyst is reduced, which results in the decrease of the work function. This phenomenon has also been demonstrated in a porous TiO_2 layer with Pd electrodes [98,99].

Chemisorbed oxygen species formed on a Pd surface at an elevated temperature ranging from 200 – 600°C leads to an increase in the work function of Pd. This also increases the barrier height at the interface of Pd and TiO_2, resulting in high resistance. In the presence of a reducing gas, such as hydrogen, the chemisorbed oxygen on the Pd surface reacts with hydrogen. This removal of oxygen lowers barrier height, displaying a decrease of resistance. The chemical concept proposes that a deposited catalyst promotes the dissociation of hydrogen molecules, which spill over onto the oxide surface [15,100,101]. The hydrogen molecules adsorbed on the catalyst produce a Pd hydride, which reacts with ionic oxygen. This process releases the electrons back to the oxide surface, resulting in a decrease of the potential barrier and resistance. The effect of a thin Pd layer on a TiO_2 layer was demonstrated in Publication IV.

2.8 Anodic oxidation of titanium

Anodization has commonly been used to decorate the surface of some metals to enhance its surface properties, because uniform and adhesive oxide layers on metals can be produced cost-effectively [102,103]. By varying chemical or electrical parameters during anodization, it is feasible to produce a compact or a porous structured oxide layer that creates insulating or semi-conductive properties on metals or semiconductors [104]. By using anodization, a Ti surface can be covered with an oxide layer in an acid electrolyte involving field-assisted migration of metal (Ti^{4+}) ions through the oxide layer. This process induces the reduction of the current density during the anodization. While the oxide layer is growing, gas generation (O_2 and H_2) is generally observed. In 1999, Zwilling and coworkers [5] initially reported anodization using Ti and its alloys (TA6V) that formed a compact oxide layer in an electrolyte containing chromium acid and a nanoporous oxide structure in HF/chromium acidic electrolyte. Grimes et al. accomplished a significant contribution on the anodization of Ti by discovering a nanotubular structure prepared in an aqueous electrolyte containing HF [6]. Based on relevant studies, it has been found that the morphologies of anodic TiO_2 can be controlled by varying experimental parameters including the voltage, the electrolyte and the anodization time. To date, the anodic TiO_2 layer can ultimately be grown in thicknesses ranging from few hundreds of nanometers to approximately

1000 μm and pore diameters ranging from 10 to hundreds nanometers [105,106].

2.9 Evolution of anodic TiO_2 nanostructures

The majority of the research on the anodic TiO_2 layer has focused on tubular structures and their applications. The evolution of the materials and the modifications has been categorized as four generations depending on the morphological structures of the oxide in different electrolytes (1^{st} –3^{rd} generation) and base substrates (4th generation).

2.9.1 First generation

The first generation of TiO_2 nanotubes, which was prepared in aqueous HF or its mixture electrolyte using Ti foil, were grown with tube lengths up to 500 nm by varying the electrolyte concentration [5,6]. Also, the anodization bath temperature is an important experimental parameter that influences chemical dissolution rates and etching rates during anodic oxidation [107]. In this work, anodization at different bath temperatures (5°C, 25°C, 35°C and 50°C) in an electrolyte containing acetic acid and HF (1 : 7 ratio) showed that the decrease of bath temperature increases wall thicknesses and tube lengths.

2.9.2 Second generation

Increasing the number of attempts to grow TiO_2 tubes with high–aspect ratio (tube length/tube diameter) by anodization in electrolytes containing HF, it was found that the thickness of the TiO_2 layer was limited up to several hundred nanometers by the fast rate of TiO_2 dissolution. Several μm long nanotubes, as called second generation materials, were grown in neutral electrolytes containing KF or NaF [108]. The morphologies of tubes were modified by varying the pH of the electrolyte [108,109]. It was found that the increase of pH resulted in longer nanotubes.

2.9.3 Third generation

The usage of various organic electrolytes, such as formamide, dimethyl sulfoxide, and ethylene glycol can increase tube lengths forming smooth tube walls [110,111] as seen in Figure 7. During anodization in non-aqueous electrolytes, a low current density and low etching rate of the oxide layer were observed. These are responsible for the formation of a thinner initial oxide layer on Ti than that in an aqueous electrolyte. The thin oxide layers

incorporate high ionic conductivity and low Ti oxidation rate, resulting in substantial increases in nanotube lengths [110]. Using organic electrolytes, a thick oxide layer up to thickness of 1000 μm was grown successfully, and the oxide layer could be separated from the Ti base substrate [110].

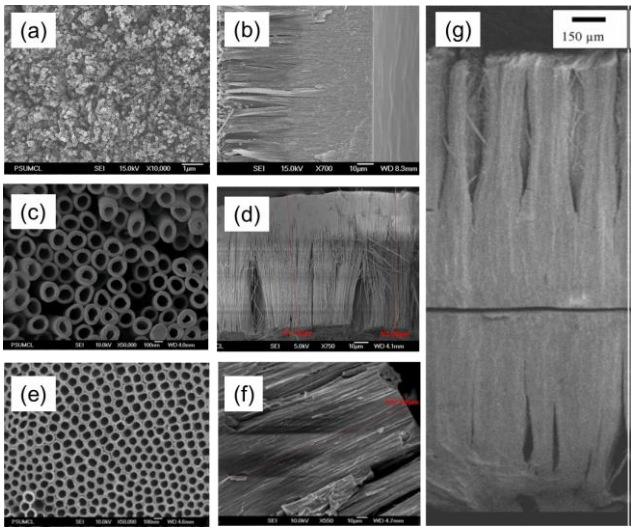

Figure 7: FESEM images of TiO_2 nanotube arrays grown in various organic electrolytes. a, b) Formamide based electrolyte at 35 V for 48 h; c, d) 60 V in a DMSO electrolyte containing 2% HF for 70 h; e, f) 60 V in an ethylene glycol electrolyte containing 0.25 wt. % NH_4F for 17 h, Reprinted with permission from [111]. Copyright 2015 IOP Publishing Ltd., g) cross sectional image of oxide membrane obtained from 2 mm Ti foil at 60 V for 216 h in 0.5 wt. % NH_4F and 3.0% water in ethylene glycol. Reprinted with permission from [106]. Copyright 2007 American Chemical Society.

2.9.4 Fourth generation: Anodization of Ti deposited on alternative substrates

TiO_2 nanostructural layers can easily be grown by the anodization of a Ti foil. However, the structure of the Ti foil underneath the oxide layer is not optimal considering its usage in electronic applications due to following reasons [87]: As mentioned earlier in section 2.5, an electrical short-circuit can possibly be caused by the metal (Pt or Pd) electrodes deposited on the oxide layer. The contact between the oxide layer and the electric device, which is typically made by wire-bonding, can be broken by mechanical shock or vibration [85,87]. Finally, Ti is not suitable to use in micro sized devices due to its difficulty of reducing material size. Therefore, the

formation of a TiO_2 layer on alternative substrates is required and some effort has been made on using Si, SiO_2, Al_2O_3, glass [86] and In_2O_3 [112,113] substrates. However, it is still challenging to form uniform TiO_2 nanostructures on these alternative substrates. The Ti layer deposited on the substrate can be damaged during the anodization. For instance, if the anodization parameters are not optimized, a significant loss of the deposited Ti layer may occur at the interface between the electrolyte and air where intense etching occurs [86].

Also, the deposited Ti layer may not be oxidized completely due to an irregular electric potential on the Ti layer. Some research groups have attempted to overcome the challenges of preparing TiO_2 nanostructures on the alternative substrates. Macak and co-workers [114] achieved TiO_2 nanotubular layers with a thickness of 500 nm on a Si wafer using a H_2SO_4/HF mixed electrolyte at a low temperature (–2°C). This work clearly showed that a low bath temperature is advantageous in preparing regular tubular structures on the wafer, as irregular morphology was found from the sample anodized at 20°C. Mor et al. [86] used a double Ti layer on the interface region and indicated that the deposition needs to be done at a high temperature (500°C). The high deposition temperature improves the density of the Ti layer and the adhesion between Ti layer and the base substrate [112,115,116].

2.10 Growth model of anodic TiO_2 nanostructures

Ti is a good candidate to form self-organized oxide structures, such as porous and tubular structures, by anodization [66]. Theories about how to understand the growth of anodic TiO_2 nanostructures have been brought from Al anodization, which has been used to grow alumina (Al_2O_3) [117-119]. For the last decade, the comprehensive studies on the Ti anodization mechanism have been accomplished [120,121]. These studies showed that the fluorine ion in the electrolyte is an important factor for the formation of the oxide structure. The formation mechanism of porous and tubular TiO_2 in the electrolyte with/without fluoride ions is described in Figure 8. In both cases, the anodization process is explained by two competitive reactions; (Eq. 3) field-assisted anodic oxide formation and (Eq. 4) chemical dissolution of the oxide.

$$Ti + 2H_2O \rightarrow TiO_2 + 4H^+ + 4e^- \quad (3)$$

$$TiO_2 + 4H^+ + 6F^- \rightarrow TiF_6^{2-} + 2H_2O \quad (4)$$

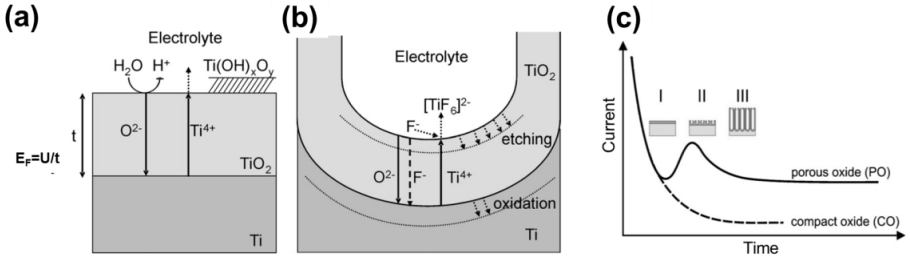

Figure 8: Schematic representation of Ti anodization. (a) in absence of fluorides (results in flat layers), and (b) in the presence of fluorides (results in the tube). Reprinted with permission from [120]. Copyright 2007 Elsevier Ltd., (c) current-time plot of anodization using fluoride ion free (----) and fluoride ion containing (—) electrolyte. Reprinted with permission from [121] Copyright 2011 WILEY-VCH Verlag GmbH & Co. KGaA, Weinheim.

In case of the fluoride free electrolyte, the formation of the oxide layer starts, when Ti reacts with O^{2-} ions in H_2O (Eq. 3) as in Figure 8a. The oxide growth continues by field-assisted ion transport (O^{2-} and Ti^{4+} ions) through the growing oxide layer. During this process, the field effect $E_F = U/t$ with a constant voltage U decreases drastically during the oxide growth, which leads to the decrease of the driving force, until the field effect is diminished and thickness of the oxide layer reaches the finite thickness [121].

The fluorides in the electrolyte play an important role in the formation of either a porous or tubular structure. If the fluoride concentration is low ($\leq$ 0.05 wt. %), anodization forms a compact oxide layer like in fluoride-free anodization. If fluoride concentration is high ($\geq$ 1 wt. %), oxide is no longer obtained on the metal surface because the fluoride ions react with Ti^{4+} forming soluble $[TiF_6]^{2-}$ ions, which may cause electro-polishing [121,122].

The formation of porous/tubular structures in fluoride ion containing electrolytes has often been described using a current-time curve [121] that is divided in three phases. First, an oxide layer grows at the interface of metal/electrolyte by the reaction of metal Ti with O^{2-} and OH^-. If anodization is stopped at this stage, a compact oxide layer can be obtained. Next, nanoscaled pores start forming on the oxide surface and a sharp increase of current is observed. This results from the localized dissolution of the oxide (Eq. 3). These pores form all over the oxide surface, leading to the current increase. Last, the current decreases slowly because the depth of the porous structure increases and the growth rate of the oxide at the metal/oxide interface becomes equal to that of the oxide dissolution at the pore bottom/electrolyte interface.

Chapter 3

Aims of the thesis

The main purpose of this work is to develop a highly sensitive hydrogen gas sensor using anodically prepared TiO_2 nanostructures. This sensor can be integrated with microelectronic systems and be mass-produced. In order to develop such a sensor, anodization was used to prepare a nanostructured TiO_2 layer.

Publication I investigated the relation of the morphological and color properties of TiO_2 layers prepared by the anodization of Ti foil in an aqueous electrolyte. Anodization is a known method for coloring metal surfaces. Therefore, knowledge of the coloration of Ti during anodization can be utilized to identify the morphological structure of the oxide layer.

In Publication II, a hydrogen sensor was fabricated using TiO_2 nanotubes prepared in the same manner as in Publication I. The sensor was tested with various hydrogen concentrations at room temperature. Despite of the appreciable performance of the sensor in detecting hydrogen, the sensor based on Ti foil showed some clear drawbacks that encouraged developing a gas sensor based on anodic TiO_2 nanostructures on alternative substrates.

The anodization of a Ti layer on a semiconducting or an insulating substrate requires different experimental parameters than that of Ti foil. This method enables the sensor to be reduced in size and to be integrated into micro-electronic system. Thus, Publication III and Publication IV demonstrated hydrogen gas sensors using TiO_2 nanostructures.

In Publication III, mesoporous TiO_2 on a Si wafer was prepared and was used for hydrogen gas sensing. As the most compatible substrate for micro-electric system, the Si wafer was selected as the base substrate to form TiO_2.

In Publication IV, a hydrogen sensor was prepared by using a Pd decorated TiO_2 tubular layer on an insulating substrate, thermally oxidized silicon (SiO_2/Si). Typically the electrode structures, which are made by wire bonding, can be broken by physical disturbances, such as vibration. In order to develop a reliable gas sensor, metal electrodes were patterned under the oxide layer. By using this method, it is also possible to produce multiple sensor elements via a single anodization process and to reduce sensor size. A thin Pd layer as a catalyst was decorated on the oxide layer to improve the sensing properties.

Chapter 4

Materials and methods

4.1. Anodization set-up (Publication I–IV)

The anodic oxidation set-up in this thesis consists of a conventional two electrode configuration with a platinum foil as a counter electrode as seen in Figure 9. The anodization apparatus includes a beaker made of Teflon, two sample holders, a thermometer and a refrigerated circulator (Neslab Instruments, Inc., Newington, NH). Depending on the purpose of the studies, different anode electrodes (Ti foil and deposited Ti layer) are used. The details of the anode electrode preparation are described in section 5.
The voltage was applied using a power supply (GW, GPG-3030, US). The current during anodization was recorded with a precision multimeter (Fluke 8846A 6.5 digit precision multimeter, Fluke UK Ltd, Norwich, UK).

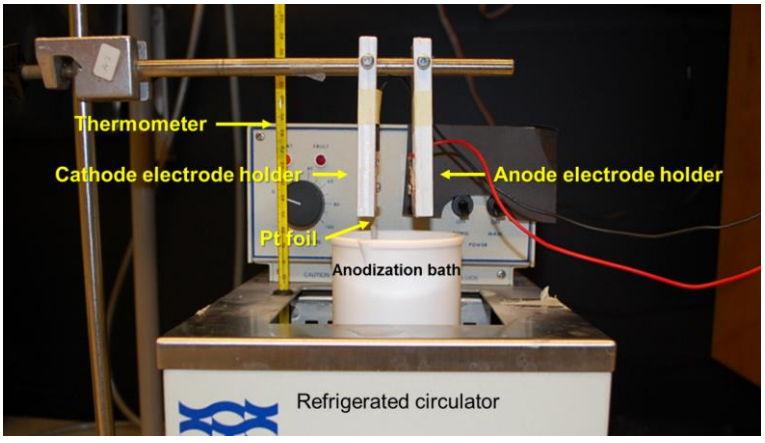

Figure 9: Image of the anodization apparatus.

4.2. Heat treatment for crystallization (Publication II – IV)

Prior to sensor preparation, the as-anodized TiO_2 was annealed at 500°C with a heating/cooling rate of 1°C/min by a multi-stage programmable electric furnace (Vulcan, 3-130 Furnace, US) in ambient atmosphere for crystal phase transition.

4.3 Gas sensor preparation (Publication II – IV)

This study presents different sensors using anodic TiO_2 nanostructures on different base substrates including metal Ti foil, Si and SiO_2/Si. After heat treatment, the substrates (Ti, Si, SiO_2/Si), which were cut to compatible size (5 mm × 10 mm) were fixed on an alumina substrate (20 mm × 10 mm) using a silicon glue. Then, copper (Cu) or gold (Au) wires were adhesively bonded to metal electrodes using a silver (Ag) paste (Conductive epoxy CW2400, Chemtronics, USA) in order to create electrical contacts.

4.4 Characterization

4.4.1 Field Emission scanning electron microscope (FESEM, Publication I – IV)

Morphology and cross sectional observations of the samples were carried out by field emission scanning electron microscopy (FESEM, Hitachi S-4800, Tokyo, Japan). Cross sectional images in Publication I and II were taken by bending or scratching samples. A FESEM sample holder for cross sections was used for the TiO_2 layers formed on Si and the thermally oxidized silicon substrate in Publication III and IV. Prior to FESEM analysis for cross sectional images, the Si and SiO_2/Si substrates were mechanically cracked.

4.4.2 Spectrophotometer (Publication I)

The optical properties of the TiO_2 layer on metal Ti foil were characterized using a spectrophotometer (Konica Minolta Sensing Inc., CM-700d, Japan). The device provides information on reflectance spectra within the visible wavelength (400 – 700 nm). The interference color of the samples was estimated in the CIElab color scale using a D65 light source.

4.4.3 Energy-dispersive X-ray spectroscopy (EDX, Publication III and IV)

An energy-dispersive X-ray spectroscopy (EDX) equipped to FESEM was used to analyze material elements.

4.4.4 X-ray diffraction (XRD, Publication I, III and V)

X-ray diffraction was used to identify the crystalline structure of the material. The crystal structure in this study was characterized by XRD (Philips X'Pert Pro MPD X-raypowder diffractometer, Netherland) using CuK_{α} radiation over a 2θ range of 20–65°.

4.4.5 Current-Voltage characterization (Publication III and IV)

The resistance between the metal electrodes (Pt or Au) was detected by making direct needle contacts to the Pt electrodes with a needle probe station (Rucker & Kolls 666). The current–voltage characteristics were measured by a semiconductor parameter analyzer (Hewlett Packard HP4145B)

4.4.6 Gas sensing measurement (Publication II, III and IV)

The gas sensor measurements in this thesis were carried out using three set-ups. These set-ups were changed and developed during the progress of the sensor development process.

The first measurement in Publication II, which dealt with a sensor consisting of TiO_2 nanotubes prepared from Ti foil, was implemented in a 56 liter glass chamber at room temperature. An exact volume of hydrogen was injected into the chamber using a syringe. Two fans were installed to circulate the air in the chamber.

In Publication III, the sensor was placed on an aluminum block, where a ceramic heater (15 mm × 15 mm, Ultramic 600, Watlow) was placed to control operation temperature. A thermocouple was attached to the aluminum to observe the sensor temperature (Figure 10a). A precision multi-meter (Keithley 6487 Picoammeter Voltage Source, Keithley Instruments Inc., OH, USA) was used to record the resistance of the sensor with the applied DC voltage of 5 V. This sensor module was installed in a 56 liter closed glass chamber with continuous air circulation.

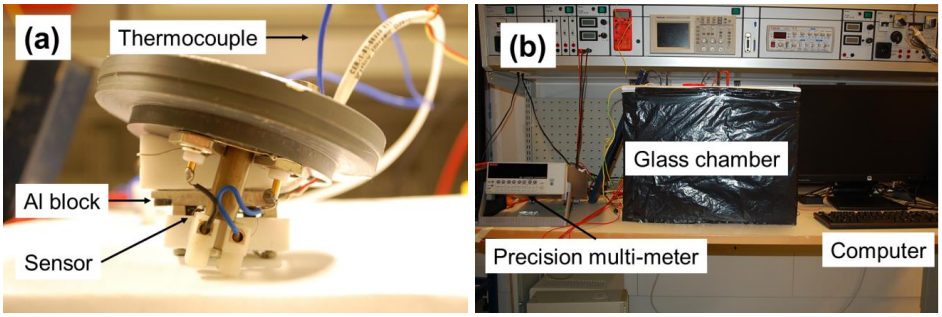

Figure 10: Images of the gas sensing measurement system: (a) gas sensor module, (b) gas sensing measurement chamber and recording devices consisting of a computer to record data from the precision multi-meter.

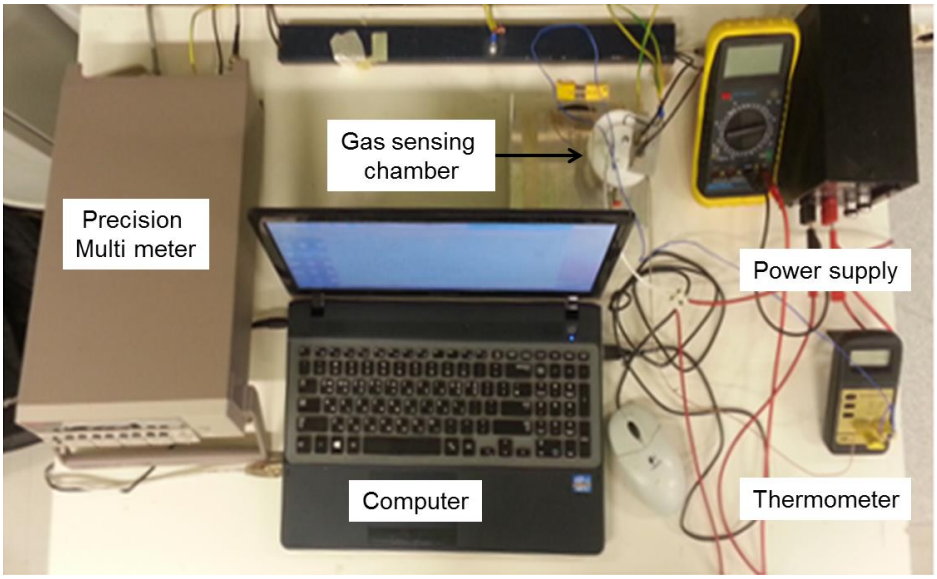

Figure 11: Image of the gas sensor measurement set-up.

An exact volume of H_2 was injected into the chamber and a commercial H_2 sensor (SX917, Sensorex, Finland) was used to verify the H_2 concentration during the measurement (Figure 10b).

In Publication IV, an Al chamber was made with a volume of 75 cm^3 to test the sensor in different atmospheres. The gas sensor module (Figure 10a) was used. Gas mixtures were made from high purity gases controlled by mass flow controllers. The total gas flow through the chamber was 1000 sccm. The gas sensor measurement system is shown in Figure 11.

Chapter 5

Summary of results and discussion

5.1 Anodization of Ti foil and interference colors of TiO_2 (Publication I)

In nature, Ti is covered by a natural thin oxide layer. Like other valve metals, when Ti is anodized, oxide growth takes place on the Ti surface via field-assisted migration of Ti^{4+} ions through the oxide layer. The morphological properties of the oxide depend on the electrochemical parameters of the anodization including the current density, the electrolyte concentration and the electrolyte temperature [103,123]. The anodization of Ti using electrolytes containing fluoride ion enables the forming of porous/tubular TiO_2 structures.

Table 7: Morphological parameters of TiO_2 nanotube arrays anodized at different voltages for 30 min.

Voltage (V)	Pore diameter (nm)	Wall thickness (nm)	Tube length (nm)	Porosity (%)
7	17	16	134	23
10	32	10	231	41
15	45	14	271	51
20	90	29	340	60

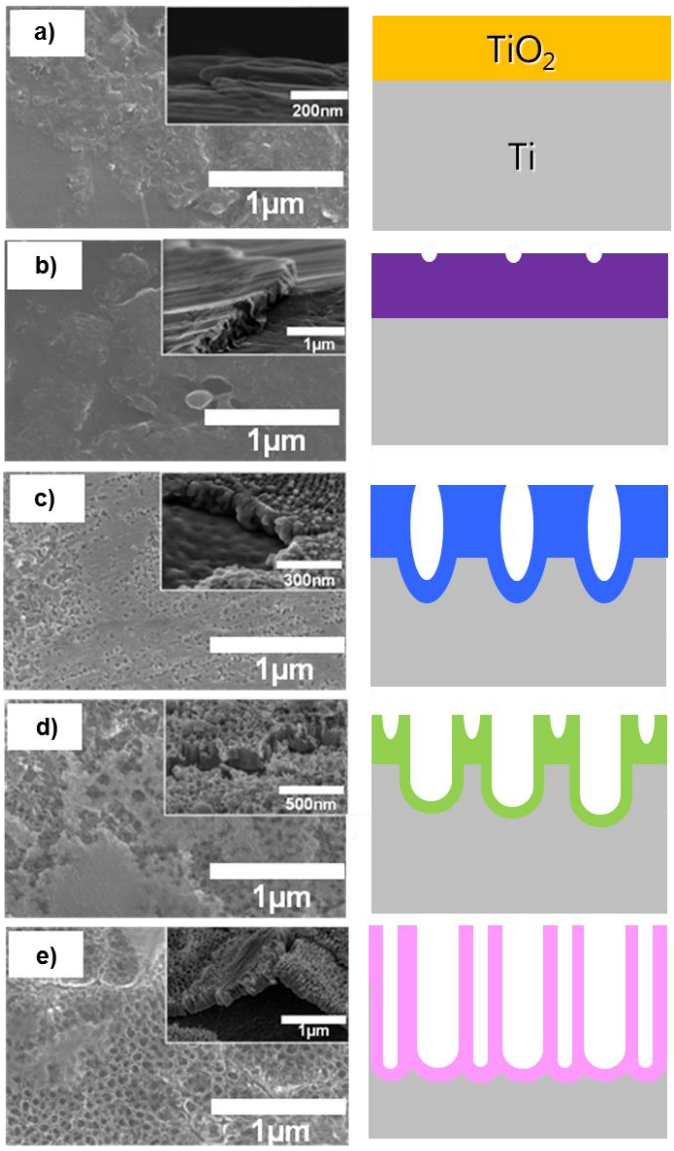

Figure 12: The comparison between the growth procedure and the interference colors of TiO_2 nanotube arrays formed at 20 V a) 1-2 s after immersion: Formation of oxide layer on Ti foil, b) 34 s, development of oxide layer, c) 66 s: formation of slits and cracks on oxide layer, d) 126 s: sequential pore growth, e) 400 s: pore growth completed and remaining tubular structure.

To study the growth of TiO_2 nanotubes, anodization of Ti foil was carried out using an aqueous electrolyte containing HF 0.5 wt. % at different voltages (7, 10, 15 and 20 V). The FESEM analysis of TiO_2 nanotubes showed that the tube morphologies including the pore diameter, the tube lengths and the wall thickness increased as a function of the applied voltages. The estimated porosities of the TiO_2 nanotubes increased as a function of increased voltages. The summary of the morphologies and the porosities is shown in Table 7.

When white light is illuminated, particular colors can be seen by naked eye due to the interference phenomena in the oxide layer on the Ti foil. In order to investigate the coloration, a group of TiO_2 nanotube samples were prepared by varying the anodization time and their morphologies were examined by FESEM as seen in Figure 12. The oxide layer formed in the initial stage of the anodization was a compact layer with a thickness of 70 nm (< several seconds) and 90 nm (34 s), displaying a gold hue and a purple hue, respectively. Then the oxide layer started forming porous structures on the oxide surface. Tubular structures were formed when the oxide thickness reached 173 nm displaying light green color. The oxide layer growth continued up to 240 nm resulting in a pink hue.

5.2 Empirical studies for optical properties of anodic TiO_2 nanotube layers (Publication I)

The optical properties of thin oxide layers are influenced by grain boundaries, voids and disordered regions. These morphological properties also influence interference colors. Based on the correlation of optical and morphological properties, thus, the empirical knowledge of TiO_2 coloration is clearly beneficial in understanding oxide structures.

A spectrophotometer was used to obtain the reflectance spectra. The reflectance spectra of the oxide layers prepared at different voltages have a broad maximum reflectance within the visible wavelength region as seen in Figure 13a. The results indicated that the reflectance decreased when the thickness of TiO_2 layer increased. The reflectance curves of the sample group determined by anodization time in Figure 13b showed that when the thickness of the oxide layer became thick enough (> 240 nm), the interference effect and the reflectance became weak. This result is in good agreement with the study of Al_2O_3 prepared by anodization, which showed the disappearance of interference effect when the oxide layer reached a critical thickness [124].

The color properties obtained by the spectrophotometer were determined by the L*a*b* system, where L*, a* are b* are hue, saturation and degree of

lightness, respectively. The pure Ti foil was characterized first as a reference. The total color difference (TCD) was estimated as

$$\mathrm{TCD} = \sqrt{(\Delta L^*)^2 + (\Delta a^*)^2 + (\Delta b^*)^2} \quad (5)$$

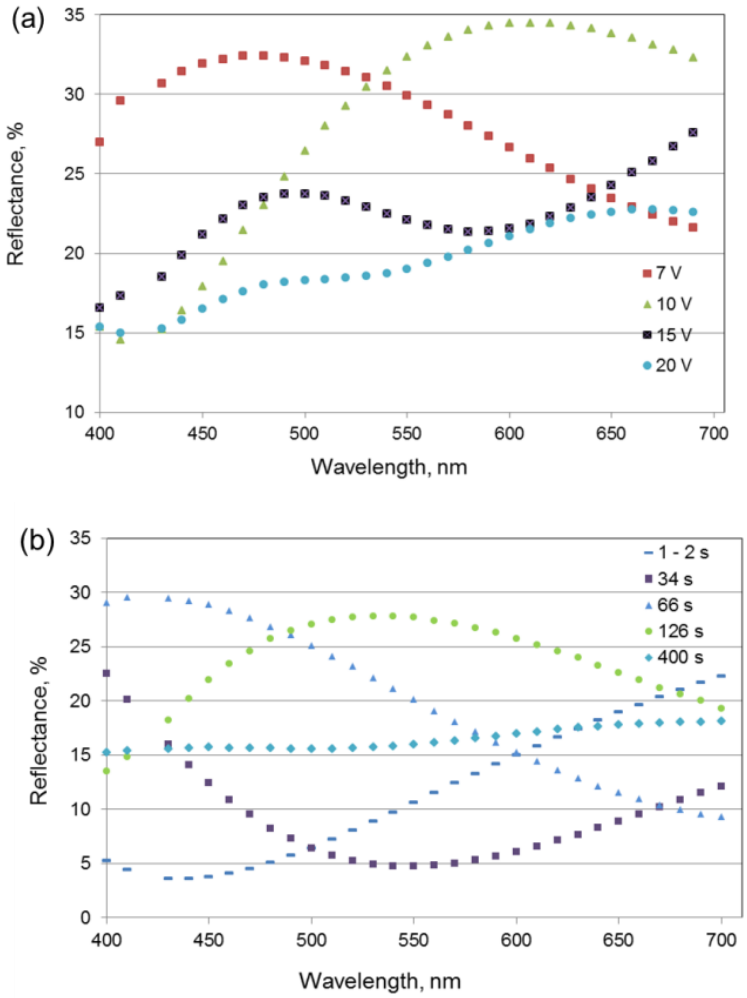

Figure 13: Optical reflectance spectra of TiO_2 nanotube arrays prepared a) at different voltages, b) varying anodization time with a constant voltage (20V).

The anodization parameters, the oxide thicknesses and color properties are summarized in Table 8. These results indicate that the samples anodized less than 1 min showed high TCD values. In the other hands, it indicates that the compact layers have a greater coloration effect than porous layers on Ti foil as the sample anodized for longer time showed a lower TCD value.

The phenomenon causing the interference colors has been explained by the multiple-beam interference theory [102]. When the oxide surface is illuminated with white light, an interference phenomenon occurs. In the case of the anodization of Ti foil, the coloration is therefore mainly dependent on the thickness of the oxide layer, while the surface structures influence the lightness. According to the results of this study, the coloration can be used as an indication of the morphological structures and to predict the thickness of the oxide structure.

Table 8: Summary of the chromaticity diagram of TiO_2 nanotube arrays prepared at different voltages.

Sample	Time (s)	Voltage (V)	Thickness (nm)	L	a*	b*	TCD (D65)
Ti		-	-	60.66	1.47	5.24	-
(a)	1800	7	134	61.29	-5.41	-2.51	10.54
(b)	1800	10	231	61.80	0.02	22.39	17.27
(c)	1800	15	271	54.46	-4.00	4.53	8.46
(d)	1800	20	340	57.27	1.89	8.43	4.66
(e)	1	20	73	39.28	9.62	25.98	30.82
(f)	34	20	91	29.32	14.82	-21.64	43.32
(g)	66	20	113	51.42	-6.82	-14.92	23.76
(h)	126	20	173	58.57	-6.51	8.19	8.99
(i)	400	20	240	52.05	2.70	2.35	9.14

5.3 Porous TiO_2 layer prepared on Si substrate (Publication III)

In order for anodization using alternative substrates, such as Si, it is crucially important to control the concentration of the electrolyte. In many cases, anodizations to form TiO_2 contain F^- ions that have a considerably high chemical dissolution rate [114,125]. This type of electrolyte may damage the oxide layer or the base substrate if special attention is not paid. In the case of a thin Ti layer (<100 nm) deposited on Si, the anodization ends in few tens of seconds. Thus, the oxide structures do not fully form into porous or tubular structures due to the short anodization time [126]. In order to lower the dissolution rate, Macak et al. [127] pointed out that a low anodization bath temperature below 5°C can be a key to synthesize tubular structures. In addition, the usage of a neutral electrolyte containing 1M $(NH_4)_2SO_4$ and 0.5 wt. % NH_4F was suggested to reduce the dissolution rate.

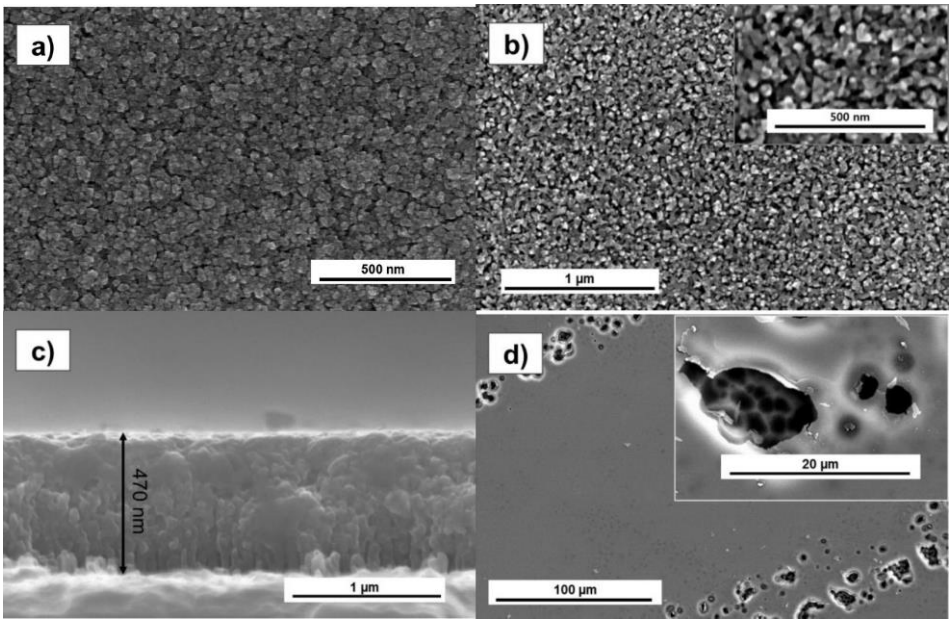

Figure 14: FESEM images of Ti and TiO_2 layers on Si substrate: (a) Ti layer deposited on Si, (b) top view of a mesoporous TiO_2 layer on Si after anodization in HF 0.5% in DI water; inset is with high magnification, (c) cross-sectional image of a TiO_2 layer, (d) top image of a TiO_2 layer anodized for 10 min; inset shows partially porous silicon formation.

The crucial parameters in this study were Ti deposition temperature and anodization time. At the start of this experiment, the sample in the sputter could be heated up to 200°C, which is lower than the optimal temperature previously reported [87]. Therefore, the Ti layer was deposited at 150°C on the Si substrate. This process improved the adhesion of the Ti layer on the Si substrate [115]. The sample was anodized an aqueous electrolyte containing hydrofluoric acid (HF) 0.5 vol.% in DI water for 5 min at room temperature. FESEM images in Figure 14 show the deposited Ti layer (a), which has grain diameters of 10-25 nm and the anodized TiO_2 (b, c) with grain diameters of 20 – 40 nm and a thickness of 470 nm. The long anodization time caused the dissolution of the TiO_2 and the formation of porous Si as seen Figure 14d. It can be assumed that the electrolyte reaches the interface between the Ti layer and the Si surface and starts dissolving the Si [127]. Furthermore, the time when to remove the sample from the anodization bath needs to be carefully considered.

5.4 Tubular TiO_2 layer prepared on metal electrode patterned SiO_2/Si (Publication IV)

TiO_2 nanostructures have been prepared by anodization on various substrates including glass, silicon and alumina [85,86,114]. Essentially, SiO_2/Si is a good base substrate due to its compatibility for microelectronic applications and feasibility to reduce the device size. However, the anodization of Ti on alternative substrates has suffered from substantial TiO_2 loss by chemical dissolution [128]. Several approaches have been reported, such as low temperature anodization, double Ti layer deposition and high Ti deposition temperature [85,86,114].

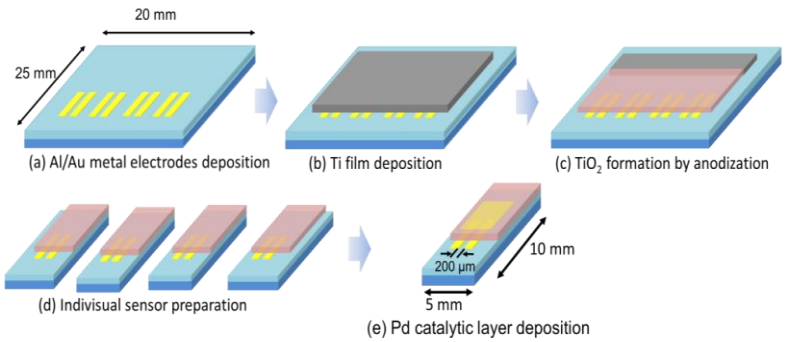

Figure 15: Schematic of the sensor fabrication procedure.

In Publication IV, anodically formed tubular TiO_2 structures were prepared on a SiO_2/Si slice with patterned metal electrodes. The sample preparation is schematically described in Figure 15.

High quality Ti (thickness of 500 nm) was deposited on a SiO_2/Si substrate patterned with metal electrodes (Al/Au) by a DC magnetron sputter. Anodization was carried out in organic electrolyte containing 0.3 wt. % NH_4F in ethylene glycol for 40 min at 5°C. The applied potential was 60 V with 1 V/s ramp rate. This experimental arrangement was chosen after a series of experiments with various parameters, such as the bath temperature (5-20°C), the applied voltage (20-60V) and the electrolyte concentration.

The obtained TiO_2 layer had a thickness of 350 nm, an average pore diameter of 40 nm and an average wall thickness of 15 nm (Figure 16). After the anodization, a thin Pd layer (2 nm) as a catalytic material was deposited to enhance the hydrogen adsorption/desorption effect. EDS analysis confirmed the existence of the TiO_2 and Pd layers on the metal electrodes and SiO_2 layer.

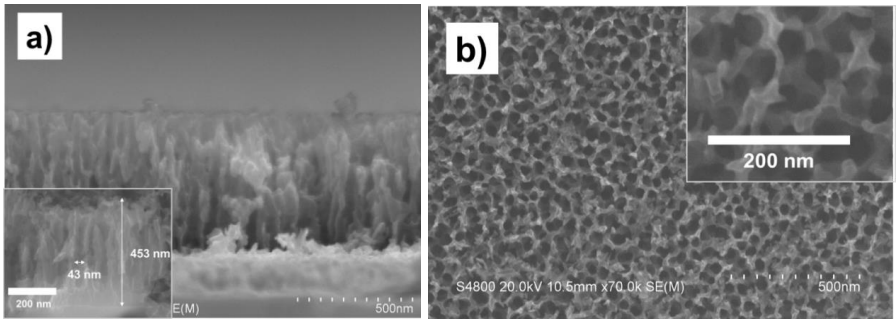

Figure 16: FESEM image of tubular TiO_2 structures obtained from the anodization of a Ti layer on a SiO_2/Si substrate in an electrolyte containing NH4F 0.3 wt. % in ethylene glycol at 5 °C.

5.5 Crystalline structures of anodic TiO_2 (Publication I, III and IV)

The crystallinity of TiO_2 plays a significant role in determining its usage in different applications. The as-anodized TiO_2 layer is typically observed to be amorphous. The crystallinity of the TiO_2 can be converted from amorphous to anatase or rutile by annealing at an elevated temperature in an ambient atmosphere [56]. The as-anodized TiO_2 prepared by varying the anodization parameters can have compact, porous or tubular structures. X-ray diffraction patterns from the samples anodized in aqueous HF electrolyte are proven to be amorphous as seen in Figure 17. Interestingly, some studies have reported that a mixture of amorphous and anatase was observed in an as-anodized TiO_2 layer [120]. For instance, Yoriya et al. [129] demonstrated that as-anodized TiO_2, which were anodized in diethylene glycol electrolytes containing 0.5 wt. % NH_4F and 2% H_2O, showed the anatase peak as a proof of partial crystallization of the oxide layer without any heat treatment.

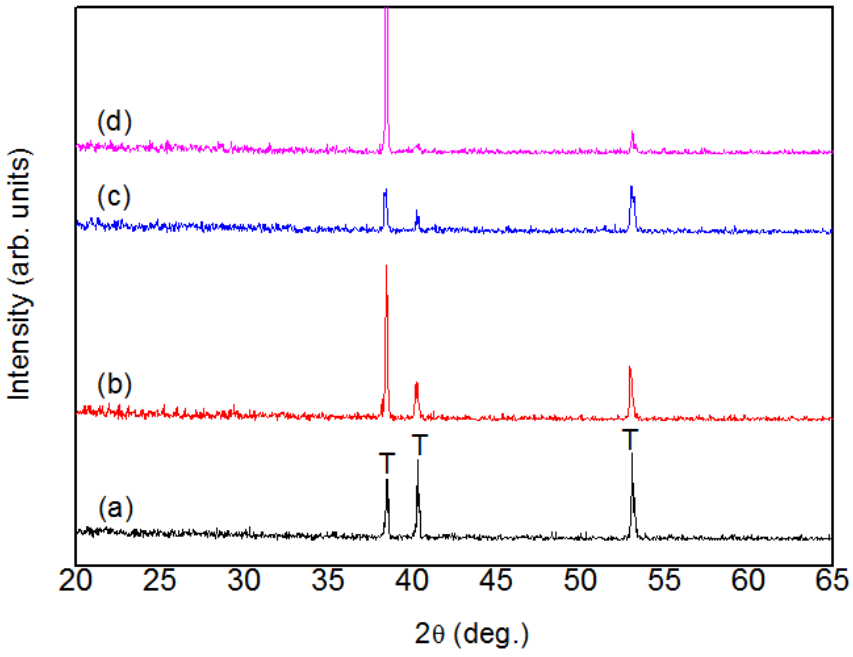

Figure 17: XRD patterns of as prepared TiO_2 layers by anodization of Ti foil in an electrolyte containing HF at different applied voltages (a) 7 V, (b) 10 V, (c) 15 V and (d) 20 V. T represents titanium.

The XRD patterns of TiO_2 nanotube arrays are shown in Figure 18, after annealing the samples at different temperatures (300-700°C). It can be seen that the crystallization takes place at 300°C. The phase transition from anatase to rutile was observed at the annealing temperature of 500°C. The anatase phase almost disappeared at 600°C and 700°C. In the case of the anodization of a Ti thin layer on an alternative substrate, such as SiO_2/Si, only the anatase phase exists at 500°C, as seen in Figure 19. This result is in contrast with the XRD patterns of TiO_2 from Ti foil, which possess a mixture of anatase and rutile at the same temperature. It was noted that during the anodization of the Ti foil, rutile starts growing at the interface between the bottom of the oxide layer and the Ti surface by thermal oxidation. The situation at the interface between TiO_2 and SiO_2 makes the phase transition of anatase phase to rutile [56,86].

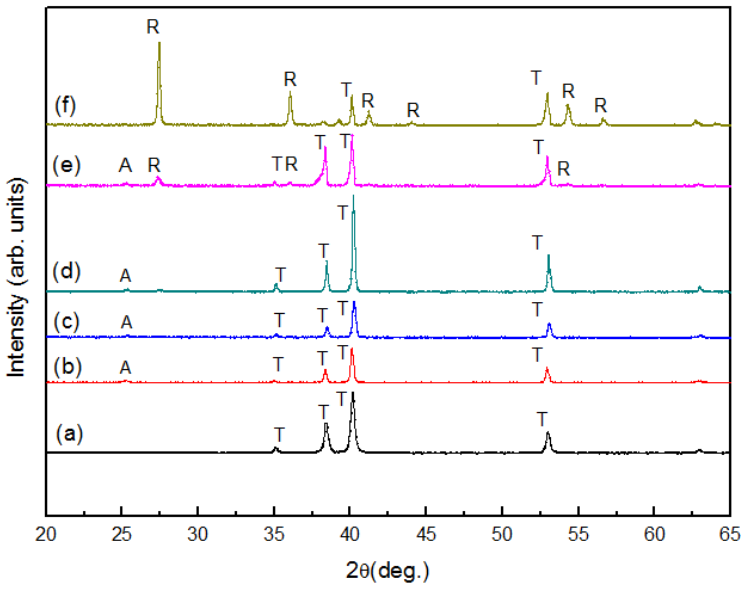

Figure 18: X-ray diffraction patterns of TiO_2 nanotubes annealed at various temperatures: (a) without annealing, (b) 300°C, (c) 400°C, (d) 500°C, (e) 600°C and (f) 700°C for 4 hours in ambient air. A, R and T represent anatase, rutile and titanium, respectively.

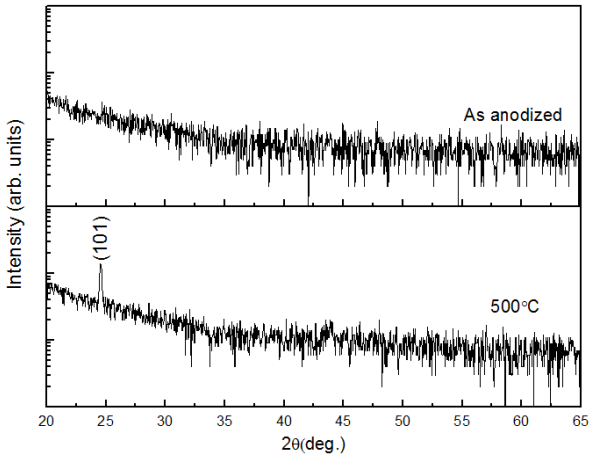

Figure 19: XRD patterns of the TiO_2 layer before and after the heat treatment at 500°C for 6 hours in ambient atmosphere.

5.6 Electrical properties (Publication III and IV)

The current-voltage (IV) characteristics were characterized by measuring two point resistances at different temperatures in air as seen in Figure 20. The result indicated that the current of both sensors increased with increasing temperature. The sensor using mesoporous TiO_2 with Pt electrodes showed non-ohmic behavior as a result of the different work function of Pt and TiO_2. This creates a Schottky barrier at their interface [130-132].

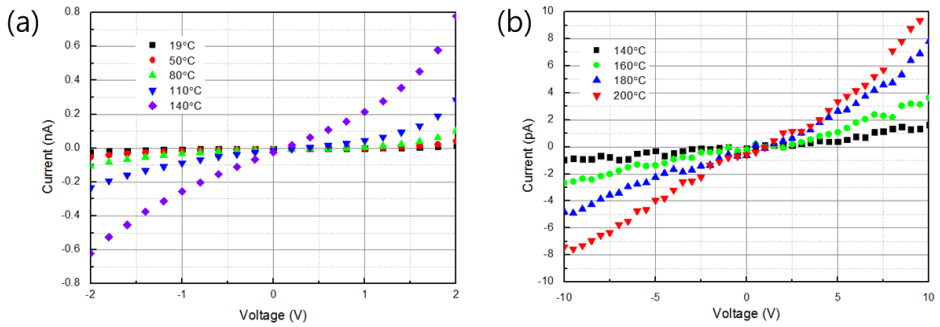

Figure 20: Current–voltage characteristics of TiO_2 layers measured at different temperatures (a) mesoporous TiO_2 prepared on Si and (b) tubular TiO_2 prepared on SiO_2/Si.

Using SiO_2/Si substrate, the current is expected to flow only through TiO_2 layer. The resistance measured between metal electrodes under tubular TiO_2 had clearly higher resistance than that made on a Si substrate and showed non-ohmic behavior. The base resistances of the sensors in case of pure Si substrate were in the range of GΩ, while in case of SiO_2/Si in TΩ. This indicated that the current partially flows from Pt metal electrode directly through Si, which is less resistive, resulting in lower resistance. However, it will be shown in the section 5.7 that the sensor response to H_2 is mainly dominated by the reaction of TiO_2 with H_2

5.7 Hydrogen sensing properties

5.7.1 Hydrogen sensing using TiO_2 nanotube arrays formed on Ti foil (Publication II)

Publication II was carried out to demonstrate the sensor using TiO_2 nanotubes on Ti foil. A number of gas sensors using anodic TiO_2 nanostructures, which are mostly prepared from Ti foil, have been studied [99,133,134]. These sensors can simply be constructed with having metal electrodes deposited on the oxide layer as illustrated in Figure 21. The TiO_2 nanotube samples were prepared in the same manner as in Publication I at 15 V. After the crystallization of the TiO_2 nanotube arrays at 600°C, two Pt electrodes (thickness 20 nm, diameter 1 mm, distance 1 mm) were deposited using a shadow mask on the oxide layer in order to form the electrical contacts. The resistance between the Pt electrodes was about 60 MΩ in ambient atmosphere. The range of sensor response was from 0.008 to 4.2 in the presence of hydrogen (0.1 – 4%) as shown in Figure 22.

The reason for low sensor response is from the conductive Ti metal underneath the oxide layer [135]. The base resistance of a Ti foil based sensor can vary from several kΩ to several 100 GΩ due to the conductive underlying Ti foil and the Schottky diode effect at the interface between TiO_2 and Pt electrodes [84,133]. This makes the sensor using Ti foil based TiO_2 difficult to calibrate in practical applications. In addition, the lifespan of the sensors may not be satisfactory due to resistance changes caused by the diffusion of metal electrodes. This encouraged us to develop more reliable sensor structures using anodic TiO_2 nanostructures on alternative base substrates.

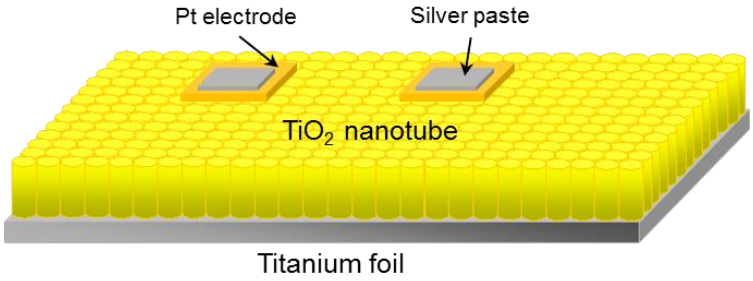

Figure 21: Schematic of the sensor using TiO_2 nanotube arrays prepared from Ti foil.

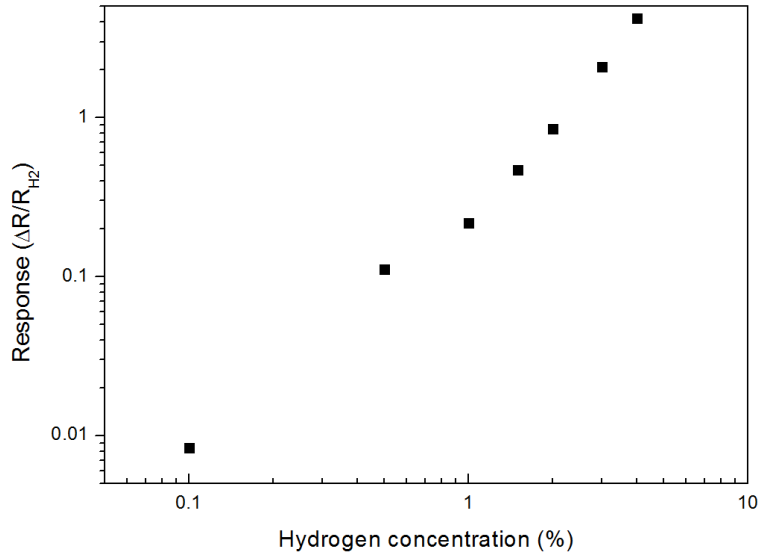

Figure 22: Responses of the sensor using TiO_2 nanotube arrays when exposed to hydrogen concentrations ranging from 0.1% to 4% in air at room temperature.

5.7.2 Hydrogen sensor using mesoporous TiO_2 on Si (publication III)

The formation of anodic TiO_2 nanostructures on a Si slice and its importance for microelectronic applications has been reported [114,136]. However, few studies have reported gas sensors using anodically prepared TiO_2 on Si [114,126,137].

In this study, a gas sensor using anodically oxidized porous TiO_2 on Si (Section 5.3) was fabricated for hydrogen detection. Pt electrodes (thickness 100 nm, diameter 1.4 mm, and distance 0.4 mm) were deposited on a TiO_2 layer by DC magnetron sputtering. After the crystallization procedure at 500°C, the sensor was then attached on an alumina substrate (20 mm × 10 mm × 1 mm). Au wires (25 µm diameter) were connected to the Pt electrodes and Cu sheet using Ag paste. The sensor structure is schematically illustrated in Figure 23.

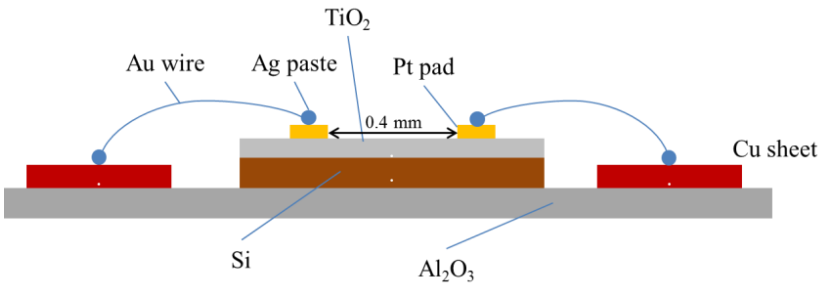

Figure 23: Schematic drawing of TiO_2 sensor on Si substrate.

The influence of the operating temperatures (50°C, 80°C, 110°C and 140°C) to H_2 detection was investigated as shown in Figure 24a. The increase of the operating temperature decreased the base resistance and reduced the noise level. The sensor response as a function of hydrogen concentrations at different operating temperature is shown in Figure 24b. The best H_2 sensing properties were achieved at 140°C with a low noise level and a high response. The trend line (red line in Figure 24b) equation of the response obtained at 140°C is $S=0.4402\ln(x)-1.1607$, where x is the hydrogen concentration (ppm) and the correlation coefficient of R^2 is 0.995.

With this sensor structure, the Schottky barriers are created at the interface of Pt and TiO_2 after annealing the sensor at 600°C. In this case, there are two Schottky diodes reverse biased one against the other and the total current may be limited by the saturation current of the first or the

second Schottky barrier, depending on the polarity of the applied voltage. The response results were obtained from the applied voltage of 0.5 V.

The variation of sensor resistance at 140°C to different hydrogen concentrations is seen in Figure 25a. The sensor resistance after removal of hydrogen did not return to the initial resistance. This small difference of the resistance is mostly caused by minor changes of the operating temperature.

The response/recovery times are seen in Figure 25b. The sensor showed slow response (30–50 s) at a low hydrogen concentration (≤ 20 ppm) and a fast response (< 10 s) above 300 ppm hydrogen. The recovery time showed an opposite trend as the recovery time became slow with increasing hydrogen concentration.

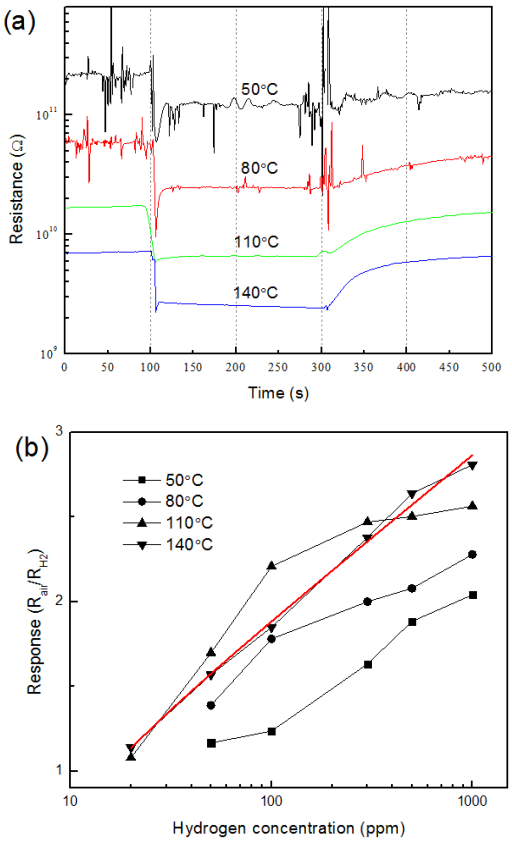

Figure 24: Hydrogen sensing properties of the TiO_2 sensor at different operating temperatures: a) Resistance plot upon exposure to 1000 ppm H_2 in air at different operating temperatures, b) Responses obtained at 20–1000 ppm H_2.

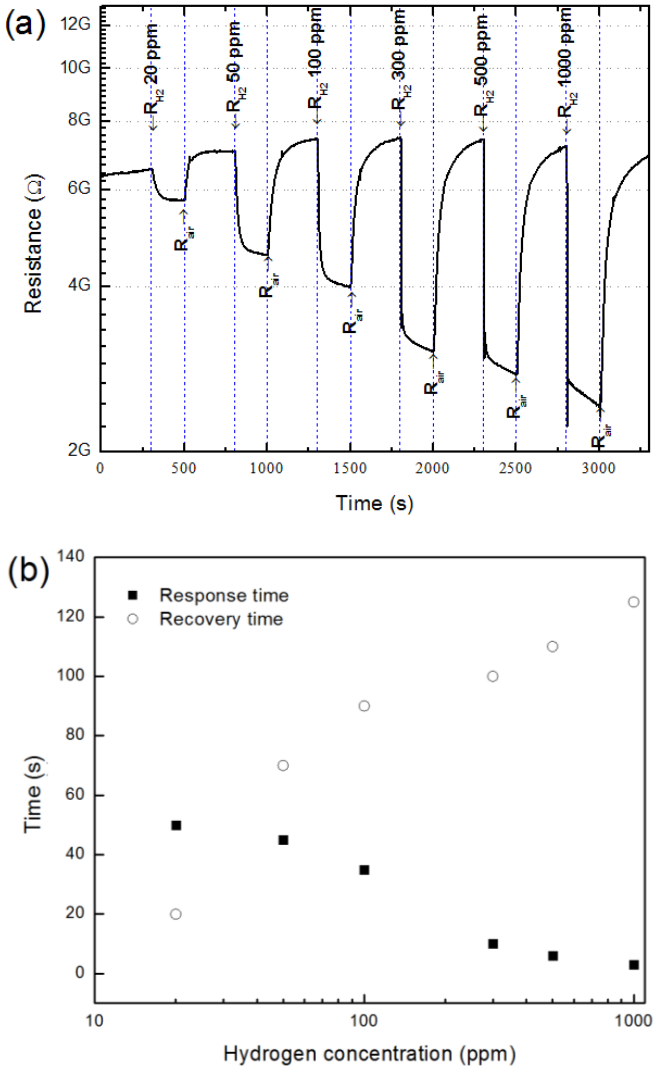

Figure 25: Hydrogen sensing properties of the TiO_2 sensor prepared on a Si substrate: (a) Resistance plot of the TiO_2 sensor upon exposure to H_2 concentrations from 20 to 1000 ppm in air at 140°C operating temperature, (b) Response and recovery time of the TiO_2 sensor as a function of H_2 concentration.

5.7.3 Hydrogen sensing measurement using Pd decorated tubular TiO_2 layer on metal electrodes patterned on SiO_2/Si substrate (Publication IV)

In Publication IV, the preparation of a tubular TiO_2 layer (tube diameter 40 nm and thickness 450 nm) on a SiO_2/Si slice with patterned metal electrodes was demonstrated. This approach enables the sensor to be wire-bonded to chips in microelectronic devices and to increase the compatibility of the sensor with IC technologies. The oxide surface was decorated with a catalytic material, Pd, in order to improve the adsorption/desorption of hydrogen. For further investigation of the hydrogen sensing mechanism, the sensor was tested in different atmospheric environments.

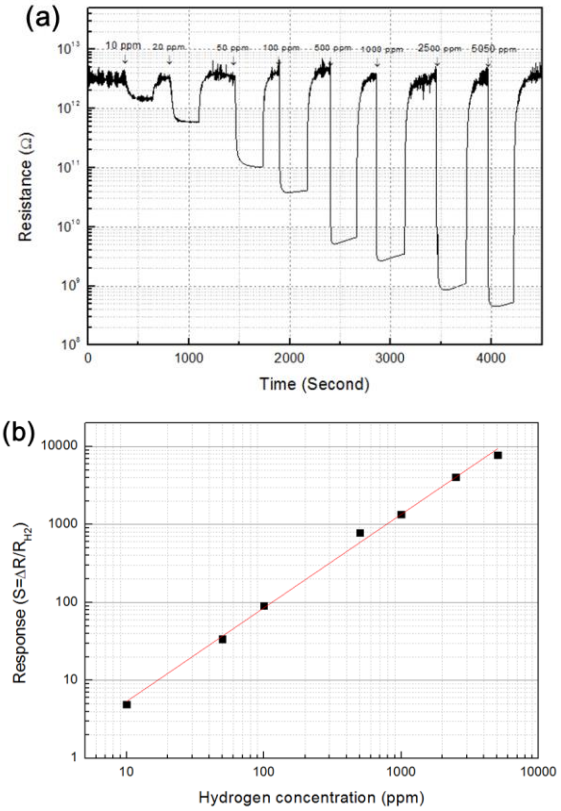

Figure 26: Hydrogen sensing properties of the Pd decorated TiO_2 sensor to 10-5050 ppm H_2 in dry air at 180°C. (a) Resistance variation and (b) response plot.

The results of the hydrogen sensing measurement in dry synthetic air at 180°C indicated that the sensor has a wide hydrogen concentration detection range (Figure 26a). Its response followed the power law, $S = 0.102x^{1.3701}$, where x is hydrogen concentration (ppm), with good correlation ($R^2 = 0.98$) (Figure 26b). The response time ($\leq$ 10s) decreased as the hydrogen concentration increased. In N_2 atmosphere, as the sensor resistance is controlled by the accumulation layer, the lower base resistances were observed (4 GΩ in N_2 and 3 TΩ in air). The response time of the sensor in oxygen free atmosphere was similar to that in dry air, while the recovery ($\geq$ 30 min) was slow. From Figure 26b, the resistance in H_2 500-5050 ppm started increasing after reaching the minimum value. This phenomenon has not clearly been explained yet, although has been observed in elsewhere [99,138-140]. The concentrations of adsorbed H_2 molecules are dependent on the oxide surface and the operating temperature [141]. Thus, the operating temperature needs to be optimized to obtain the maximum adsorption of H_2. However, when the sensor is operated at non-optimal temperature, the sensor may experience some imbalance of adsorption and desorption. When this adverse effect occurs, the desorption may be more dominant than adsorption process [142].

The Pd layer decorated on the oxide surface played a significant role in enhancing the hydrogen sensing properties. The Pd layer either adsorbs or dissociates hydrogen molecules, which are spilled over to the oxide layer for chemisorption. As seen in Figure 27, the response of the Pd decorated TiO_2 sensor was about two orders of magnitude higher than the pristine TiO_2.

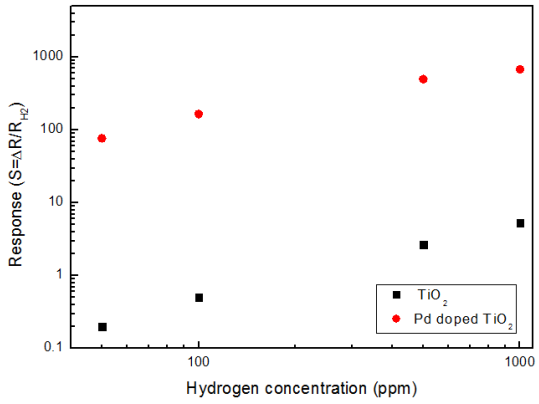

Figure 27: Comparison of responses between a pure and Pd doped TiO_2 sensor.

Figure 28a shows a resistance variation of the sensor in dry air at different relative humidities (dry air, 5, 10 and 20%) to 1000 ppm H_2. In general, water molecules adsorbed on the oxide surface decreases the sensor resistance and may have a negative effect on sensor performance due to disturbing the chemisorption of oxygen molecules. By switching the atmosphere from dry to humid air (5% RH), the sensor showed a fast decrease in sensor resistance. However, the general hydrogen sensing properties of the sensor were not significantly influenced in the measured RH as shown in Figure 28b.

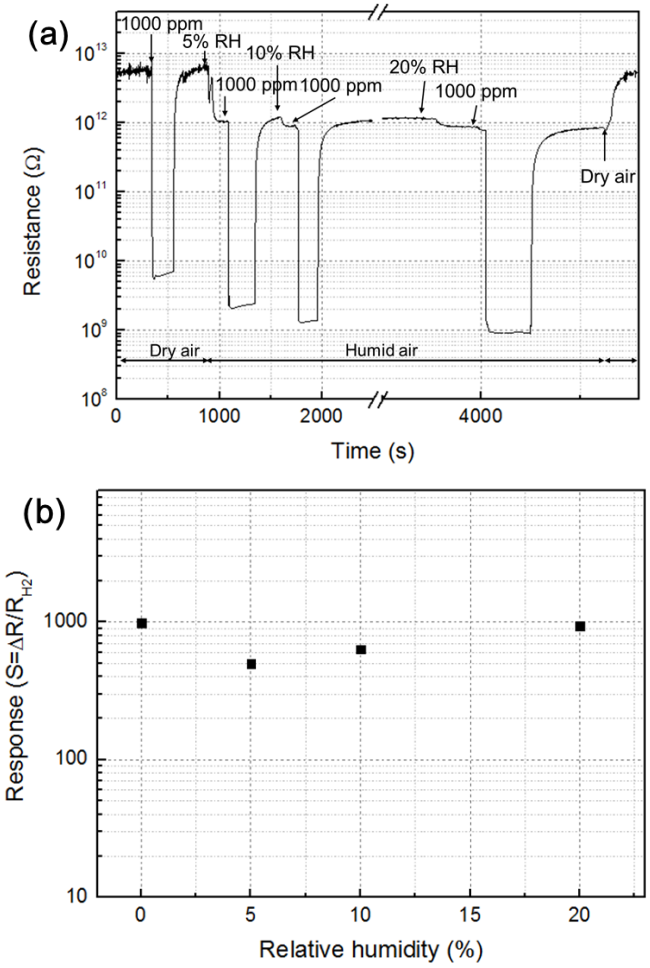

Figure 28: Hydrogen sensing properties of the Pd decorated TiO_2 sensor to 1000 ppm H_2 at 0 – 20% RH in synthetic air at 180°C: (a) the resistance variation; (b) the response to 1000 ppm H_2.

Table 9: Summary of gas sensors using various metal oxides in the literature.

Material	Structure	Synthesis Method	Catalyst	Detection limit (ppm)	Operating Temp (°C)	Ref.
SnO_2	Thin film	Magnetron sputtering	Pd	100	175	[143]
	Nanopore	Anodization		9	80	[144]
ZnO	Nanofiber	Electrospinning		0.1	350	[145]
	Nanofiber	Electrospinning	Graphene oxide	0.1	300	[146]
In_2O_3	Nanotower	Thermal evaporation		10	240	[147]
	Nanopowder	Hydrothermal process	Pt	500	RT	[148]
Fe_2O_3	Nanotubes	Thermal decomposition		10	RT	[149]
WO_3	Thin film	Sol–gel	Pt	100	200	[150]
VO_2	Nanobelts	Hydrothermal process		0.17	RT	[151]
Nb_2O_5	Nanopores	Anodization		600	50	[152]
NiO	Thin film	RF sputtering		50	350	[153]
TiO_2	Nanowire	Thermal evaporation	Pd	500	100	[39]
	Nanotube arrays on polymer film	ALD		100-1000	100	[40]
	Single nanotube	Anodization		1000	RT	[41]
	Thin film	Sol-gel	Graphene	5000	75	[154]
	Nanotubes on SiO_2/Si	Anodization	Pd	1-10000	140-180	Present work

In addition, a selectivity test was carried out with CO, CO_2, ethanol and acetone. The response of the sensor was negligible to those gases. The reason for this good selectivity is still not clear. The distinct properties of this sensor can be due to the crystalline structure (anatase), the low operating temperature and the Pd layer deposited on the oxide layer. The tubular TiO_2 layer formed on SiO_2/Si only consists of anatase. The anatase structure of TiO_2 is known to be more sensitive to H_2 than rutile due to higher electron mobilities [69]. Additionally, the great response only to hydrogen can be achieved by adding the Pd layer, which promotes high hydrogen adsorption.

H_2 sensors have been developed using various metal oxide materials as previously mentioned in section 2.5. For the last decade, studies in this field have attempted to improve gas sensing properties, such as sensitivity, operating temperature and response/recovery time. The comparison of the

recently developed H_2 sensors and the sensor in this study is summarized in Table 9. It shows that the detection limit of ZnO is less than 1 ppm of H_2 at 300°C. This high sensitivity makes the ZnO sensor possible to be used in various hydrogen industries as well as biomedical applications [155]. Some metal oxides, such as In_2O_3, Fe_2O_3, TiO_2, provide the advantage of low temperature use (≤ 100°C). Nevertheless, the response and recovery time of these sensors are mostly slow (≥ 100 s). The Pd-decorated TiO_2 sensor is capable of detecting a wide concentration range of hydrogen and has a fast response and recovery time at 180°C. However, the high resistance of the sensor in ambient air needs to be lowered in future work.

Chapter 6

Conclusions

The aim of this thesis was to develop a highly sensitive and reliable hydrogen sensor using TiO_2 nanostructures prepared by anodization. Through understanding the relation of the growth process and coloration properties of TiO_2 nanotubes, it was found that the morphological properties of the nanostructures can be identified by the coloration. Hydrogen sensors which consisted of nanotubes typically grown on metal foil showed incompatibility to microelectronic devices because of the underlying Ti foil.

In order to achieve more compatible gas sensor using an anodic TiO_2 layer, the anodization of the Ti layer was carried out on alternative substrates. A mesoporous TiO_2 layer was made on the Si wafer. In some cases porous silicon formed on the Si substrate during the anodization and the TiO_2 layer could dissolve under non-optimized anodization condition. The gas sensor using the mesoporous TiO_2 could detect hydrogen at low operating temperatures (50–140°C). However, in both sensors (on Ti foil and Si) the current can partially flow through the conductive base substrates, leading to low base resistance and unreliable response to hydrogen.

Finally, the use of an insulating substrate, SiO_2/Si, for the formation of TiO_2 layers enabled the sensor to have a reliable base resistance. Essentially, the patterned metal electrodes under the oxide layer were beneficial in producing mechanically robust and compatible sensors in microelectronic applications. Pd decoration significantly improved the response of the sensor in the presence of hydrogen. The sensor showed a wide detection range, fast response/recovery time, and good performance in humid atmosphere. It was also found that the experimental results and theoretical values of the conduction models are in a good agreement, which helps to understand the H_2 sensing behavior of metal oxide sensors. It is yet challenge to decrease the high resistance of the sensor at relatively low operating temperature (≤ 200°C) and to make the hydrogen detection of the sensor independent from humid atmosphere.

Reference List

[1] M. Lenzen, Current state of development of electricity-generating technologies: a literature review, Energies 3 (2010) 462-591.

[2] R. Ramachandran, R. Menon, An overview of industrial uses of hydrogen, Int. J. Hydrogen Energy 23 (1998) 593-598.

[3] W. J. Buttner, M. B. Post, R. Burgess, C. Rivkin, An overview of hydrogen safety sensors and requirements, Int. J. Hydrogen Energy 36 (2011) 2462-2470.

[4] T. Huebert, L. Boon-Brett, G. Black, U. Banach, Hydrogen sensors - A review, Sens. Actuators B 157 (2011) 329-352.

[5] V. Zwilling, M. Aucouturier, E. Darque-Ceretti, Anodic oxidation of titanium and TA6V alloy in chromic media. An electrochemical approach, Electrochim. Acta 45 (1999) 921-929.

[6] D. Gong, C. Grimes, O. Varghese, W. Hu, R. Singh, Z. Chen, E. Dickey, Titanium oxide nanotube arrays prepared by anodic oxidation, J. Mater. Res. 16 (2001) 3331-3334.

[7] A. Hulanicki, S. Glab, F. Ingman, Chemical Sensors Definitions and Classification, Pure Appl. Chem. 63 (1991) 1247-1250.

[8] W. H. Brattain, J. Bardeen, Surface properties of germanium, Bell Syst. Tech. J. 32 (1953) 1-41.

[9] Figaro Products Catalogue, Figaro Gas Sensors 1-Series 8-Series, Figaro Engineering Inc., European Office, Oststrasse 10, 40211 Düsseldorf, Germany.

[10] I. Simon, N. Bârsan, M. Bauer, U. Weimar, Micromachined metal oxide gas sensors: opportunities to improve sensor performance, Sens. Actuators B 73 (2001) 1-26.

[11] J. S. Suehle, R. E. Cavicchi, M. Gaitan, S. Semancik, Tin oxide gas sensor fabricated using CMOS micro-hotplates and insitu processing, IEEE Electron Device Lett. 14 (1993) 118-120.

[12] M. Graf, S. K. Muller, D. Barrettino, A. Hierlemann, Transistor heater for microhotplate-based metal-oxide microsensors, IEEE Electron Device Lett. 26 (2005) 295-297.

[13] W. Shin, K. Tajima, Y. Choi, N. Izu, I. Matsubara, N. Murayama, Planar catalytic combustor film for thermoelectric hydrogen sensor, Sens. Actuators B 108 (2005) 455-460.

[14] I. Simon, M. Arndt, Thermal and gas-sensing properties of a micromachined thermal conductivity sensor for the detection of hydrogen in automotive applications, Sens. Actuators A 97–98 (2002) 104-108.

[15] A. Kolmakov, M. Moskovits, Chemical sensing and catalysis by one-dimensional metal-oxide nanostructures, Annu. Rev. Mater. Sci. 34 (2004) 151-180.

[16] N. Wu, S. Wang, I. Rusakova, Inhibition of crystallite growth in the sol-gel synthesis of nanocrystalline metal oxides, Science 285 (1999) 1375-1377.

[17] H. Chiu, C. Yeh, Hydrothermal synthesis of SnO_2 nanoparticles and their gas-sensing of alcohol, J. Phys. Chem. C 111 (2007) 7256-7259.

[18] Y. Liu, E. Koep, M. Liu, Highly sensitive and fast-responding SnO_2 sensor fabricated by combustion chemical vapor deposition, Chem. Mat. 17 (2005) 3997-4000.

[19] B. Wang, L. F. Zhu, Y. H. Yang, N. S. Xu, G. W. Yang, Fabrication of a SnO_2 nanowire gas sensor and sensor performance for hydrogen, J. Phys. Chem. C 112 (2008) 6643-6647.

[20] L. L. Fields, J. P. Zheng, Y. Cheng, P. Xiong, Room-temperature low-power hydrogen sensor based on a single tin dioxide nanobelt, Appl. Phys. Lett. 88 (2006) 263102.

[21] J. Huang, N. Matsunaga, K. Shimanoe, N. Yamazoe, T. Kunitake, Nanotubular SnO_2 templated by cellulose fibers: Synthesis and gas sensing, Chem. Mater. 17 (2005) 3513-3518.

[22] S. H. Jeong, S. Kim, J. Cha, M. S. Son, S. H. Park, H. Kim, M. H. Cho, M. Whangbo, K. Yoo, S. Kim, Hydrogen Sensing under Ambient Conditions Using SnO_2 Nanowires: Synergetic Effect of Pd/Sn Codeposition, Nano Lett. 13 (2013) 5938-5943.

[23] Z. Wang, Z. Li, T. Jiang, X. Xu, C. Wang, Ultrasensitive hydrogen sensor based on Pd-0-Loaded SnO_2 electrospun nanofibers at room temperature, ACS Appl. Mater. Interfaces 5 (2013) 2013-2021.

[24] S. Shukla, P. Zhang, H.J. Cho, S. Seal, L. Ludwig, Room temperature hydrogen response kinetics of nano-micro-integrated doped tin oxide sensor, Sens. Actuators B 120 (2007) 573-583.

[25] G. De, R. Koehn, G. Xomeritakis, C.J. Brinker, Nanocrystalline mesoporous palladium activated tin oxide thin films as room-temperature hydrogen gas sensors, Chem. Commun. (2007) 1840-1842.

[26] Z. L. Wang, Nanostructures of zinc oxide, Mater.Today 7 (2004) 26-33.

[27] N. H. Al-Hardan, M. J. Abdullah, A. A. Aziz, Sensing mechanism of hydrogen gas sensor based on RF-sputtered ZnO thin films, Int. J. Hydrogen Energy 35 (2010) 4428-4434.

[28] H. S. Al-Salman, M. J. Abdullah, N. Al-Hardan, ZnO thin film nanostructures for hydrogen gas sensing applications, Ceram. Int. 39 (2013) S447-S450.

[29] O. Lupan, G. Chai, L. Chow, Novel hydrogen gas sensor based on single ZnO nanorod, Microelectron. Eng. 85 (2008) 2220-2225.

[30] O. Lupan, V. V. Ursaki, G. Chai, L. Chow, G. A. Emelchenko, I. M. Tiginyanu, A. N. Gruzintsev, A. N. Redkin, Selective hydrogen gas nanosensor using individual ZnO nanowire with fast response at room temperature, Sens. Actuators B 144 (2010) 56-66.

[31] T. Rashid, D. Phan, G. Chung, A flexible hydrogen sensor based on Pd nanoparticles decorated ZnO nanorods grown on polyimide tape, Sens. Actuators B 185 (2013) 777-784.

[32] Y. T. Lim, J. Y. Son, J. S. Rhee, Vertical ZnO nanorod array as an effective hydrogen gas sensor, Ceram. Int. 39 (2013) 887-890.

[33] L. C. Tien, P. W. Sadik, D. P. Norton, L. F. Voss, S. J. Pearton, H. T. Wang, B. S. Kang, F. Ren, J. Jun, J. Lin, Hydrogen sensing at room temperature with Pt-coated ZnO thin films and nanorods, Appl. Phys. Lett. 87 (2005) 222106.

[34] Y. Liu, C. Gao, X. Pan, X. An, Y. Xie, M. Zhou, J. Song, H. Zhang, Z. Liu, Q. Zhao, Y. Zhang, E. Xie, Synthesis and H_2 sensing properties of aligned ZnO nanotubes, Appl. Surf. Sci. 257 (2011) 2264-2268.

[35] M. Lin, C. Chen, W. Wang, C. Lin, S. Chang, Fabrication of the selective-growth ZnO nanorods with a hole-array pattern on a p-type GaN/Mg layer through a chemical bath deposition process, Thin Solid Films 518 (2010) 7398-7402.

[36] C. Zhang, A. Boudiba, C. Navio, C. Bittencourt, M. Olivier, R. Snyders, M. Debliquy, Highly sensitive hydrogen sensors based on co-

sputtered platinum-activated tungsten oxide films, Int. J. Hydrogen Energy 36 (2011) 1107-1114.

[37] J. Zhou, L. Gong, S. Z. Deng, J. Chen, J. C. She, N. S. Xu, R. S. Yang, Z. L. Wang, Growth and field-emission property of tungsten oxide nanotip arrays, Appl. Phys. Lett. 87 (2005) 223108.

[38] M. Ahsan, M. Z. Ahmad, T. Tesfamichael, J. Bell, W. Wlodarski, N. Motta, Low temperature response of nanostructured tungsten oxide thin films toward hydrogen and ethanol, Sens. Actuators B 173 (2012) 789-796.

[39] S. An, S. Park, H. Ko, C. Lee, Fabrication of WO_3 nanotube sensors and their gas sensing properties, Ceram.Int. 40 (2014) 1423-1429.

[40] M. Yang, N. K. Shrestha, P. Schmuki, Thick porous tungsten trioxide films by anodization of tungsten in fluoride containing phosphoric acid electrolyte, Electrochem. Commun. 11 (2009) 1908-1911.

[41] N. Mukherjee, M. Paulose, O.K. Varghese, G. K. Mor, C. A. Grimes, Fabrication of nanoporous tungsten oxide by galvanostatic anodization, J. Mater. Res. 18 (2003) 2296-2299.

[42] R. Hahn, J.M. Macak, P. Schmuki, Rapid anodic growth of TiO_2 and WO_3 nanotubes in fluoride free electrolytes, Electrochem. Commun. 9 (2007) 947-952.

[43] J. Kukkola, J. Maklin, N. Halonen, T. Kyllonen, G. Toth, M. Szabo, A. Shchukarev, J. Mikkola, H. Jantunen, K. Kordas, Gas sensors based on anodic tungsten oxide, Sens. Actuators B 153 (2011) 293-300.

[44] W.P. Jakubik, Hydrogen gas-sensing with bilayer structures of WO_3 and Pd in SAW and electric systems, Thin Solid Films 517 (2009) 6188-6191.

[45] J. Choi, J. Kim, Highly sensitive hydrogen sensor based on suspended, functionalized single tungsten nanowire bridge, Sens. Actuators B 136 (2009) 92-98.

[46] J. Kukkola, M. Mohl, A. Leino, J. Maklin, N. Halonen, A. Shchukarev, Z. Konya, H. Jantunen, K. Kordas, Room temperature hydrogen sensors based on metal decorated WO_3 nanowires, Sens. Actuators B 186 (2013) 90-95.

[47] L. Trengove, William Gregor discoverer of titanium, Ann. Sci. 29 (1972) 361-395.

[48] A. Russel, The Rev. William Gregor (1761-1817), discoverer of titanium. Mineral. Mag. (1955) 617-624.

[49] A. Fujishima, K. Honda, Electrochemical Photolysis of Water at a Semiconductor Electrode, Nature 238 (1972) 37-38.

[50] S. Frank, A. Bard, Heterogeneous photocatalytic oxidation of cyanide and sulfite in aqueous-solutions at semiconductor powders, J. Phys. Chem. 81 (1977) 1484-1488.

[51] S. N. Frank, A. J. Bard, Heterogeneous photocatalytic oxidation of cyanide Ion in aqueous-solutions at TiO_2 powder, J. Am. Chem. Soc. 99 (1977) 303-304.

[52] A. Wisitsoraat, A. Tuantranont, E. Comini, G. Sberveglieri, W. Wlodarski, Characterization of n-type and p-type semiconductor gas sensors based on NiO_x doped TiO_2 thin films, Thin Solid Films 517 (2009) 2775-2780.

[53] D. P. Macwan, P. N. Dave, S. Chaturvedi, A review on nano-TiO_2 sol-gel type syntheses and its applications, J. Mater. Sci. 46 (2011) 3669-3686.

[54] T. Kasuga, M. Hiramatsu, A. Hoson, T. Sekino, K. Niihara, Formation of titanium oxide nanotube, Langmuir 14 (1998) 3160-3163.

[55] Z. Miao, D. Xu, J. Ouyang, G. Guo, X. Zhao, Y. Tang, Electrochemically induced sol-gel preparation of single-crystalline TiO_2 nanowires, Nano Lett. 2 (2002) 717-720.

[56] O. K. Varghese, D. W. Gong, M. Paulose, C. A. Grimes, E. C. Dickey, Crystallization and high-temperature structural stability of titanium oxide nanotube arrays, J. Mater. Res. 18 (2003) 156-165.

[57] H. Cheng, J. Ma, Z. Zhao, L. Qi, Hydrothermal preparation of uniform nanosize rutile and anatase particles, Chem. Mat. 7 (1995) 663-671.

[58] Y. Hu, H.-. Tsai, C.-. Huang, Phase transformation of precipitated TiO_2 nanoparticles, Mater. Sci. Eng. A 344 (2003) 209-214.

[59] V. C. Fuertes, C. F. A. Negre, M. Belen Oviedo, F. P. Bonafe, F. Y. Oliva, C. G. Sanchez, A theoretical study of the optical properties of nanostructured TiO_2, J. Phys.: Condens. Matter 25 (2013) 115304.

[60] P. Hoyer, Formation of a titanium dioxide nanotube array, Langmuir 12 (1996) 1411-1413.

[61] P. Hu, G. Du, W. Zhou, J. Cui, J. Lin, H. Liu, D. Liu, J. Wang, S. Chen, Enhancement of ethanol vapor sensing of TiO_2 nanobelts by surface engineering, ACS Appl. Mater. Interfaces 2 (2010) 3263-3269.

[62] M. Wu, A. Sapi, A. Avila, M. Szabo, J. Hiltunen, M. Huuhtanen, G. Toth, A. Kukovecz, Z. Konya, R. Keiski, W. Su, H. Jantunen, K. Kordas, Enhanced photocatalytic activity of TiO_2 nanofibers and their flexible composite films: decomposition of organic dyes and efficient H_2 generation from ethanol-water mixtures, Nano Res. 4 (2011) 360-369.

[63] K. Fujihara, A. Kumar, R. Jose, S. Ramakrishna, S. Uchida, Spray deposition of electrospun TiO_2 nanorods for dye-sensitized solar cell, Nanotechnology 18 (2007) 365709.

[64] Z. Y. Yuan, B. L. Su, Titanium oxide nanotubes, nanofibers and nanowires, Colloids Surf. A 241 (2004) 173-183.

[65] H. Ou, S. Lo, Review of titania nanotubes synthesized via the hydrothermal treatment: Fabrication, modification, and application, Sep. Purif. Technol. 58 (2007) 179-191.

[66] G. K. Mor, O. K. Varghese, M. Paulose, K. Shankar, C. A. Grimes, A review on highly ordered, vertically oriented TiO_2 nanotube arrays: Fabrication, material properties, and solar energy applications, Sol. Energy Mater. Sol. Cells 90 (2006) 2011-2075.

[67] U. Kirner, K. D. Schierbaum, W. Göpel, B. Leibold, N. Nicoloso, W. Weppner, D. Fischer, W.F. Chu, Low and high temperature TiO_2 oxygen sensors, Sens. Actuators B 1 (1990) 103-107.

[68] A. Ruiz, G. Sakai, A. Cornet, K. Shimanoe, J. Morante, N. Yamazoe, Cr-doped TiO_2 gas sensor for exhaust NO_2 monitoring, Sens. Actuators B 93 (2003) 509-518.

[69] H. Tang, K. Prasad, R. Sanjines, F. Levy, TiO_2 anatase thin-films as gas sensors, Sens. Actuators B 26 (1995) 71-75.

[70] L. D. Birkefeld, A. M. Azad, S. A. Akbar, Carbon-monoxide and hydrogen detection by anatase modification of titanium-dioxide, J. Am. Ceram. Soc. 75 (1992) 2964-2968.

[71] D. Manno, G. Micocci, R. Rella, A. Serra, A. Taurino, A. Tepore, Titanium oxide thin films for NH_3 monitoring: Structural and physical characterizations, J. Appl. Phys. 82 (1997) 54-59.

[72] G. N. Chaudhari, D. R. Bambole, A. B. Bodade, P. R. Padole, Characterization of nanosized TiO_2 based H_2S gas sensor, J. Mater. Sci. 41 (2006) 4860-4864.

[73] A.A. Haidry, J. Puskelova, T. Plecenik, P. Durina, J. Gregus, M. Truchly, T. Roch, M. Zahoran, M. Vargova, P. Kus, A. Plecenik, G. Plesch, Characterization and hydrogen gas sensing properties of TiO_2 thin films prepared by sol-gel method, Appl. Surf. Sci. 259 (2012) 270-275.

[74] Y. Jun, H. Kim, J. Lee, S. Hong, High H_2 sensing behavior of TiO_2 films formed by thermal oxidation, Sens. Actuators B 107 (2005) 264-270.

[75] G. Munuera, A.R. Gonzalezelipe, A. Munoz, A. Fernandez, J. Soria, J. Conesa, J. Sanz, Mechanism of hydrogen gas-sensing at low-temperatures using Rh/TiO_2 systems, Sens. Actuators B 18 (1989) 337-348.

[76] G. Yamamoto, T. Yamashita, K. Matsuo, T. Hyodo, Y. Shimizu, Effects of polytetrafluoroethylene or polyimide coating on H_2 sensing properties of anodized TiO_2 films equipped with Pd–Pt electrodes, Sens. Actuators B 183 (2013) 253-264.

[77] M. Paulose, O. K. Varghese, G. K. Mor, C. A. Grimes, K. G. Ong, Unprecedented ultra-high hydrogen gas sensitivity in undoped titania nanotubes, Nanotechnology 17 (2006) 398-402.

[78] T. Iwanaga, T. Hyodo, Y. Shimizu, M. Egashira, H_2 sensing properties and mechanism of anodically oxidized TiO_2 film contacted with Pd electrode, Sens. Actuators B 93 (2003) 519-525.

[79] S. Joo, I. Muto, N. Hara, Hydrogen gas sensor using Pt- and Pd-added anodic TiO_2 nanotube films, J. Electrochem. Soc. 157 (2010) J221-J226.

[80] D. Meng, T. Yamazaki, T. Kikuta, Preparation and gas sensing properties of undoped and Pd-doped TiO_2 nanowires, Sens. Actuators B 190 (2014) 838-843.

[81] G. Devi, T. Hyodo, Y. Shimizu, M. Egashira, Synthesis of mesoporous TiO_2-based powders and their gas-sensing properties, Sens. Actuators B 87 (2002) 122-129.

[82] S. Hwang, H. Kwon, S. Chhajed, J.W. Byon, J.M. Baik, J. Im, S.H. Oh, H.W. Jang, S.J. Yoon, J.K. Kim, A near single crystalline TiO_2 nanohelix array: enhanced gas sensing performance and its application as a

monolithically integrated electronic nose, Analyst 138 (2013) 443-450.

[83] M. Epifani, E. Comini, R. Díaz, C. Force, P. Siciliano, G. Faglia, TiO_2 colloidal nanocrystals surface modification by V_2O_5 species: Investigation by Ti MAS-NMR and H_2, CO and NO_2 sensing properties, Appl. Surf. Sci. 351 (2015) 1169-1173.

[84] O. K. Varghese, D. W. Gong, M. Paulose, K. G. Ong, E. C. Dickey, C. A. Grimes, Extreme changes in the electrical resistance of titania nanotubes with hydrogen exposure, Adv. Mater. 15 (2003) 624-627.

[85] D. H. Kim, Y. Shim, H. G. Moon, H. J. Chang, D. Su, S. Y. Kim, J. Kim, B. K. Ju, S. Yoon, H. W. Jang, Highly ordered TiO_2 nanotubes on patterned substrates: Synthesis-in-place for ultrasensitive chemiresistors, J. Phys. Chem. C 117 (2013) 17824-17831.

[86] G. K. Mor, O. K. Varghese, M. Paulose, C. A. Grimes, Transparent highly ordered TiO_2 nanotube arrays via anodization of titanium thin films, Adv. Funct. Mater. 15 (2005) 1291-1296.

[87] G. K. Mor, O. K. Varghese, M. Paulose, K. G. Ong, C. A. Grimes, Fabrication of hydrogen sensors with transparent titanium oxide nanotube-array thin films as sensing elements, Thin Solid Films 496 (2006) 42-48.

[88] Y. Kimura, S. Kimura, R. Kojima, M. Bitoh, M. Abe, M. Niwano, Micro-scaled hydrogen gas sensors with patterned anodic titanium oxide nanotube film, Sens. Actuators B 177 (2013) 1156-1160.

[89] N. Yamazoe, New approaches for improving semiconductor gas sensors, Sens. Actuators B 5 (1991) 7-19.

[90] N. Barsan, M. Schweizer-Berberich, W. Gopel, Fundamental and practical aspects in the design of nanoscaled SnO_2 gas sensors: a status report, Fresenius J. Anal. Chem. 365 (1999) 287-304.

[91] S. Samson, C. Fonstad, Defect structure and electronic donor levels in stannic oxide crystals, J. Appl. Phys. 44 (1973) 4618-4621.

[92] Z. M. Jarzebski, J. P. Marton, Physical-Properties of SnO_2 Materials .1. Preparation and defect structure, J. Electrochem. Soc. 123 (1976) C199-C205.

[93] W. Gopel, K. Schierbaum, SnO_2 sensors - current status and future-prospects, Sens. Actuator B 26 (1995) 1-12.

[94] M. E. Franke, T. J. Koplin, U. Simon, Metal and metal oxide nanoparticles in chemiresistors: Does the nanoscale matter? Small 2 (2006) 36-50.

[95] N. Barsan, M. Huebner, U. Weimar, Conduction mechanisms in SnO_2 based polycrystalline thick film gas sensors exposed to CO and H_2 in different oxygen backgrounds, Sens. Actuator B 157 (2011) 510-517.

[96] N. Barsan, U. Weimar, Conduction model of metal oxide gas sensors, J. Electroceram. 7 (2001) 143-167.

[97] N. Yamazoe, K. Shimanoe, Receptor function and response of semiconductor gas sensor, J. Sens. (2009) Article ID 875704 21.

[98] N. Yamamoto, S. Tonomura, T. Matsuoka, H. Tsubomura, A study on a palladium-titanium oxide Schottky diode as a detector for gaseous components, Surf. Sci. 92 (1980) 400-406.

[99] Y. Shimizu, T. Hyodo, M. Egashira, H_2 sensing performance of anodically oxidized TiO_2 thin films equipped with Pd electrode, Sens. Actuators B 121 (2007) 219-230.

[100] A. Kolmakov, D. O. Klenov, Y. Lilach, S. Stemmer, M. Moskovits, Enhanced gas sensing by individual SnO_2 nanowires and nanobelts functionalized with Pd catalyst particles, Nano Letters 5 (2005) 667-673.

[101] U. Roland, T. Braunschweig, F. Roessner, On the nature of spilt-over hydrogen, J. Mol. Catal. A: Chem. 127 (1997) 61-84.

[102] J.L. Delplancke, M. Degrez, A. Fontana, R. Winand, Self-color anodizing of titanium, Surf. Technol. 16 (1982) 153-162.

[103] Y. Sul, C. Johansson, Y. Jeong, T. Albrektsson, The electrochemical oxide growth behaviour on titanium in acid and alkaline electrolytes, Med. Eng. Phys. 23 (2001) 329-346.

[104] L. Majewski, R. Schroeder, M. Grell, Low-voltage, high-performance organic field-effect transistors with an ultra-thin TiO_2 layer as gate insulator, Adv. Funct. Mater. 15 (2005) 1017-1022.

[105] S. P. Albu, A. Ghicov, J. M. Macak, P. Schmuki, 250 μm long anodic TiO_2 nanotubes with hexagonal self-ordering, Phys. Status Solidi RRL 1 (2007) R65-R67.

[106] M. Paulose, H. E. Prakasam, O. K. Varghese, L. Peng, K. C. Popat, G. K. Mor, T. A. Desai, C. A. Grimes, TiO_2 nanotube arrays of 1000 μm

length by anodization of titanium foil: Phenol red diffusion, J. Phys. Chem. C 111 (2007) 14992-14997.

[107] G. K. Mor, K. Shankar, M. Paulose, O. K. Varghese, C. A. Grimes, Enhanced photocleavage of water using titania nanotube arrays, Nano Letters 5 (2005) 191-195.

[108] Q. Y. Cai, M. Paulose, O. K. Varghese, C. A. Grimes, The effect of electrolyte composition on the fabrication of self-organized titanium oxide nanotube arrays by anodic oxidation, J. Mater. Res. 20 (2005) 230-236.

[109] J.M. Macak, H. Tsuchiya, P. Schmuki, High-aspect-ratio TiO_2 nanotubes by anodization of titanium, Angew. Chem. Int. Ed. 44 (2005) 2100-2102.

[110] M. Paulose, K. Shankar, S. Yoriya, H. E. Prakasam, O. K. Varghese, G. K. Mor, T. A. Latempa, A. Fitzgerald, C. A. Grimes, Anodic growth of highly ordered TiO_2 nanotube arrays to 134 μm in length, J. Phys. Chem. B 110 (2006) 16179-16184.

[111] K. Shankar, G. K. Mor, H. E. Prakasam, S. Yoriya, M. Paulose, O. K. Varghese, C. A. Grimes, Highly-ordered TiO_2 nanotube arrays up to 220 μm in length: use in water photoelectrolysis and dye-sensitized solar cells, Nanotechnology 18 (2007) 065707.

[112] C. Chen, K. Chen, J. He, Transparent conducting oxide glass grown with TiO_2-nanotube array for dye-sensitized solar cell, Curr. Appl Phys. 10 (2010) S176-S179.

[113] A. Z. Sadek, H. Zheng, K. Latham, W. Wlodarski, K. Kalantar-zadeh, Anodization of Ti Thin Film Deposited on ITO, Langmuir 25 (2009) 509-514.

[114] J.M. Macak, H. Tsuchiya, S. Berger, S. Bauer, S. Fujimoto, P. Schmuki, On wafer TiO_2 nanotube-layer formation by anodization of Ti-films on Si, Chem. Phys. Lett. 428 (2006) 421-425.

[115] J. Tupala, M. Kemell, E. Harkonen, M. Ritala, M. Leskela, Preparation of regularly structured nanotubular TiO_2 thin films on ITO and their modification with thin ALD-grown layers, Nanotechnology 23 (2012) 125707.

[116] N. Jang, M. S. Kim, S. Kim, S. Lee, J. Kim, Direct growth of titania nanotubes on plastic substrates and their application to flexible gas sensors, Sensors and Actuators B 199 (2014) 361-368.

[117] W. Lee, R. Ji, U. Goesele, K. Nielsch, Fast fabrication of long-range ordered porous alumina membranes by hard anodization, Nat. Mater. 5 (2006) 741-747.

[118] S. Chu, K. Wada, S. Inoue, M. Isogai, A. Yasumori, Fabrication of ideally ordered nanoporous alumina films and integrated alumina nanotubule arrays by high-field anodization, Adv. Mater. 17 (2005) 2115-2119.

[119] J. E. Houser, K. R. Hebert, The role of viscous flow of oxide in the growth of self-ordered porous anodic alumina films, Nat. Mater. 8 (2009) 415-420.

[120] J. M. Macak, H. Tsuchiya, A. Ghicov, K. Yasuda, R. Hahn, S. Bauer, P. Schmuki, TiO_2 nanotubes: Self-organized electrochemical formation, properties and applications, Curr. Opin. Solid State Mater. Sci. 11 (2007) 3-18.

[121] P. Roy, S. Berger, P. Schmuki, TiO_2 Nanotubes: Synthesis and Applications, Angew. Chem. Int. Ed. 50 (2011) 2904-2939.

[122] R. Beranek, H. Hildebrand, P. Schmuki, Self-organized porous titanium oxide prepared in H_2SO_4/HF electrolytes, Electrochem. Solid-State Lett. 6 (2003) B12-B14.

[123] M. V. Diamanti, B. Del Curto, M. Pedeferri, Interference colors of thin oxide layers on titanium, Color Res. Appl. 33 (2008) 221-228.

[124] T. Shih, P. Wei, Y. Huang, Optical properties of anodic aluminum oxide films on Al1050 alloys, Surf. Coat. Technol. 202 (2008) 3298-3305.

[125] X. F. Yu, Y. X. Li, W. Y. Ge, Q. B. Yang, N. F. Zhu, K. Kalantar-Zadeh, Formation of nanoporous titanium oxide films on silicon substrates using an anodization process, Nanotechnology 17 (2006) 808-814.

[126] X. Yu, Y. Li, W. Wlodarski, S. Kandasamy, K. Kalantar-zadeh, Fabrication of nanostructured TiO_2 by anodization: A comparison between electrolytes and substrates, Sens. Actuators B 130 (2008) 25-31.

[127] M. Rauscher, H. Spohn, Porous silicon formation and electropolishing, Phys. Rev. E 64 (2001) art. no.031604 (1-10).

[128] S. Berger, A. Ghicov, Y.-C. Nah, P. Schmuki, Transparent TiO_2 nanotube electrodes via thin layer anodization: Fabrication and use in electrochromic devices, Langmuir 25 (2009) 4841-4844.

[129] S. Yoriya, G. K. Mor, S. Sharma, C. A. Grimes, Synthesis of ordered arrays of discrete, partially crystalline titania nanotubes by Ti anodization using diethylene glycol electrolytes, J. Mater. Chem. 18 (2008) 3332-3336.

[130] Z. Zhang, Y. Yu, P. Wang, Hierarchical top-porous/bottom-tubular TiO_2 nanostructures decorated with Pd nanoparticles for efficient photoelectrocatalytic decomposition of synergistic pollutants, ACS Appl. Mater. Interfaces. 4 (2012) 990-996.

[131] J. Yoon, T. Sasaki, N. Koshizaki, Dispersion of nanosized noble metals in TiO_2 matrix and their photoelectrode properties, Thin Solid Films 483 (2005) 276-282.

[132] H. Kobayashi, K. Kishimoto, Y. Nakato, Reactions of hydrogen at the interface of palladium-titanium dioxide Schottky diodes as hydrogen sensors, studied by workfunction and electrical characteristic measurements, Surf. Sci. 306 (1994) 393-405.

[133] O. K. Varghese, D. W. Gong, M. Paulose, K. G. Ong, C. A. Grimes, Hydrogen sensing using titania nanotubes, Sens. Actuators B 93 (2003) 338-344.

[134] S. K. Asl, B. Alavi, S. Ahmadi, The effect of highly ordered titania nanotube structures on hydrogen gas detection, Surf. Interface Anal. 44 (2012) 1051-1053.

[135] H. Miyazaki, T. Hyodo, Y. Shimizu, M. Egashira, Hydrogen-sensing properties of anodically oxidized TiO_2 film sensors-ffects of preparation and pretreatment conditions, Sens. Actuators B 108 (2005) 467-472.

[136] J. Moon, M. Kemell, J. Kukkola, R. Punkkinen, H. Hedman, A. Suominen, E. Mäkilä, M. Tenho, A. Tuominen, H. Kim, Gas sensor using anodic TiO_2 thin film for monitoring hydrogen, Procedia Eng. 47 (2012) 791-794.

[137] J. Moon, H. Hedman, M. Kemell, A. Suominen, E. Makila, H. Kim, A. Tuominen, R. Punkkinen, A study of monitoring hydrogen using mesoporous TiO_2 synthesized by anodization, Sens. Actuators B 189 (2013) 246-250.

[138] Y. Shimizu, A. Jono, T. Hyodo, M. Egashira, Preparation of large mesoporous SnO_2 powder for gas sensor application, Sens. Actuators B 108 (2005) 56-61.

[139] Q. Kuang, C. Lao, Z.L. Wang, Z. Xie, L. Zheng, High-sensitivity humidity sensor based on a single SnO_2 nanowire, J. Am. Chem. Soc. 129 (2007) 6070- 6071.

[140] Y. Shen, T. Yamazaki, Z. Liu, D. Meng, T. Kikuta, Hydrogen sensors made of undoped and Pt-doped SnO_2 nanowires, J.Alloys Compounds 488 (2009) L21-L25.

[141] J. Mitsei, How can sensitive and selective semiconductor gas sensors be made, Sens. Actuators B 23 (1995) 173-176.

[142] S. K. Hazra, S. Basu, High sensitivity and fast response hydrogen sensors based on electrochemically etched porous titania thin films, Sens. Actuators B 115 (2006) 403-411.

[143] L. Yang, C. Yin, Z. Zhang, B. Zhu, A study of hydrogen sensing properties and microstructure for highly dispersed Pd SnO_2 thin films with high response magnitude, Appl. Surf. Sci. 311 (2014) 74-82.

[144] A. Palacios-Padros, M. Altomare, A. Tighineanu, R. Kirchgeorg, N. K. Shrestha, I. Diez-Perez, F. Caballero-Briones, F. Sanz, P. Schmuki, Growth of ordered anodic SnO_2 nanochannel layers and their use for H_2 gas sensing, J. Mater. Chem.A 2 (2014) 915-920.

[145] A. Katoch, S. Choi, H. W. Kim, S. S. Kim, Highly sensitive and selective H_2 sensing by ZnO nanofibers and the underlying sensing mechanism, J. Hazard. Mater. 286 (2015) 229-235.

[146] Z. U. Abideen, H. W. Kim, S. S. Kim, An ultra-sensitive hydrogen gas sensor using reduced graphene oxide-loaded ZnO nanofibers, Chem. Commun. 51 (2015) 15418-15421.

[147] Z. Q. Zheng, L. F. Zhu, B. Wang, In_2O_3 nanotower hydrogen gas Sensors based on both schottky junction and thermoelectronic emission, Nanoscale Res. Lett. 10 (2015) 293.

[148] Y. Wang, B. Liu, D. Cai, H. Li, Y. Liu, D. Wang, L. Wang, Q. Li, T. Wang, Room-temperature hydrogen sensor based on grain-boundary controlled Pt decorated In_2O_3 nanocubes, Sens. Actuators B 201 (2014) 351-359.

[149] J. Chen, L.N. Xu, W. Y. Li, X. L. Gou, α-Fe_2O_3 nanotubes in gas sensor and lithium-ion battery applications, Adv Mater 17 (2005) 582-586.

[150] Y. Yamaguchi, S. Imamura, S. Ito, K. Nishio, K. Fujimoto, Influence of oxygen gas concentration on hydrogen sensing of Pt/WO_3 thin film prepared by sol–gel process, Sens. Actuators B 216 (2015) 394-401.

[151] A. Simo, B. Mwakikunga, B. T. Sone, B. Julies, R. Madjoe, M. Maaza, VO_2 nanostructures based chemiresistors for low power energy consumption hydrogen sensing, Int. J. Hydrogen Energy 39 (2014) 8147-8157.

[152] R. A. Rani, A. S. Zoolfakar, J. Z. Ou, M. R. Field, M. Austin, K. Kalantar-zadeh, Nanoporous Nb_2O_5 hydrogen gas sensor, Sens. Actuators B 176 (2013) 149-156.

[153] P. Chou, H. Chen, I. Liu, C. Chen, J. Liou, K. Hsu, W. Liu, Hydrogen sensing performance of a nickel oxide (NiO) thin film-based device, Int. J. Hydrogen Energy 40 (2015) 729-734.

[154] D. Dutta, S. K. Hazra, J. Das, C. K. Sarkar, S. Basu, Studies on p-TiO_2/n-graphene heterojunction for hydrogen detection, Sens. Actuators B 212 (2015) 84-92.

[155] C. A. Grimes, K. G. Ong, O. K. Varghese, X. P. Yang, G. Mor, M. Paulose, E. C. Dickey, C. M. Ruan, M. V. Pishko, J. W. Kendig, A. J. Mason, A sentinel sensor network for hydrogen sensing, Sensors 3 (2003) 69-82.

Publication reprints

Publication I

The correlation between the interference colour and growth procedure of anodic titanium dioxide nanotube arrays, 2014, Coloration Technology, 130, 1, 1-7.

Jongyun Moon, Marianna Kemell, Byungki Park, Arho Suominen, Ermei Mäkilä, Risto Punkkinen, Hannu‐Pekka Hedman, Hong Kim, Lippo V Lassila, Aulis Tuominen

doi: 10.1111/cote.12067

The correlation between the interference colour and growth procedure of anodic titanium dioxide nanotube arrays

Jongyun Moon,[a,*] Marianna Kemell,[b] Byungki Park,[c] Arho Suominen,[a] Ermei Mäkilä,[d] Risto Punkkinen,[a] Hannu-Pekka Hedman,[a] Hong Kim,[e] Lippo V Lassila[f] and Aulis Tuominen[a]

[a]*Department of Information Technology, University of Turku, FI-20014, Turku, Finland Email: jong.moon@utu.fi*

[b]*Department of Chemistry, University of Helsinki, FI-00014, Helsinki, Finland*

[c]*Industrial and Academic Collaboration Foundation, Hoseo University, 336-795, Asan, Korea*

[d]*Department of Physics, University of Turku, FI-20014, Turku, Finland*

[e]*Department of Safety Engineering, Hoseo University, 336-795, Asan, Korea*

[f]*Department of Biomaterials Science and Turku Clinical Biomaterials Centre, University of Turku, FI-20520, Turku, Finland*

Received: 2 April 2012; Accepted: 30 April 2013

Titanium dioxide nanotube arrays were anodised from titanium foils in an aqueous electrolyte solution of hydrofluoric acid. The formed oxide showed visually different colours owing to light interference in the titanium dioxide layer. The behaviour of interference colour in anodic titanium dioxide film was investigated by varying anodisation parameters such as the applied voltage and the anodisation time. The morphologies and the crystalline phases of anodised samples were studied on a field emission scanning electron microscope and X-ray diffractometer. The correlation between the interference colour and growth procedure of anodic titanium dioxide nanotube arrays was studied. The anodic films prepared under different conditions consisted of a compact oxide film with a nanoporous/tubular structure upon/beneath it. The crystalline phase of the anodic oxide layer was amorphous. The optical properties of the oxide film were investigated on a spectrophotometer. Optical interference could be detected in compact oxide layers when the thickness of the titanium dioxide was as small as 70 nm. In general, the interferences of the nanoporous/tubular structures were lower than those for compact structures. The empirical colour properties were estimated by the *L*a*b** system. The relationships between the interference colour of anodic titanium dioxide film and its thickness and morphology are discussed.

Editor-in-Chief's recommendation: *Nature does not need colorants to create vivid coloration in living things. Rather than relying solely on absorption of light by pigmentation, She is able to produce striking colours by manipulating the physical structure of matter. Tiny surface features interact with light, generating 'structural colour' through interference effects. Feathers, butterfly wings, and berries are a few examples where appearance depends on this kind of coloration. Just as technologists draw inspiration from Nature when developing lighter, stronger, stickier, and more resilient materials, structural colour attracts great interest from researchers because it offers a means of crafting robust and novel effects that might not otherwise be feasible with conventional colorants. In this Feature article, the authors present a fascinating example of structural coloration. They demonstrate how the colour of titanium foil can be tuned through the controlled growth of nanoscale features on its surface. Alterations to the dimensions of these surface structures generate large changes in hue. It is all the more remarkable that these structures are made up of titanium dioxide, a material that is the basis for what is by far the most industrially important group of white pigments.*

Introduction

Titanium dioxide (TiO_2) is an oxide semiconductor with a large electronic band gap of over 3.0 eV, absorbing light primarily in the UV region. TiO_2 nanostructures have a wide range of functional applications, for example as photocatalysts, gas sensors, and dye-sensitised solar cells [1–3]. TiO_2 can be fabricated into different nanostructures by various methods such as anodisation, electrochemical lithography, the photoelectrochemical process, the sol–gel method, hydrothermal synthesis, and DC magnetron sputtering [4–11].

Anodic TiO_2 nanotube arrays have attracted much attention owing to their various advantages, such as a relatively simple fabrication process and some physical/chemical properties that provide remarkable electron percolation pathways for physical charge transfer between interfaces [12]. The fabrication of TiO_2 nanotube arrays via anodisation was first reported in 2001 [13]. The proposed growth mechanism explains initial oxidation of titanium (Ti) during oxide layer formation by anodisation, which causes the subsequent localised dissolution of TiO_2 by fluorine ions in an electrolyte according to the following reactions [14]:

$$Ti + 2H_2O \rightarrow TiO_2 + 4H^+ + 4e^- \quad (1)$$

$$TiO_2 + 4H^+ + 6F^- \rightarrow TiF_6^{2-} + 2H_2O \quad (2)$$

The anodically formed oxide layers typically exhibit various colours that are caused by the interference of light which is reflected at the outer air/oxide and the inner oxide/metal interface [15]. Some studies have suggested that the

interference colours can be utilised in predicting the thickness of the oxide layer [16–18].

Most recent studies have concentrated on controlling the nanotube structures, including their pore size, wall thickness, and length, which are controlled by various experimental parameters, such as the applied potential and the electrolyte composition, as well as the anodisation time and temperature [19–21]. The tube structures are known to play an important role in determining optical properties, which in turn are related to photocatalytic properties, photoconversion efficiency for the photovoltaic device, and hydrogen detection capacity [22–24]. The light-absorbing properties of TiO_2 nanotube arrays grown on transparent (glass) and opaque (metal) substrates have been estimated by an electromagnetic computational technique known as the finite difference time domain [25]. Joo *et al.* [26] used ellipsometric methods to monitor the anodisation procedure for TiO_2 nanotube growth.

In the present study, TiO_2 nanotube arrays were prepared from pure Ti foil in an aqueous electrolyte that contained fluoride ions. The current density was measured to monitor the electrical behaviour during anodisation. The surface structure and the crystalline phase of the TiO_2 nanotube arrays were studied to observe the growth and to understand its correlation with the interference colour. The optical properties and interference colours were studied on a spectrophotometer. The properties of the interference colours were estimated using the $L^*a^*b^*$ system as a function of the applied voltage and the anodisation time.

Experimental

Anodisation was performed as follows: a Ti foil (20 mm × 20 mm × 0.1 mm, 99.5%) was used as an anode substrate to fabricate TiO_2 nanotube arrays, and a platinum foil (20 mm × 20 mm × 0.1 mm, 99.98%) was used as a cathode. The Ti foil was ultrasonicated in deionised (DI) water and isopropanol and dried in an air stream. All samples were anodised in an electrolyte containing 0.5 wt% hydrogen fluoride (HF) in DI at room temperature (22 °C) for 30 min. A constant voltage (7, 10, 15, or 20 V) was applied, and the current density was measured on a Fluke 8846 precision multimeter (Fluke Calibration, USA). After anodisation, the samples were immediately rinsed with DI water and dried in an air stream.

A specific set of samples were anodised in the same electrolyte at 20 V for varying times in order to investigate the interference colour. Each time the surface colour of the Ti foil changed, anodisation of the sample was stopped for analysis of the colour properties.

The morphologies of the prepared samples were observed with an S-4800 field emission scanning electron microscope (FESEM) (Hitachi, Japan). The crystalline structure of the obtained samples was determined by X-ray-diffraction (XRD) on an X'Pert Pro MPD X-ray powder diffractometer (Philips) using CuK_α radiation over a 2θ range of 20–65°.

A CM-700D spectrophotometer (CM-700d, Konica Minolta Sensing Inc., Japan) was used for studying the optical properties of the anodised Ti samples, including reflectance spectra within the visible wavelength range (400–700 nm) and the interference colours of the anodised Ti, which were estimated by the CIELab colour scale on the spectrophotometer with a D65 light source.

Jongyun Moon *is a PhD candidate at the Department of Information Technology, University of Turku, Finland. He received his MEng from the Department of Safety Engineering at Hoseo University, Republic of Korea, in 2008. His research interests are focused on the synthesis and characterisation of self-organised metal oxide materials and their gas sensor applications.*

Risto Punkkinen *received his MSc Degree in Physics from the University of Turku, Finland, in 1976 and received his PhD in Physics from the University of Turku in 1990. He has worked at the University for most of his career. He was a Senior Assistant in the Department of Physics and is now an Adjunct Professor and the Head of the Microelectronics Laboratory in the Department of Information Technology. His research interests are in semiconductor manufacturing, processing, electrical characterisation of semiconductors, and silicon-based radiation detectors. He is also the author or coauthor of ca. 50 publications.*

Results and Discussion

Anodisation of titanium foil at different voltages

Figure 1 shows the current density behaviour of Ti anodisation at different voltages (7, 10, 15, and 20 V) in an electrolyte solution containing HF. The total anodisation time was 30 min. The current density initially decreased very sharply on account of the formation of a compact oxide layer and then entered a steady stage in which the rate of oxide formation slowed down owing to the thick oxide layer, and thus the current density was reduced [10]. The sample anodised at 7 V displayed a higher current density; this may have been due to the thinner oxide layer formed by comparison with the other samples. Therefore, the current density remained higher than in the samples anodised at higher voltages.

Figure 2 shows surface and cross-sectional FESEM images of TiO_2 films prepared by anodisation at different voltages (7–20 V). Tubular structures were observed on all the anodised samples. The top surfaces of the nanotubes

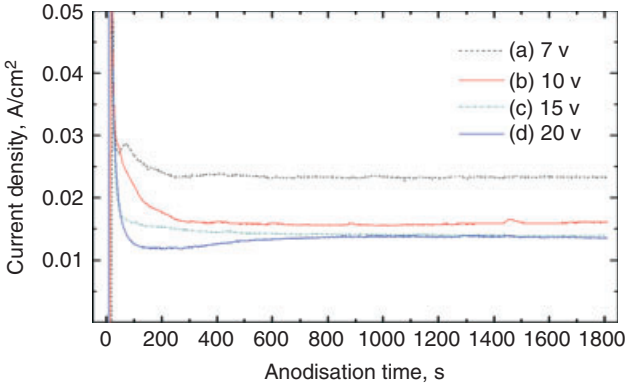

Figure 1 The current density during Ti anodisation at different voltages

Table 1 The morphology parameters of TiO_2 nanotube arrays at different voltages for 30 min

Voltage, V	Pore diameter, nm	Wall thickness, nm	Tube length, nm
7	17	16	134
10	32	10	231
15	45	14	271
20	90	29	340

were open and the bottoms were closed, as commonly observed in Ti anodisation, and the tube surfaces had rings (ripples) on the outer wall, as can be seen in the cross-section images shown in the inset of Figure 2. The sample anodised at 7 V showed irregular and tightly interconnected pores. The geometrical features and anodisation parameters of the samples are summarised in Table 1. According to these results, the applied voltage seems to play an important role in influencing the morphology of TiO_2 nanotube arrays. The porosity (P) of the oxide film can be estimated by using the formula:

$$P = \left[1 - \frac{2\pi(d_p w + w^2)}{\sqrt{3}l^2}\right] \times 100\% \quad (3)$$

where d_p, w, and l are the inner pore diameter, the wall thickness, and the centre-to centre distance between nanotubes respectively [27]. According to calculations using Eqn (3), the porosities of the samples anodised at 7, 10, 15, and 20 V were 23, 41, 51, and 60% respectively.

Titanium coloration as a function of anodisation time

The relationship between the anodisation time, morphology, and the visual interference colour is summarised in Figure 3, and its correlation with the formation of TiO_2 nanotube arrays is described in Figure 4. The samples displayed the following interference colours during anodisation: gold, purple, blue, light green, and light pink. This order of the interference colours is in agreement with some results that have been observed from the anodisation of Ti and its alloys [16,17]. The order of appearance of the interference colours has been explained by multiple-beam interference theory [28].

The oxidation of Ti started as soon as Ti was immersed in the electrolyte and the voltage was applied. An oxide layer (about 70 nm thick) (Figure 4a) formed within seconds and displayed a gold hue. The oxide layer continued to grow and showed a purple hue at a thickness of 90 nm (Figure 4b). As anodisation continued, small pores caused

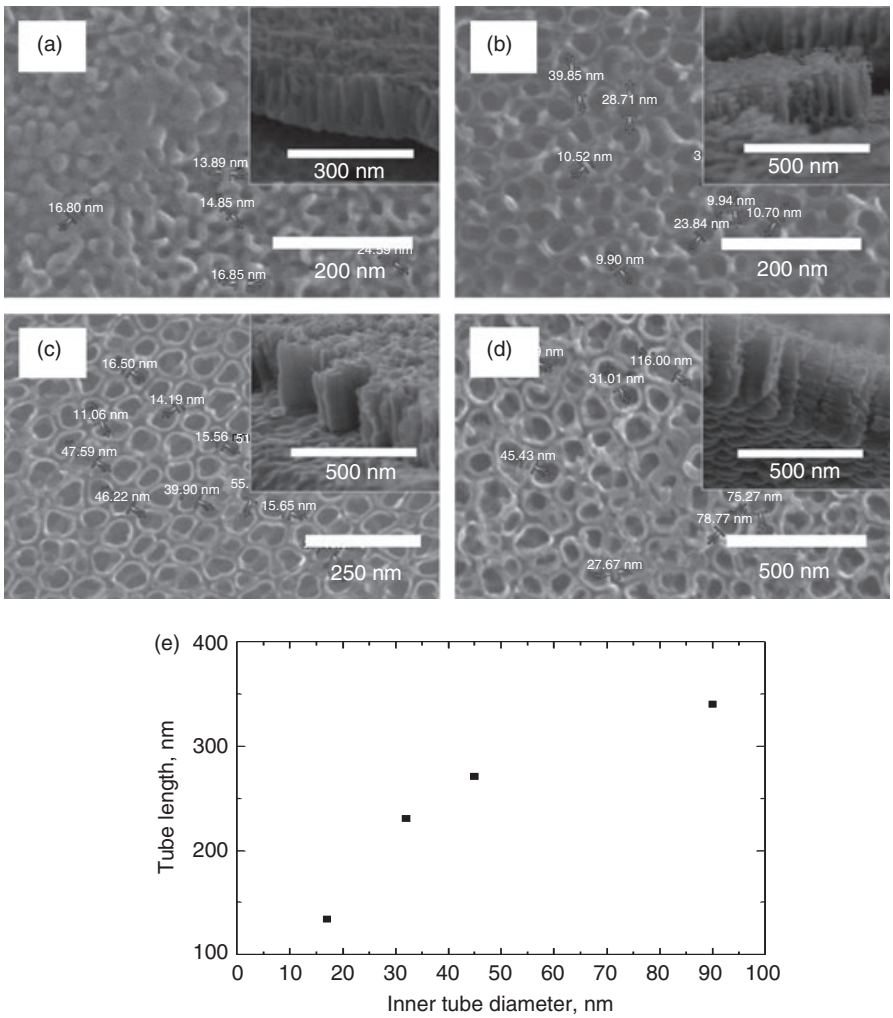

Figure 2 Field emission-scanning electron microscope images of the top view and cross-section of TiO_2 nanotube arrays anodised at (a) 7 V, (b) 10 V, (c) 15 V, and (d) 20 V, and (e) the variation in length versus the inner diameter of the TiO_2 nanotubes

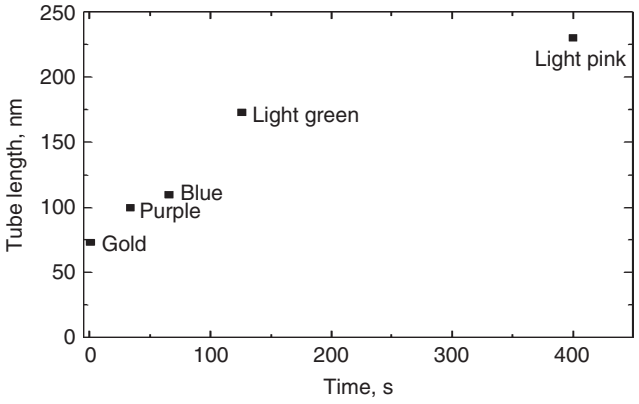

Figure 3 The relationship between anodising time, oxide thickness, and colours of Ti foil anodised at 20 V in an aqueous electrolyte containing 0.5 wt% HF

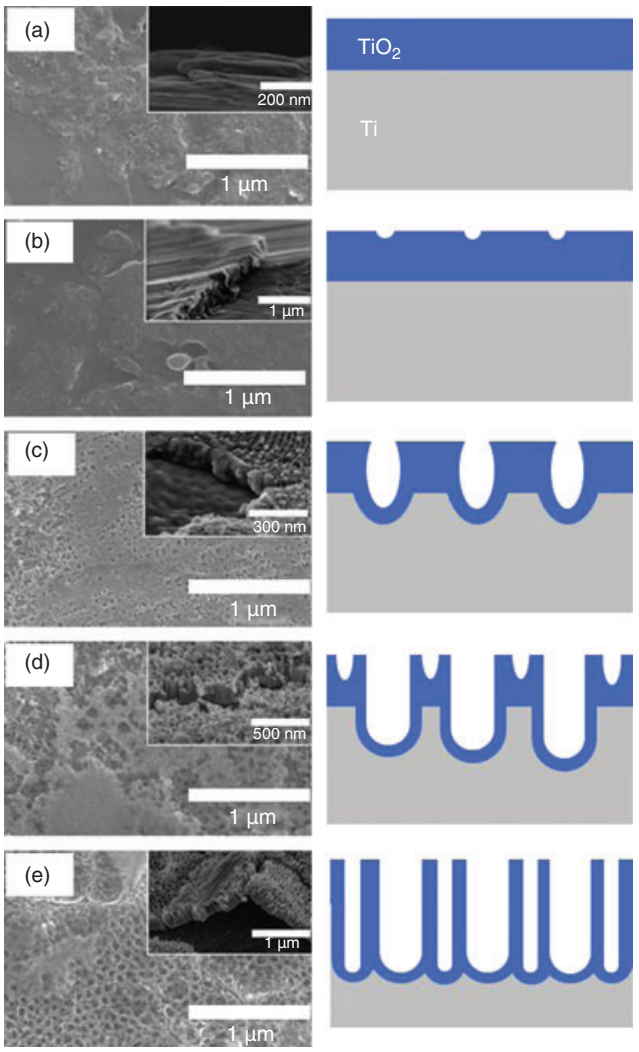

Figure 4 A comparison between the growth procedure and the interference colours of TiO_2 nanotube arrays formed at 20 V: (a) 1–2 s after immersion: formation of an oxide layer on the Ti sheet; (b) 34 s after immersion: development of the oxide layer; (c) 66 s after immersion: formation of slits and cracks on the oxide layer; (d) 126 s after immersion: sequential pore growth; (e) 400 s after immersion: pore growth completed and remaining tubular structure

by localised dissolution of the oxide emerged on the oxide layer (110 nm thick), showing a blue interference colour. A barrier layer could be seen at the bottom (Figure 4c). The

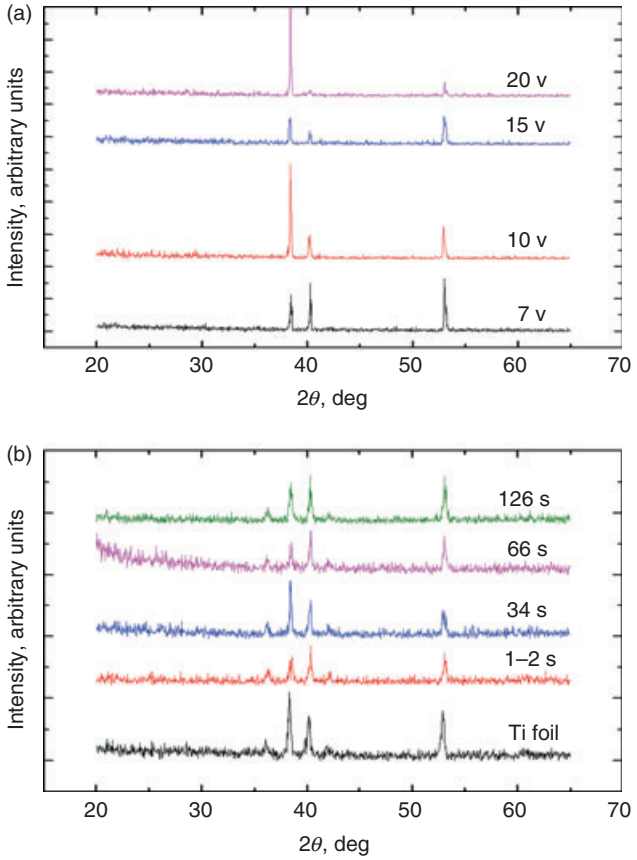

Figure 5 X-ray-diffraction patterns of a TiO_2 film grown on Ti as a function of (a) the applied voltages and (b) the anodisation time with interference colour change

pores spread out over the entire oxide surface and had thin walls owing to the relatively low ion mobility and relatively high chemical solubility of the oxide in the electrolyte, as expected [29]. When the interference colour changed to light green, the thickness of the TiO_2 layer reached 170 nm and the pores formed particular tubular structures (Figure 4d). When anodisation was continued, TiO_2 nanotubes formed at a thickness of 240 nm, showing an interference colour of pink hue with a green shade (Figure 4e). The development of oxide layer thickness, structures, and coloration with anodisation time in this study is in good agreement with the growth procedure of TiO_2 nanotube arrays previously reported [10].

Material crystalline phase

A TiO_2 film prepared by anodisation without subsequent heat treatment is typically amorphous. The XRD patterns in Figure 5 indicate that all the TiO_2 thin films were amorphous, as only Ti peaks were observed from all samples. This result is in agreement with findings previously reported by Mor *et al.* [10].

It has been shown that the crystalline phase of as-prepared TiO_2 film formed by Ti anodisation can be modified by varying experimental parameters such as the applied potential [30]. For instance, Yoriya *et al.* [31] demonstrated that an as-anodised TiO_2 layer, synthesised in DEG + 0.5 wt% NH_4F + 2% H_2O electrolyte and anodised at 80 V, showed an anatase peak intensity indicating partial crystallisation of the oxide film without heat treatment. In their study, the intensity of the anatase peak increased with

the NH_4F concentration. Diamanti *et al.* [16] also demonstrated that an oxide film obtained by anodisation in a phosphoric acid electrolyte at voltages between 10 and 103 V was amorphous, but anodisation in sulphuric acid electrolyte at 70 V produced a semi-crystalline oxide containing anatase or rutile in an amorphous oxide layer. In their study, the intensity of the anatase reflections increased with applied voltage. The experiments in the present study were performed at considerably lower voltages (maximum 20 V) in order to form TiO_2 nanotube arrays in aqueous HF electrolytes, and no indications of rutile or anatase crystallites were found.

Reflectance and colour properties of the oxide film

The applied voltages and the anodisation times clearly have an effect on the reflectance spectra of the TiO_2 films within the visible wavelength range, as seen in Figure 6. The reflectivity depends strongly on the wavelength. In general, the reflectance spectra of the samples seem to have a broad maximum located within the visible wavelength region or outside it [28]. In the case of a very thin oxide film, a rising curve can be seen.

Samples anodised at low voltages (7 and 10 V) show a broad reflectance maximum, while for samples anodised at higher voltages (15 and 20 V) the maximum moved out of the visible region, lowering the observed reflectance and saturation. The reflectance generally decreases with increasing anodisation voltage. Samples anodised at different voltages show reflectances oscillating between 15% and 35%. One broad maximum and no distinct minimum were observed from samples anodised at 7 and 10 V. The reflectance at higher voltages (15 and 20 V) shows only one local maximum and minimum value. This result indicates that the measured reflectance decreases as the thickness of the film increases.

The samples controlled by anodisation time show a reflectance oscillating between 4 and 30%. The samples with a compact film (1 and 34 s) show one single broad minimum without a distinct maximum. The oscillation range of the reflectance becomes smaller as the anodisation time increases. When the oxide film reaches a thickness of over 240 nm, interference disappears and the reflectance is smooth, varying between 15% and 18%. Similar results were observed when growing an oxide layer on aluminium alloys. When the oxide layer grows to critical thickness, the interference disappears [32].

The colour of the samples were expressed in the $L^*a^*b^*$ system, which is based on the colour sensitivity and perception of human eyes. The parameters a^* and b^* (hue and saturation) represent colours, while L^* expresses the degree of lightness, ranging from white to black. In order to investigate the colour difference between a pure Ti sample and an anodised sample, the total colour difference (TCD) of two observations (ΔE^*ab) was calculated by means of the formula [33]

$$\Delta E*ab = \sqrt{(\Delta L*)^2 + (\Delta a*)^2 + (\Delta b*)^2} \qquad (4)$$

The properties of the interference colours of the samples are summarised in Table 2. The Ti sample showed the highest lightness and a grey hue. The sample group controlled by the anodisation voltages have L values between 54 and 61. Their colours estimated by a^* and b^* were uniform on the entire surface of each sample, and

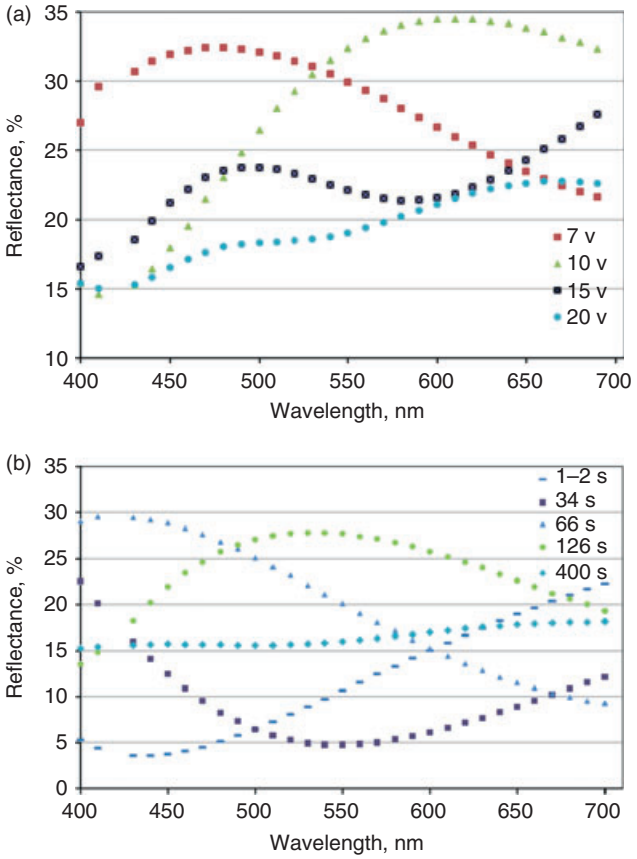

Figure 6 Optical reflectance spectra of TiO_2 nanotube arrays (a) prepared at different voltages and (b) as a function of anodisation time and coloration

Table 2 Interference colour properties of anodic TiO_2 films prepared at different voltages

Sample	Time, s	Voltage, V	Thickness, nm	L	a^*	b^*	ΔE^*ab (D65)
Ti				60.66	1.47	5.24	
a	1800	7	134	61.29	−5.41	−2.51	10.54
b	1800	10	231	61.80	0.02	22.39	17.27
c	1800	15	271	54.46	−4.00	4.53	8.46
d	1800	20	340	57.27	1.89	8.43	4.66
e	1	20	73	39.28	9.62	25.98	30.82
f	34	20	91	29.32	14.82	−21.64	43.32
g	66	20	113	51.42	−6.82	−14.92	23.76
h	126	20	173	58.57	−6.51	8.19	8.99
i	400	20	240	52.05	2.70	2.35	9.14

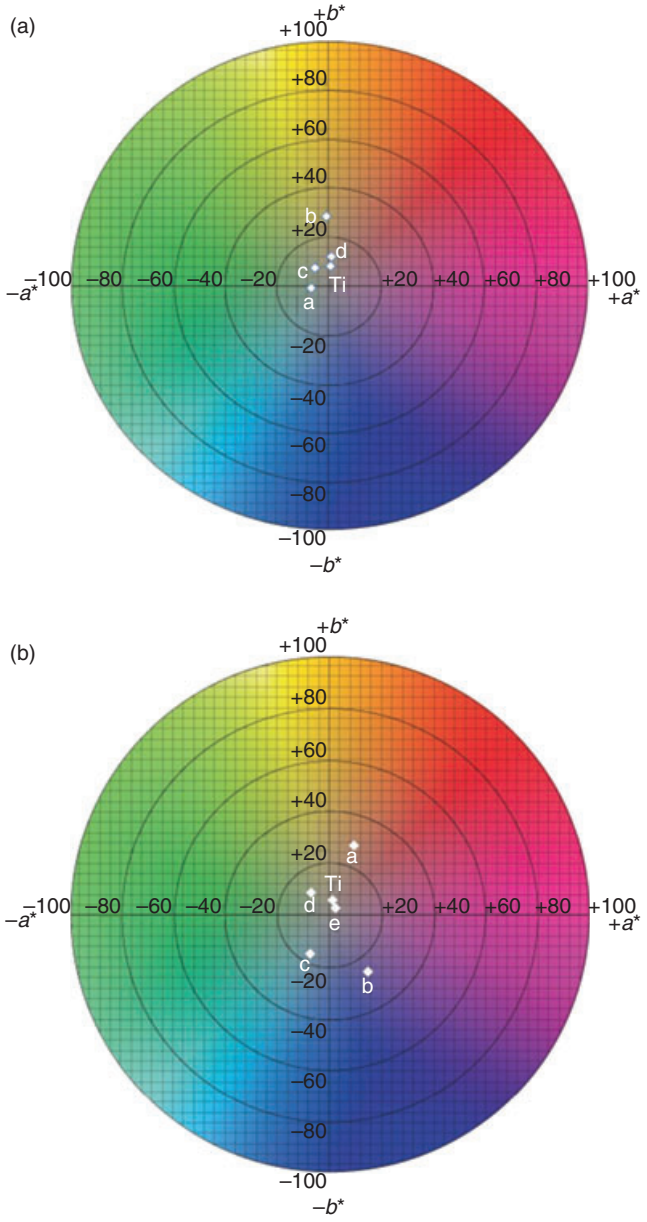

Figure 7 Chromaticity diagram of TiO_2 nanotube arrays (a) prepared at different voltages (a: 7 V; b: 10 V; c: 15 V; d: 20 V) and (b) as a function of anodisation time and coloration (a: 1–2 s; b: 34 s; c: 66 s; d: 126 s; e: 400 s): $-a^*$ = green; $+a^*$ = red; $-b^*$ = blue; $+b^*$ = yellow

their TCD value decreased when the anodisation voltage was increased.

The samples controlled as a function of anodisation time showed L values between 29 and 58. The lightness of samples with an oxide layer thickness of over 113 nm was in almost the same range as that of the previous sample group. The range of TCD values of these samples was wider (between 9 and 43) than for the oxide layer anodised for 30 min. The samples known to have a compact oxide layer had high TCD values, indicating greater interference.

It is known that several factors, including particle size, porosity, surface texture, chemical composition, and incident light wavelength, influence the reflectance of the material [34]. Based on observed results in the present study, the thickness and morphology of the oxide layer are dominant factors for the interference colours. Incident light was partly reflected by specular reflection from samples consisting of smooth compact oxide layers (samples e and f). Some influence of surface morphology on interference colour was observed. The chromaticity diagram in Figure 7 was drawn in order to elucidate the phenomena. The $L^*a^*b^*$ values of the sample anodised at 20 V for 126 s were nearly the same as the $L^*a^*b^*$ values of the sample anodised at 15 V for 30 min, even though the difference in their oxide layer thicknesses was nearly 100 nm, and the reflectance spectra differed notably. Liu *et al.* [34] suggested that the reflectance of SnO_2 nanoparticles prepared by the sol–gel method was affected by the crystal size, morphology, and particle boundary; for instance, reflectance decreased as particle size increased. This suggestion [34] is somewhat in keeping with present results indicating that reflectance decreases with increasing tube diameter (see Figure 6a).

Conclusions

TiO_2 nanotube arrays were prepared from Ti foil by anodisation in an aqueous electrolyte solution containing 0.5 wt% HF. The morphology of TiO_2 nanotube arrays was influenced by the anodisation voltage (7–20 V), which increased the diameter and length of the nanotubes. The surface structure of samples anodised at 20 V was studied during various stages of anodisation on the basis of interference colour in relation to anodisation time. Crystallisation of as-anodised samples to anatase or rutile phase did not occur in the present study. The reflectance spectra showed that the samples with porous or tubular structures expressed relatively low reflectance. The results from studying the colour properties on a spectrophotometer indicated that the compact TiO_2 film showed great colour difference, while nanoporous/tubular surfaces displayed high lightness values influenced by their surface structure and thickness. The interference colour of Ti can be a means of predicting not only the thickness of the oxide layer but also its surface structure according to optical properties.

Acknowledgements

Jongyun Moon gratefully acknowledges a fellowship (number TM-08-574/CIMO, http://www.cimo.fi/) from the Centre for International Mobility of Finland and the Fortum Foundation (grant number 11-134).

References

1. D M Chien, N N Viet, N T Van and N T Phong, *J. Exp. Nanosci.*, **3** (2009) 221.
2. B Karunagaran, P Uthirakumar, S J Chung, S Velumani and E K Suh, *Mater. Charact.*, **58** (2007) 680.
3. J M Macák, H Tsuchiya, A Ghicov and P Schmuki, *Electrochem. Commun.*, **7** (2005) 1133.
4. C C Wang, C Y Yu, C C Kei, C T Lee and T P Perng, *Nanotechnology*, **20** (2009) 285601.
5. M Luo, K Cheng, W Weng, C Song, P Du, G Shen, G Xu and G Han, *Mater. Lett.*, **62** (2007) 1965.
6. H A Bullen and S J Garrett, *Nano Lett.*, **2** (2002) 739.
7. H Masuda, K Kanezawa, M Nakao, A Yokoo, T Tamamura, T Sugiura, H Minoura and K Nishio, *Adv. Mater.*, **15** (2003) 159.
8. G Pecchi, P Reyes, P Sanhueza and J Villaseñor, *Chemosphere*, **43** (2001) 141.
9. S Afshar and M Hakamizadeh, *J. Exp. Nanosci.*, **4** (2009) 77.
10. G K Mor, O K Varghese, M Paulose, K Shankar and C A Grimes, *Sol. Energy Mater. Sol. Cells*, **90** (2006) 2011.
11. F Meng and Z Sun, *Appl. Surf. Sci.*, **255** (2009) 6715.

12. C A Grimes, *J. Mater. Chem.*, **17** (2007) 1451.
13. D Gong, C A Grimes, O K Varghese, W Hu, R S Singh, Z Chen and E C Dickey, *J. Mater. Res.*,**16** (2001) 3331.
14. K Yasuda, J M Macak, S Berger, S Ghicov and P Schmuki, *J. Electrochem. Soc.*, **154** (2007) C472.
15. D Velten, V Biehl, A B Valeske, W Possart and J Breme, *J. Biomed. Mater. Res.*, **59** (2002) 18.
16. M V Diamanti, B D Curto and M P Pedeferri, *Color Res. Appl.*, **33** (2008) 221.
17. Y T Sul, C B Johansson, Y Jeong and T Albrektsson, *Med. Eng. Phys.*, **23** (2001) 329.
18. F Reizman and W van Gelder, *Solid State Electron.*, **10** (1967) 625.
19. Z Lockman, S Sreekantan, S Ismail, L Schmidt-Mende and J L MacManus-Driscoll, *J. Alloys Compd.*, **503** (2010) 359.
20. G K Mor, K Shankar, M Paulose, O K Varghese and C A Grimes, *Nano Lett.*, **5** (2005) 191.
21. V M Prida, E Manova, V Vega, M Hernandez-Velez, P Aranda, K R Pirota, M Vazquez and E Ruiz-Hitzky, *J. Magn. Magn. Mater.*, **316** (2007) 110.
22. H Liu, G Liu and Q Zhou, *J. Solid State Chem.*, **182** (2009) 3238.
23. H Tsuchiya, J M Macak, L Taveira, E Balaur, A Ghicov, K Sirotna and P Schmuki, *Electrochem. Commun.*, **7** (2005) 576.
24. G K Mor, O K Varghese, M Paulose, K G Ong and C A Grimes, *Thin Solid Films*, **496** (2006) 42.
25. K G Ong, O K Varghese, G K Mor and C A Grimes, *J. Nanosci. Nanotechnol.*, **5**(2005) 1801.
26. S Joo, I Muto and N Hara, *J. Electrochem. Soc.*, **155** (2008) C154.
27. K Zhu, N R Neale, A Miedaner and A J Frank, *Nano Lett.*, **7** (2007) 69.
28. J Delplancke, M Degrez, A Fontana and R Winand, *Surf. Tech.*, **16** (1982) 153.
29. G Mor, O K Varghese, M Paulose, N Mukherjee and C A Grimes, *J. Mater. Res.*, **18** (2003) 2588.
30. J M Macak, H Tsuchiya, A Ghicov, K Yasuda, R Hahn, S Bauer and P Schmuki, *Curr. Opin. Solid State Mater. Sci.*, **11** (2007) 3.
31. S Yoriya, G K Mor, S Sharma and C A Grimes, *J. Mater. Chem.*, **18** (2008) 3332.
32. T S Shin, P S Wei and Y S Huang, *Surf. Coat. Technol.*, **202** (2008) 3298.
33. L Gao, W Ren, F Li and H M Cheng, *ACS Nano*, **2** (2008) 1625.
34. J Liu, Y Lu, J Liu, X Yang and X B Yu, *J. Alloys Compd.*, **496** (2010) 261.

Publication II

Hydrogen sensing performance of TiO_2 nanotubes at room temperature, 2010, Electronics Conference (BEC) 12th Biennial Baltic, 73-76.

Jongyun Moon, Ilkka Tuokko, Arho Suominen, Aulis Tuominen, Dongseok Oh, Byungki. Park, Hong Kim

Hydrogen sensing performance of TiO_2 nanotubes at room temperature

J. Y. Moon[1], I. Tuokko[1], A.Suominen[1], A.Tuominen[1], D. S. Oh[2], B. K. Park[3], H. Kim[2]

[1]*Department of Information Technology, University of Turku, FI-20010 Turku, Finland, E-mail: jong.moon@utu.fi*
[2] *Department of Safety Engineering, Hoseo University, Asan, Republic of Korea*
[3]*Industry Academic Cooperation Foundation, Hoseo University, Asan, Republic of Korea*

ABSTRACT: We report the hydrogen sensing properties of a sensor using TiO_2 nanotube arrays. The TiO_2 nanotube arrays were fabricated by anodization on titanium foil, in an electrolyte containing 0.5 wt% hydrofluoric acid mixed with water, the electric potential being 15V. TiO_2 nanotube arrays were annealed at 600 Celsius for 1 h. The sensors were equipped with platinum electrodes. These two were connected with a metal wire using silver paste. The measurements of the sensor's electrical resistance were performed in NTP. The hydrogen sensor using TiO_2 nanotube arrays shows a linear sensitivity with various hydrogen concentrations. After repeating exposure to hydrogen at room temperature, the sensor's resistance indicated a stable recovery to its initial resistance. The reproducibility of this exam is reliable.

1 Introduction

Hydrogen is becoming more important, since hydrogen fuel energy has been considered as a renewable resource, because it is clean and abundant in the air. So far hydrogen has been considered as a dangerous energy resource to use, because of the hydrogen explosion risk at 40,000 ppm in the air. Therefore, a safety system is required to prevent a leak of hydrogen in hydrogen generation, transportation, storage, and use. At the core of a hydrogen safety system are hydrogen sensor technologies which detect the leak of hydrogen.

In order to use hydrogen in various applications, a hydrogen sensor with high competence in sensitivity, reducibility and low price is needed. Therefore, many sensor technologies such as Schottky junction [1], fiber optic [2], catalytic [3], electrochemical [4], field effect transistor (FET) [5] and oxide semiconductor [6], have been developed.

Sensors using oxide semiconductor technology have been used for a variety of applications and paid considerably attention to, because of its diverse advantages such as compact size, low cost and low power consumption.[7] However, semiconductor sensors need an elevated temperature (100 – 500 Celsius) to operate. This is a significant factor hindering the commercialization of semiconductor sensors, esepecially with explosive gases such as hydrogen. Only few studies reported metal oxide sensors for operating at room temperature[8-9].

Titanium dioxide (TiO_2) is one of the most widely used functional semiconductors with applications in gas sensors [10], dye-sensitized solar cells [11], and photo-catalysis [12]. The gas sensing capability of TiO_2 is based on the changes in the film conductivity in the presence of oxidizing gases [13]. Since Varghese et al. [14] reported the hydrogen sensing performance of TiO_2 nanotubes, there have been several studies on hydrogen sensing properties of sensors using TiO_2 nanotubes. Hydrogen sensors using palladium doped TiO_2 nanotubes were reported to have both a remarkable surface resistance change at room temperature and photo-catalytic properties ,which can be used to recover the sensor's initial resistance by ultraviolet light exposure, after being contaminated [15]. To improve the sensitivity and reproductivility of the sensor, Chen et al. fabricaded a nanoporous TiO_2 layer on anodized alumina.[16] Han et al. fabricated a flat-type catalytic combustion hydrogen sensor enhancing the photocatalytic property using ultra violet light at an operating temperature of 82 Celsius [17]. Even though many studies to improve hydrogen sensing properties based TiO_2 have been made, the commercialization of hydrogen sensor's is still not as popular when compared to other sensors in the industry, because of a complex manufacturing process, high cost and reliable operation time.

In this study, we studied the hydrogen sensing properties of a hydrogen sensor which uses TiO_2 nanotube arrays equipped with a Pt electrode at room temperature.

2 Experimental

Titanium foils (0.125mm thickness, 99.5%, Sigma Aldrich) that were used as an anode electrode to grow TiO_2 nanotube arrays on, were cut in segments of 20mm × 30mm. Platinum (Pt, 0.1mm × 2.0mm × 2.0mm, 99.98%) was used as a counter electrode. Each of the electrodes were degreased by sonicating it in distilled water and rinsed with iso-propanol and distilled water. The constant voltage of 15V was applied using a power supply (DC Power Supply HY 3005D, Mastech) during the anodizing process. The titanium foil was anodized in an electrolyte containing hydrofluoric acid of 0.5% wt% with distilled water for 30 minutes. The anodization process was conducted at room temperature, at approximately 22

978-1-4244-7359-5/10/$26.00 ©2010 IEEE

Celsius.

The geometry of the sensor is described in Fig 1. The Pt electrodes, with a thickness of 20nm, were achieved by RF-sputtering (Bal-Tec Med 020) and the distance between the Pt electrodes is 10mm. The electrical contact between a Pt electrode and a wire was achieved with silver (Ag) paste. The prepared TiO_2 nanotubes were annealed at 600 Celsius for 1 hour in air atmosphere with heating and cooling rates of 1 Celsius per min by using a multi-stage programmable electric furnace (3-130 Furnace, Vulcan).

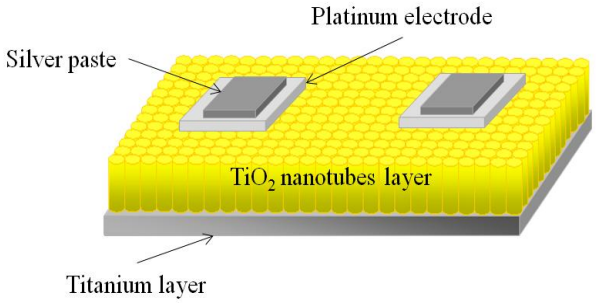

Fig. 1 The schematic diagram of the sensor's geometry

Electrical behavior during the anodizing process was observed with a multi-meter connected to a computer. The morphologies of the TiO_2 nanotubes were studied using a field emission scanning electron microscope (FESEM).

The sensor's sensitivity to hydrogen was measured with a multi-meter connected to computer in a glass chamber. The hydrogen concentration was varied in discrete steps from 0 to 40,000ppm. The sensor's reproducibility was measured by a digital multi-meter (Precision multi-meter 8846A, Fluke) connected to a computer. The hydrogen concentrations were generated by a hydrogen generator meant for lab tests.

3 Results and discussion

The current density during anodization at 15V in electrolyte containing 0.5 wt% hydroflouric acid is illustrated in Fig. 2. As shown in Fig 2, the behavior of anodization in electrolyte based on hydroflouric is explained with three steps; i) the formation of oxide layer on titanium foil ii) the growth of porous, iii) the formation of vain path and tuberal porous [17, 18].

In our previous study [19], we reported that TiO_2 nanotubes are formed in 30 min and its mophologies are controlled by suppying various electrical potentials. Through these studies, the formation mechanism of TiO_2 nanotube arrays was studied. Fig. 3 shows the surface morphology of nanotube arrays prepared by anodization using a voltage of 15V at room temperature, annealed at 600 Celsius for 1 h in air atmosphere. Fig. 3a illustrates the morphology of nanotube arrays and that they are uniform over the surface. The average tube diameter is 45nm and the average wall thickness 14nm. Out of the dimentional parameters of nanotube arrays, such as diameter, tube length and barrier thickness, the tube diameter may be a significant factor that influences the sensitivity of the sensor.[13]

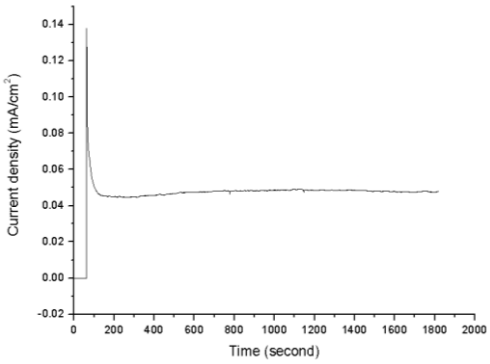

Fig. 2 Current density during anodization of titanium foil at 15V in HF-based electrolyte

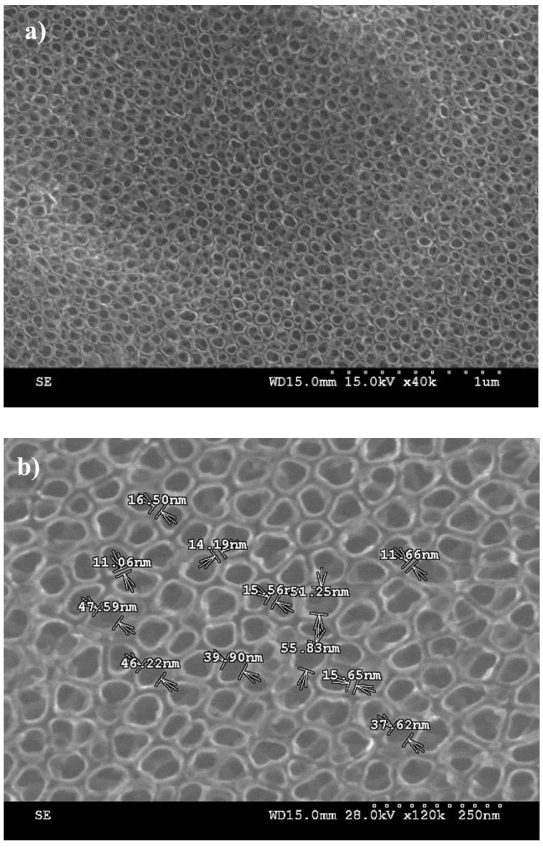

Fig. 3 FESEM images of TiO_2 nanotubes obtained by anodizing Ti foil in HF-based electrolyte for 30min, 15V, room temperature.

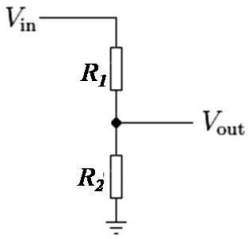

Fig. 4 Schematic diagram of Voltage divider used for hydrogen sensing measurement

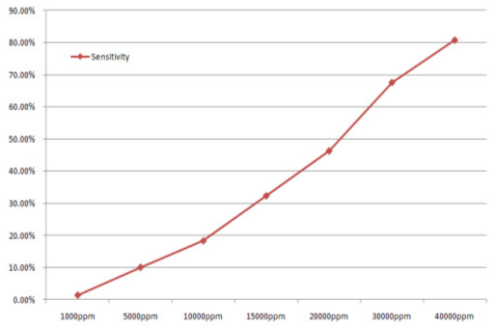

Fig. 5 Sensor's sensitivity when exposed to different concentration of hydrogen.

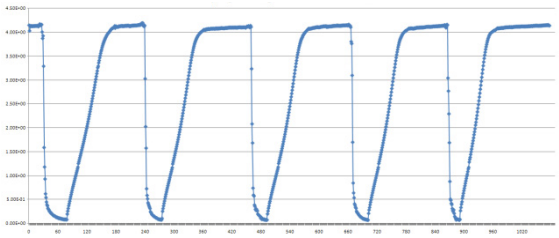

Fig. 6 Sensor's volage performance when exposed to hydrogen and flushed with air.

The typical function of a semiconductor sensor is to measure surface potential changes and surface conductivity while atomes and molecules of target gases interact with it. It is difficult to measure a presice sensitivity from the surface resistance of TiO_2 nanotube arrays because of the huge resistance of TiO_2 nanotube arrays. To measure the surface resistance more precisely, a voltage divider circuit was utilized for this experiment as shown from Fig.4. The voltage divider consists of two electrical resistances in series and a ground. The input voltage is applied across the series resistance R_1 and R_2 and the output is the voltage across R_2.R_1. The relation between the input voltage V_{in} and output voltage$_{out}$ can be described with equation 2.

$$V_{out} = \frac{R_2}{R_1 + R_2} \cdot V_{in} \qquad 2)$$

A sensor sample is used as R1 and a reference resistance of 9MΩ is used as R2. The input voltage of 5 V is supplied to obtain the output voltage. The surface resistance of the sensor is appoxiately 60MΩ obtained through the voltage diver. When the sensor was exposured to hydrogen concentration of 40,000ppm, the sensor resistance was reduced to 11.58 MΩ.

Fig. 5 illustrates the measured sensitivity of the sensors at room temperature, when they were exposed to various concentrations of hydrogen, ranging between 0 – 40,000ppm. The sensitivity of semiconductor sensor can be defined by the equation 2.

$$S = \frac{R_0 - R_{gas}}{R_{gas}} \qquad 2)$$

The measurement chamber was flushed with air after each exposure. As Fig. 5 indicates, the sensivities of the sensors indicate a linear increase up to 40,000ppm. The sensor's sensitivities hydrogen present from 1.4% in 1000ppm to 80.8% in 40,000ppm.

To study the reproducibility of the sensors, they were exposed to hydrogen repeatedly by using a hydrogen generator in a glass chamber. After being exposed to a certain concentration of hydrogen, the sensor's voltage is seen to recover to the initial voltage repeatedly. The response time of the sensor is not clear since the multi-meter's measurement time interval was set to 1 sec. Fig 6 indicates that the reaction of sensors occurred in less than 1 sec. The recovery time from the moment, which the chamber was flushed with air until the sensor reached its initial voltage, was approximately 100 sec.

The sensors using TiO_2 nanotube arrays coated with palladium indicated remarkable sensitivity at room temperature, and palladium is known to improve the sensors ability to dectect hydrogen. [13]

It can be considered that the interaction between the sensor and hydrogen may be due to the chemisorption of the dissociated hydrogen on the surface of TiO_2 nanotube arrays, because the sensor regains the initial resistance after hydrogen exposure. While the chemisorption occurs, hydrgen operates as a surface state and a partial charge transfer is caused from hydrogen to the conduction band of the TiO_2 layer. This phenomenon produce an electron accumulation layer on the surface of the nanotubes. When the chamber is flushed with air, the sensor, electron transfer returns back to hydrogen, hence it recovers the resistance. The Pt electrodes may be another factor that can effect the hydrogen sensitivity of the sensor. The Pt electrodes might act as catalyst in the interaction between hydrogen and the sensor, so far there is no clear study on how Pt electrodes affect this reaction [20].

Conclusions

The sensor using TiO_2 nanotube arrays and is fabricated by anodization was studied. The anodization using the electrolyte containing hydrofluoric acid at 15V electric potential was successfully implemented to produce TiO_2 nanotube arrays. TiO_2 nanotube arrays were equipped

with Pt electrodes. The sensor shows clear linear sensitivity to different concentrations of hydrogen. It should be noticed that the sensor using TiO_2 nanotube arrays with Pt electrodes detect hydrogen effectively at room temperature. Up until now, the general consensus has been that semiconductor gas sensors need an elevated or high temperature to function. However, this study proves that the TiO_2 nanotube sensor can have stable reproducibility and a high sensitivity, in order to meet the requirements for commercialization in the semiconductor sensor industry.

Acknowledgements

J.Y.Moon gratefully acknowledges the fellowship (No.TM-08-574/CIMO Fellowship) from the Centre for International Mobility. Dr. Lauri Heikkilä, Dr. Risto Punkkinen and Mr. Hannu-Pekka Hedman in Department of Information technology at University of Turku are greatly acknowledged for the sputtering machine and scientific advices. The authors thank the Hoseo University for the scanning electron microscope and Sensorex LTD., for the hydrogen sensing measurement.

References

[1] S. Roy, C. Jacob and S. Basu, "Studies on Pd/3C-SiC Schottky junction hydrogen sensors at high temperature", Sensors and Actuator B 94, 298-303, 2003

[2] B.Sutapun, M. Tabib-Azar and A. Kazemi, "Pd-coated elastooptic fiber optic Bragg grating sensors for multiplexed hydrogen sensing", Sensors and Actuators B 60, 27-34, 1999

[3] C. H. Han, D. W. Hong, I. J. Kim, J. H. Gwak, S. D. Han, K. C. Singh, "Synthesis of Pd or Pt/titanate nanotube and its application ot catalytic type hydrogen gas sensor", Sensors and Actuators B 128, 320-325, 2007

[4] A. V. Kroll, V. I. Smorchkov, "Electrochemical solid-state micro-sensor for hydrogen determination", Sensors and Actuators B 34, 462-465

[5] T. Yamaguchi, T. Kiwa, K. Tsukada and K. Yokosawa, "Oxygen interference mechanism of platinum–FET hydrogen gas sensor", Sensors and Actuators A 136, 244-248

[6] A.Z. Adamyan, Z.N. Adamyan, V.M. Aroutiounian, A.H. Arakelyan, K.J. Touryan and J.A. Turner, "Sol–gel derived thin-film semiconductor hydrogen gas sensor", International Journal of Hydrogen Energy 32, Issue 16, 2007, 4101-4108, 2007

[7] A. Salehi, and M. Gholizade**,** "Gas-sensing properties of indium-doped SnO2 thin Films with variations in indium concentration", Sensors and Actuators″, B 89, 173-179, 2003

[8] M.Sanchez, R. Guirado, M. E. Rincon, "Multiwalled carbon nanotubes embedded in sol-gel derived TiO_2 matrices and their use as room temperature gas sensors", J. Mater. Sci: Master Electron, 18, 1131-1136, 2007

[9] J. S. Oakely, H. T. Wang, B. S. Kang, Z. Wu, F. Ren, A. G. Rinzler and S. J. Pearton, "Carbon nanotube films for room temperature hydrogen sensing", Nanotechnology 16, 2218-2221, 2005

[10] G. C. Mather, F. M. B. Marques and J. R. Frade, "Detection Mechanism of TiO_2-based Ceramic H_2 sensor", Journal of the European Ceramic Society, 19, 887-891, 1999

[11] S. K. Deb, "Dye-sensitized TiO_2 thin-film solar cell research at the National Renewable Energy Laboratory (NREL)", Solar Energy Materials and Solar Cells 88, Issue 1, 1-10, 2005

[12] F. Meng, X. Song, Z. Sun "Photocatalytic activity of TiO_2 thin films deposited by RF magnetron sputtering", Vacuum, 83, Issue 9, 1147-1151, 2009

[13] Teppei Iwanaga, Takeo Hyodo, Yasuhiro Shimizu, Makoto Egashira, "H_2 sensing properties and mechanism of anodically oxidized TiO_2 film contacted with Pd electrode", Sensors and Actuators B: Chemical, 93, Issues 1-3, 519-525, 2003

[14] O. K. Varhese, D. Gong, M. Paulose, K.. G. Ong, C. A. Grimes, "Hydrogen sensing using titana nanotubes", Sensors and Actuators B 93, 338-344, 2003

[15] G. K. Mor, M. A. Carvalho, O. K. Varghese, M. V. Pshko, C. A. Grimes, "A room-temperature TiO_2-nanotube hydrogen sensor able to self-clean photoactively from environmental contamination", J.mater.Res., Vol. 19, No.2", 628-634.

[16] C. Lu, Z. Chen, "High-temperature resistive hydrogen sensor based on thin nanoporous rutile TiO_2 film on anodic aluminum oxide", Sensors and Actuators B: Chemical, 140, issue 1, 109-115, 2009

[17] Han, C. H., Hong, D. W., Han, S. D., Gwack, J. H., & Singh, K. C, "Catalytic combstion type hydrogen sensor using TiO_2 and UV-LED. Sensors and Acuators B 125 , 224-228, 2007

[18] X. Yu, Y. Li, W. Wlodarski, S. Kandasamy, K. Kalantar-zadeh, "fabrication of nanostructured TiO_2 by anodization : A comparison between electrolytes and substrates", Sensors and Actuators B, 1-7, 2007

[19] J. Y. Moon, A. Suominen, A. Tuominen, "The fabrication of highly ordered titania nanotube arrays by a simple anodic oxidation process", The sixth New Exploratory Technologies Conferences, 2009

[20] G.K. Mor, O. K. Varghese, M. Paulose, K. Sharnkar, C. A. Grimes, "A review on highly ordered, vertically oriented TiO_2 nanotube arrays : Fabrication, material properties, and solar energy applications", Solar Energy Materials & Solar Cells 90, 2011-2075, 2006

Publication III

A study of monitoring hydrogen using mesoporous TiO_2 synthesized by anodization, 2013, Sensors and Actuators B: Chemical, 189, 246-250.

Jongyun Moon, Hannu-Pekka Hedman, Marianna Kemell, Arho Suominen, Ermei Mäkilä, Hong Kim, Aulis Tuominen, Risto Punkkinen,

Sensors and Actuators B 189 (2013) 246–250

Contents lists available at ScienceDirect

Sensors and Actuators B: Chemical

journal homepage: www.elsevier.com/locate/snb

A study of monitoring hydrogen using mesoporous TiO_2 synthesized by anodization

Jongyun Moon[a,*], Hannu-Pekka Hedman[a], Marianna Kemell[b], Arho Suominen[a], Ermei Mäkilä[c], Hong Kim[d], Aulis Tuominen[e], Risto Punkkinen[a]

[a] Department of Information Technology, University of Turku, Turku FI-20014, Finland
[b] Department of Chemistry, University of Helsinki, FI-00014, Finland
[c] Department of Physics, University of Turku, Turku FI-20014, Finland
[d] Department of Safety and Health Engineering, Hoseo University, San 29-1, Sechul-Ri, Asan City 337-850, South Korea
[e] Business Innovation Development, University of Turku, Turku FI-20014, Finland

ARTICLE INFO

Article history:
Received 30 September 2012
Received in revised form 3 May 2013
Accepted 18 May 2013
Available online 25 May 2013

Keywords:
TiO_2
Anodization
Hydrogen
Gas sensor

ABSTRACT

We present a hydrogen sensor using mesoporous TiO_2 film on silicon and its H_2 sensing properties at different conditions. The sensor was formed by anodizing a sputtered Ti layer on silicon and having it annealed for crystallization. The material and electrical characterization included a study of morphology (FESEM), elemental composition (EDS), crystalline structure (XRD) and current–voltage behavior (semiconductor parameter analyzer). The sensor with Pt electrodes showed promising hydrogen sensing properties in air, such as good response to low hydrogen concentration (20–1000 ppm), fast response time of 5 s and recovery time of 125 s at 1000 ppm. The sensor response is shown to be independent toward relative humidity in the testing atmosphere.

1. Introduction

Among the basic elements in nature, hydrogen (H_2) is one of the most abundant elements. Because H_2 had been considered to be an attractive renewable resource, it has been studied and utilized in various applications, such as aerospace, medicine, transportation, and energy technologies [1–4]. The use of H_2 in fuel cells for transportation and power generation applications has raised interest today and can lead to less polluting vehicles because the only exhaust emission is water. H_2 is a potentially dangerous gas, regarding its operation and storage, due to the fact that leaking H_2 in air may cause easy ignition if its concentration is over 4%.

Metal oxide films, such as ZnO, SnO_2 and TiO_2, have been widely utilized for gas sensor applications [5–7]. Titanium dioxide is one of the most used gas sensor materials for H_2 detection, with operating temperature range of 250–500 °C. The gas sensing capability of TiO_2 film is based on the changes in the film resistivity in the presence of oxidizing gases and reducing gases, as typical metal oxide gas sensors [8,9]. Since one-dimensional nano-structured TiO_2 films have been widely studied, TiO_2 thin films anodically synthesized with Pd or Pt electrodes are convenient to produce and they have pronounced response to H_2 in both air and N_2 atmosphere [8,10,11]. Thin films consisted of TiO_2 nanotube arrays were successfully grown by anodization from Ti metal or deposited Ti on desired substrates. H_2 sensors utilizing such nanotubes have improved sensing performance and catalytic efficiency, since hydrogen can penetrate the inner structure of tubes [12].

However, when TiO_2 films are synthesized by anodization from Ti metal sheet, the potential applications of the film, such as microelectronic devices, become limited. For example, anodically synthesized TiO_2 nanotube arrays on Ti sheet may cause an electrical short-circuit due to diffusion of metal deposited top TiO_2 film into the Ti metal under the oxide layer. Also, vibration, physical shock, or the connection of electrical wires to the metal electrodes can damage the oxide layer and form a direct contact with the metal [13]. If mechanically reliable devices are to be produced, it is necessary to synthesize the oxide nanostructure on a desired substrate. Formation of TiO_2 films on other substrates, such as ITO film and silicon substrate, have recently been studied and used mainly for photovoltaic applications [9,14].

In this contribution, we report the fabrication and H_2 sensing properties of a gas sensor consisted of mesoporous TiO_2 thin film on Si substrate. The TiO_2 film was synthesized in an aqueous electrolyte containing fluoride ion by anodization of Ti deposited on Si. Pt electrodes were deposited by DC magnetic sputter. The anodized sample was annealed for crystallization. The structural properties

* Corresponding author. Tel.: +358 2 333 8670; fax: +358 2 333 8600.
E-mail address: jong.moon@utu.fi (J. Moon).

0925-4005/$ – see front matter © 2013 Elsevier B.V. All rights reserved.
http://dx.doi.org/10.1016/j.snb.2013.05.070

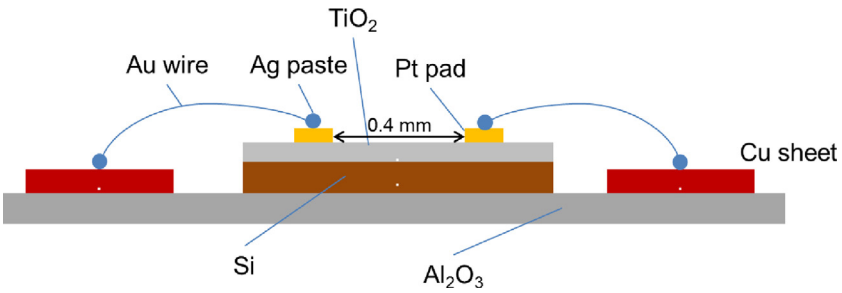

Fig. 1. Schematic of the sensor with platinum electrodes.

of the TiO_2 film were investigated by field emission scanning electron microscopy (FESEM), energy-dispersive X-ray spectroscopy (EDS), X-ray diffraction (XRD) and current–voltage measurement. Throughout H_2 sensing measurement of the sensor carried out at various concentrations with different operating temperatures in humid ambient air, the TiO_2 film gas sensor synthesized on Si shows appreciable H_2 sensing performance with fast response/recovery time at operating temperature of 140 °C.

2. Experimental

A slice of p-type Si wafer (10 mm × 20 mm × 0.6 mm) was rinsed with ethanol and deionized (DI) water and dried in air stream. High purity Ti thin film (99.9%) of 500 nm was deposited on a Si substrate by a DC magnetron sputter (BAL-TEC MED 020) in argon (Ar) at a pressure of 0.02 mbar at 150 °C. The TiO_2 thin film was synthesized via anodization of the deposited Ti film in an aqueous electrolyte containing hydrofluoric acid (HF) 0.5 vol.% in DI water for 5 min at room temperature. Only the Ti layer on Si was used as an anode and a platinum foil (Pt, 20 mm × 20 mm × 0.1 mm, 99.98%) was used as a cathode. Current density was recorded with a precision multimeter (Fluke 8846) during the anodizing process, and the sample was rinsed in DI water and dried.

Two Pt electrodes (100 nm thick, 1.4 mm diameter, 0.4 mm distance from each other) were deposited on the TiO_2 thin film by the DC magnetron sputter through a shadow mask that was placed against the film. The prepared sample was annealed at 500 °C for 6 h in air with heating and cooling rates of 1 °C/min in a multi-stage programmable electric furnace (3-130 Furnace, Vulcan).

Field emission scanning electron microscopy (FESEM, Hitachi S-4800) equipped with energy dispersive X-ray spectroscopy (EDS) was used for the surface morphology and the elemental composition analysis. X-ray diffraction (XRD, Philips X'Pert Pro MPD X-ray powder diffractometer) using Cu Kα radiation was used in studying the crystalline phase of TiO_2 film.

The sensor schematic is shown in Fig. 1. The sensor was fixed on an alumina substrate (20 mm × 10 mm × 1 mm) and thin gold wires (diameter 25 μm) were adhesively bonded for creating electrical contacts from the Pt electrodes to the copper (Cu) contacts by using silver (Ag) paste (Conductive epoxy CW2400, Chemtronics, USA).

The resistance between the Pt electrodes was detected by taking direct needle contacts to the Pt electrodes with a needle probe station (Rucker & Kolls 666). The current–voltage characteristics were measured as a function of temperature by using a semiconductor parameter analyzer (HP4145B).

The prepared sensor (10 mm × 10 mm) was placed on a small heater plate (15 mm × 15 mm, Ultramic 600, Watlow) to keep the sensor at specified temperature which was continuously observed with a thermocouple. The sensor with the heater plate was placed in a closed 56 l glass test chamber with continuous air circulation inside. The temperature inside the chamber was kept at room temperature. The desired concentrations of H_2 were created by inserting an exact volume of H_2 to the chamber and the concentration was verified with a calibrated commercial H_2 sensor (SX-917, Sensorex, Finland). The resistance of the sensor was measured by using a precision multi-meter (Keithley 6487 Picoammeter Voltage Source) connected to Cu contacts with two coaxial cables. The relative humidity (RH) inside the chamber was continuously observed with (SHT20, Sensirion). A wet paper was placed inside the chamber for adjusting the RH.

3. Results and discussion

The current density of the sputtered Ti film during anodization, as shown in Fig. 2, is similar to typical anodization of Ti, as reported elsewhere [15]. Based on the FESEM images of the samples it can be seen that the deposited Ti film has grains of Ti 10–25 nm in size (Fig. 3a) and the entire oxide layer (470 nm thick) after anodization has interconnection channels 20–40 nm in diameter (Fig. 3b and c). The result is not in good agreement with previously reported anodization of Ti sheet or Ti film on other substrates to synthesize highly ordered TiO_2 nanotube arrays using an aqueous electrolyte [15,16]. For example, Yu et al. [15] demonstrated obtaining of porous TiO_2 thin film by anodization of Ti thin film with round shape pits that have pore diameter of 25 nm and interpore distance of 40 nm on silicon substrate using an aqueous HF electrolyte at a constant voltage of 3 V at 3 °C. Particularly, when anodization was applied for a longer period of time (10 min), the TiO_2 film in our experiment was partially dissolved by acid electrolytes and, afterwards the formation of porous silicon was observed underneath TiO_2 (Fig. 3d). It is possible that the acid electrolyte dissolves TiO_2 thin layer after consuming Ti, and infiltrates on Si surface that forms the fluid–semiconductor interface, and then dissolves Si through an electrochemical reaction [17].

Only O (51.6%), Si (14.7%), and Ti (27.7%) can be detected in the EDS spectrum (Fig. 4) suggesting that the Ti peak shows more significantly than Si peak, which stems from the underlying substrate.

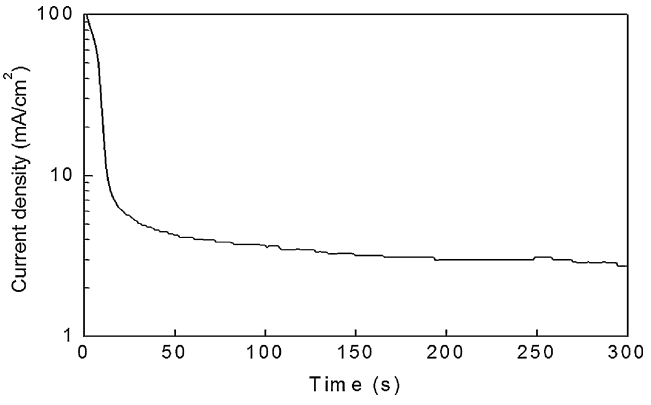

Fig. 2. Current density during anodization of Ti film deposited on Si.

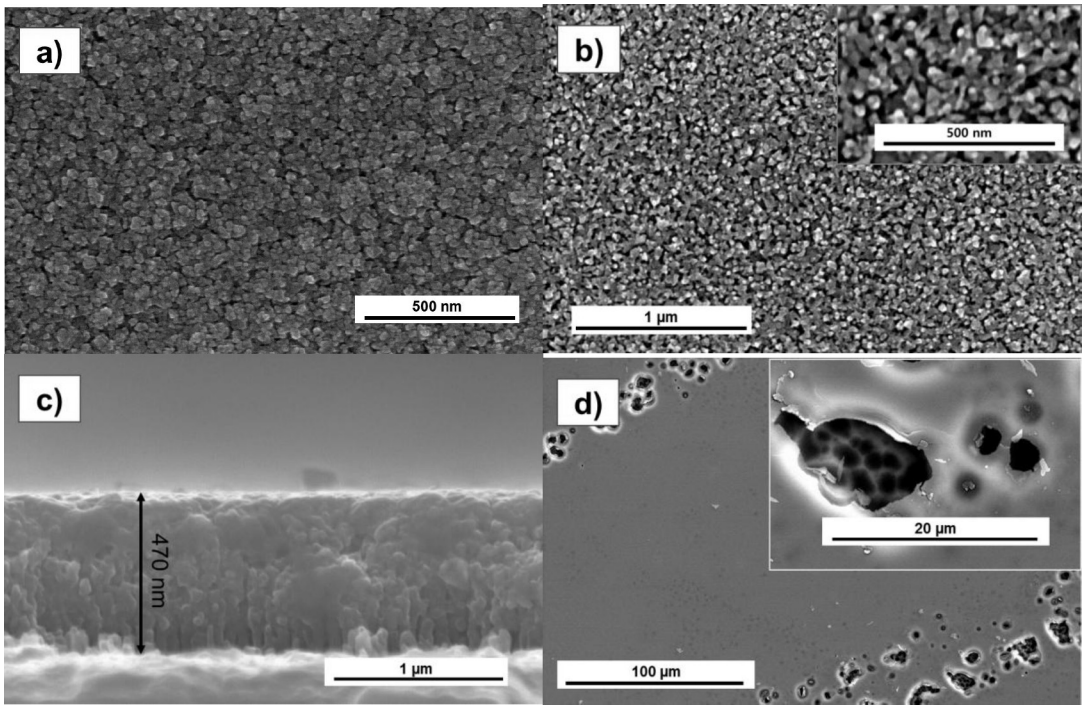

Fig. 3. FESEM images: (a) Ti film deposited on Si, (b) top view of mesoporous TiO_2 film on Si after anodization in HF 0.5% with DI water; inset is a high magnification, (c) cross-sectional image of TiO_2 film, (d) top image of TiO_2 film anodized for 10 min; inset shows partially porous silicon observed.

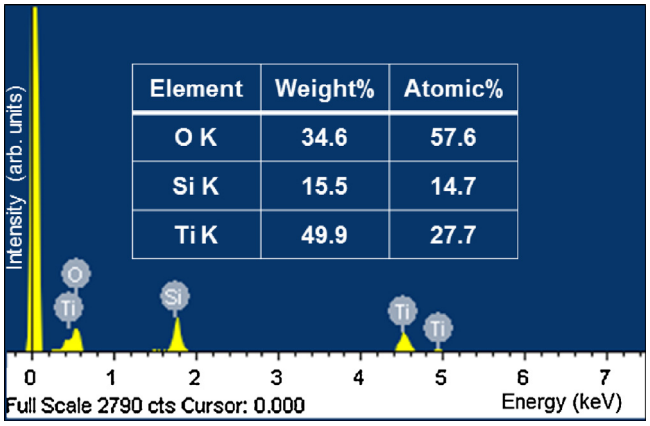

Fig. 4. EDS spectra of TiO_2 on Si substrate after annealing at 500 °C for 6 h in air.

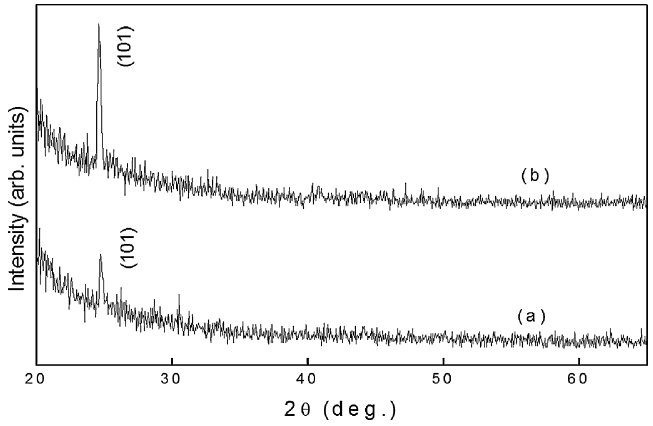

Fig. 5. XRD pattern of TiO_2 thin film (a) as anodized and (b) annealed at 500 °C.

TiO_2 nanostructures for gas sensor applications require crystallization by annealing in ambient air or oxygen atmosphere at certain temperatures for transformation of amorphous TiO_2 into anatase and/or rutile, depending on the used materials. The XRD pattern analysis is shown in Fig. 5. The as anodized TiO_2 film displays small anatase peak, but no other visible peak as seen in Fig. 5. The sample annealed at 500 °C (Fig. 5b) showed a stronger reflection than as anodized sample as shown of anatase (1 0 1) peak corresponding to an angle $2\theta = 25.3°$. But titanium peaks were not visible from this result. It is known that as anodized TiO_2 film at low anodization voltage is amorphous [15]. The existence of the slight anatase in as anodized sample shown in Fig. 5a is assumed to stem from the sputtering procedure at the elevated temperature and an existence of some air in the sputtering chamber.

The current–voltage (IV) characteristics of the sensor measured at different temperatures in air shown in Fig. 6 indicate that current tends to increase with increasing temperature. The route between the Pt pad and the Cu plate was found to be ohmic and of very low resistance. The plot of the measurement indicates that TiO_2

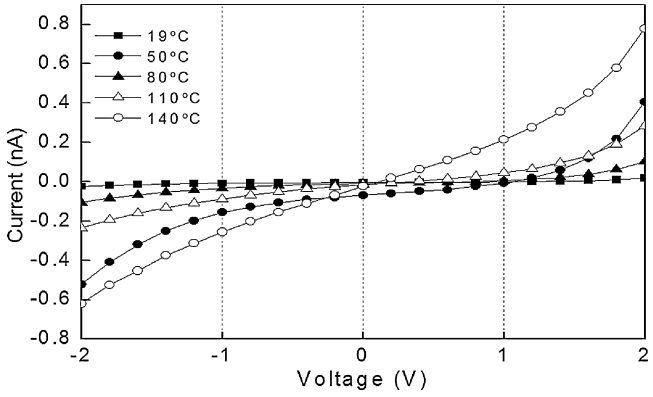

Fig. 6. Current–voltage characteristics measured at Pt electrodes of the sensor in air as a function of temperature.

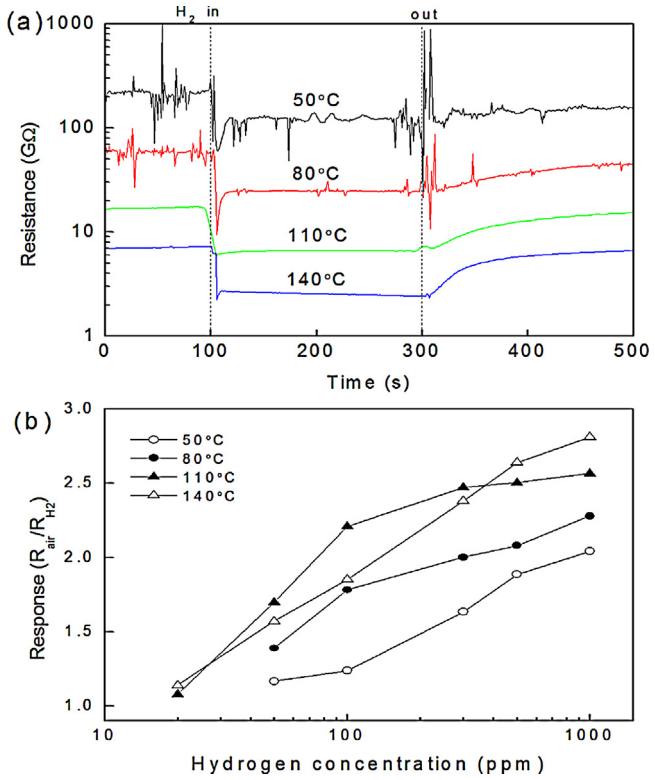

Fig. 7. (a) Resistance plot of TiO_2 sensor upon exposure to 1000 ppm H_2 in air at different operating temperature. (b) Hydrogen response of TiO_2 sensor as a function of hydrogen concentration at different operating temperature.

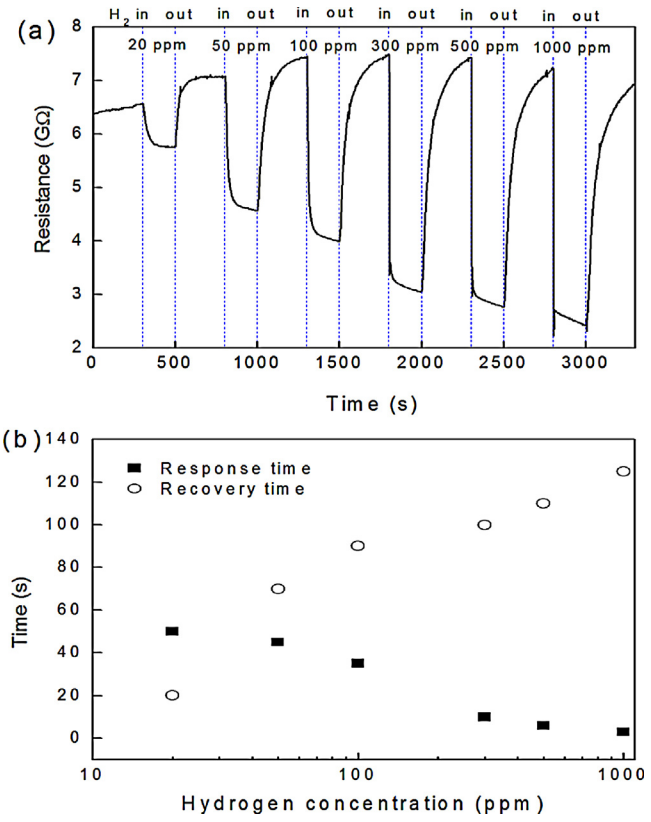

Fig. 8. (a) Resistance plot of TiO_2 sensor upon exposure to H_2 concentration range from 20 to 1000 ppm in air at 140 °C operating temperature. (b) Response and recovery time of TiO_2 sensor as a function of H_2 concentration.

film with Pt electrical contacts has non-ohmic behavior as the work function of Pt (5.65 eV) is higher than the electron affinity of anatase TiO_2 (4.12 eV). Thus, the interface between Pt film and TiO_2 forms a Schottky barrier that results in the electron transfer from the TiO_2 conduction band to Pt [18–20].

The sensor's response to hydrogen is the change in the resistance which is characterized as ratio R_{air}/R_{H_2}, where R_{air} and R_{H_2} are resistance of the sensor in absence and presence of H_2, respectively. Fig. 7 represents H_2 sensing performance at different operating temperatures. TiO_2 sensor at operating temperatures from 50 to 140 °C revealed an acceptable response upon exposure to H_2 concentration ranging from 20 ppm to 1000 ppm. However, we could only estimate the trend of the H_2 sensing response for low concentrations at operating temperatures of 50 and 80 °C which caused lots of noise for the measurement due to the very high resistance of TiO_2 sensor as shown in IV characteristics and Fig. 7a.

Fig. 7b illustrates the response of the sensor as a function of H_2 concentration. The response tends to increase with operating temperature because the properties of TiO_2 films as an n-type semiconductor. For metal semiconductor gas sensors in ambient air, oxygen chemisorbed on the metal surface increases their work function [21]. The best response for TiO_2 sensor was achieved at 140 °C, where the response is a linear function of H_2 concentration on the logarithmic scale. Thus, the trend line equation for the response at 140 °C is $0.4402\ln(x) - 1.1607$, where x is the H_2 concentration (ppm) and its correlation coefficient of R^2 is 0.995.

Fig. 8a describes a real-time variation of resistance in presence of H_2 at an operating temperature of 140 °C. In essence, the sensor exhibits noticeable H_2 sensing properties at the concentration range from 20 to 500 ppm. The response and recovery time are defined as the time for resistance to decrease and increase, respectively, toward 90% of total resistance change. The response time decreases with increasing H_2 concentration and the recovery time increases. The response time was 50 s at 20 ppm and within 10 s above 300 ppm. The recovery time was 20 s at 20 ppm and 70–125 s at 50–1000 ppm. Although the resistance change is not as great as in previously reported sensors [10,11], the low concentration response is worthy to note that anodically synthesized TiO_2 film without dopant could be able to detect low concentration H_2 and have fast response/recovery time that could be useful in determining H_2 leaks.

The influence of the relative humidity on the H_2 sensing properties was studied by observing the resistance at 100 ppm H_2 with the operating temperature of 140 °C and varying relative humidity in the test chamber. It took over 1000 s to stabilize the resistance in the targeted relative humidity during the preparation for this

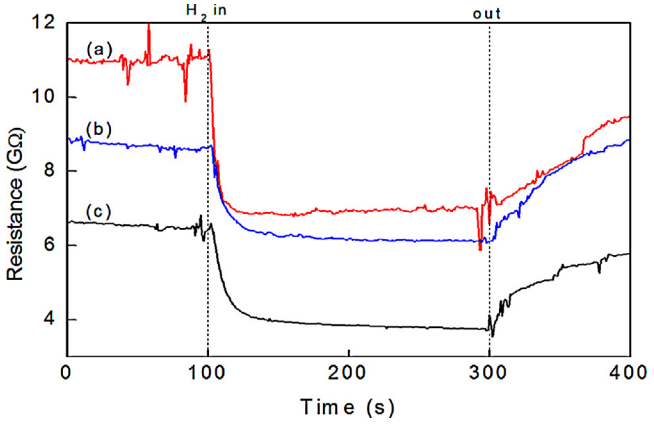

Fig. 9. The diagram of resistance variation of the TiO_2 sensor upon exposure to H_2 100 ppm in air at 140 °C as a function of humidity: (a) 5%, (b) 15%, and (c) 42%.

measurement. Fig. 9 shows that the sensor resistance decreased with increasing the humidity. The H_2 sensing behavior was similar in different humidity showing the response (1.7–1.9) to 100 ppm H_2 and response/recovery time was not significantly influenced.

4. Conclusion

A gas sensor using mesoporous TiO_2 film on Si substrate was synthesized by an anodization using an aqueous electrolyte containing HF. The obtained TiO_2 film was 470 nm thick and had small pores 25–40 nm. The crystallized TiO_2 film after annealing at 500 °C for 6 h had anatase structure. The gas sensor for H_2 detection was investigated at different operating temperatures (50–140 °C) and H_2 concentrations range from 20 to 1000 ppm in ambient air. The sensor showed that the H_2 sensing properties are clearly dependent on the operating temperatures and considering the sensor structure, the optimistic operating temperature for our sensor is 140 °C that provides the resistance reduction by a factor 2.8, the fast response time of 5 s and the recovery time of 125 s at 1000 ppm. The TiO_2 film was influenced by relative humidity in the sensing environment, showing a decrease of the resistance. However, the relative humidity change did not affect the actual response for H_2 sensing performance.

Acknowledgements

J. Moon gratefully acknowledges Fortum Foundation (B2 grant number 12-118). Authors cordially thank Sensorex Oy, Finland, for the use of their facilities in hydrogen testing.

References

[1] X. Bévenot, A. Trouillet, C. Veillas, H. Gagnaire, M. Clément, Hydrogen leak detection using an optical fibre sensor for aerospace applications, Sensors and Actuators B 67 (2000) 57–67.
[2] Y. Shen, T. Yang, T. Wang, F. Wen, Hydrogen gas: a novel antioxidant for chronic obstructive pulmonary disease? Journal of Medical Colleges of PLA 26 (2011) 94–97.
[3] T. Kojima, K. Tahara, Refinement and transportation of petroleum with hydrogen from renewable energy, Energy Conversion and Management 42 (2001) 1839–1851.
[4] C. Zamfirescu, I. Dincer, Ammonia as a green fuel and hydrogen source for vehicular applications, Fuel Processing Technology 90 (2009) 729–737.
[5] G.S.T. Rao, D.T. Rao, Gas sensitivity of ZnO based thick film sensor to NH_3 at room temperature, Sensors and Actuators B 55 (1999) 166–169.
[6] X. Du, S.M. George, Thickness dependence of sensor response for CO gas sensing by tin oxide films grown using atomic layer deposition, Sensors and Actuators B 135 (2008) 152–160.
[7] I.-D. Kim, A. Rothschild, D.-J. Yang, H.L. Tuller, Macroporous TiO_2 thin film gas sensors obtained using colloidal templates, Sensors and Actuators B 130 (2008) 9–13.
[8] T. Iwanaga, T. Hyodo, Y. Shimizu, M. Egashira, H_2 sensing properties and mechanism of anodically oxidized TiO_2 film contacted with Pd electrode, Sensors and Actuators B 93 (2003) 519–525.
[9] B. Karunagaran, P. Uthirakumar, S.J. Chung, S. Velumani, E.-K. Suh, TiO_2 thin film gas sensor for monitoring ammonia, Materials Characterization 58 (2007) 680–684.
[10] O.K. Varghese, D. Gong, M. Paulose, K.G. Ong, E.C. Dickey, C.A. Grimes, Extreme changes in the electrical resistance of titania nanotubes with hydrogen exposure, Advanced Materials 15 (2003) 624–627.
[11] Y. Shimizu, N. Kuwano, T. Hyodo, M. Egashira, High H_2 sensing performance of anodically oxidized TiO_2 film contacted with Pd, Sensors and Actuators B 83 (2002) 195–201.
[12] A. Kolmakov, M. Moskovits, Chemical sensing and catalysis by one-dimensional metal-oxide nanostructures, Annual Review of Materials Science 34 (2004) 151–180.
[13] G. Mor, O.K. Varghese, M. Paulose, C.A. Grimes, Transparent highly ordered TiO_2 nanotube arrays via anodization of titanium thin films, Advanced Functional Materials 15 (2005) 1291–1296.
[14] A.Z. Sadek, H. Zheng, K. Latham, W. Wlodarski, K. Kalantar-zadeh, Anodization of Ti thin film deposited on ITO, Langmuir 25 (2009) 509–514.
[15] X. Yu, Y. Li, W. Ge, Q. Yang, N. Zhu, K. Kakantar-zadeh, Formation of nanoporous titanium oxide films on silicon substrates using an anodization process, Nanotechnology 17 (2006) 808–814.
[16] G.K. Mor, O.K. Varghese, M. Paulose, N. Mukherjee, C.A. Grimes, Fabrication of tapered, conical-shaped titania nanotubes, Journal of Materials Research 18 (2003) 2588–2593.
[17] M. Rauscher, H. Spohn, Porous silicon formation and electropolishing, Physical Review E 64 (2001) 031604.
[18] Z. Zhang, Y. Yu, P. Wang, Hierarchical top-porous/bottom-tubular TiO_2 nanostructures decorated with Pd nanoparticles for efficient photoelectrocatalytic decomposition of synergistic pollutants, ACS Applied Materials and Interfaces 4 (2012) 990–996.
[19] K. Uosaki, R. Yoneda, H. Kita, Effect of platinization on the electrochemical behavior of titanium dioxide electrode in aqueous solution, Journal of Physical Chemistry 89 (1985) 4042–4046.
[20] J.-W. Yoon, T. Sasaki, N. Koshizaki, Dispersion of nanosized noble metals in TiO_2 matrix and their photoelectrode properties, Thin Solid Films 483 (2005) 276–282.
[21] H. Kobayashi, K. Kishimoto, Y. Nakato, Reactions of hydrogen at the interface of palladium–titanium dioxide Schottky diodes as hydrogen sensors, studied by work function and electrical characteristic measurements, Surface Science 306 (1994) 393–405.

Biographies

Jongyun Moon received his MEng at department of safety engineering from Hoseo University, Republic of Korea. Currently he is a PhD student in department of information technology at University of Turku, Finland. His research interests are laid on self-organized metal oxide materials, and semiconductor gas sensor application, and photovoltaic devices.

Hannu-Pekka Hedman studied physics and microelectronics in University of Turku, Finland where he graduated as MSc in 1993. He has worked as laboratory engineer and as research assistant in microelectronics laboratory in department of information technology (formerly in department of physics), University of Turku since 1993. His responsibilities have been to work in the clean room and process silicon wafers. Main product has been space radiation sensors. He has also measured electrical parameters of a wide range of semiconductor materials. His hobbies are electronics and computer programming.

Marianna Kemell received her PhD in inorganic chemistry in 2003 from the University of Helsinki, Finland, and her MSc in physical chemistry in 1997 from the University of Oulu, Finland. She currently holds a position as a senior lecturer of inorganic chemistry at the University of Helsinki. Her research interests include preparation of inorganic nanomaterials and thin films, especially by electrochemical methods and atomic layer deposition, and characterization by scanning electron microscopy and X-ray microanalysis. She has authored and co-authored more than 70 peer-reviewed papers.

Arho Suominen received his licentiate of technology pre-doctoral degree from University of Turku, Finland in 2009. He has previously received his MSc and BSc degrees from the University of Turku and holds a degree from the National Defense University. Currently he holds the position of university teacher teaching master level courses on new product development, leadership and electronics manufacturing. Practical experience he has gathered from working with several consulting firms as well as start-up companies. His research interests are directed toward understanding product creation and the identification and acquisition of new technology by industry.

Ermei Mäkilä received his MSc degree in physics in 2008 from the University of Turku and is currently working as a PhD student in the laboratory of industrial physics at the University of Turku. His current research interests include the fabrication and surface modification methods of porous silicon and its use in pharmaceutical applications.

Hong Kim received his PhD in department of chemistry from Chungnam National University, Republic of Korea in 1987. He is currently full professor in department of safety health engineering at Hoseo University, Republic of Korea. His research has been focused on gas explosion characteristics, toxic gas analysis and flame retardant materials.

Aulis Tuominen received his BSc from the Technical Institute of Helsinki, Finland in 1976 and his MSc from Tampere University of Technology, Finland 1991 and his DSc in Tampere University of Technology 1999, respectively. He has worked in several industry positions in companies such as Evox Oy, Reka cable factory and Nokia holding a number of positions. Since 2004 he has been a professor of electronics product development (productization) at the University of Turku. He is also an author or co-author about 150 publications. He holds five patents and several patents are applied.

Risto Punkkinen received his MSc degree in physics from the University of Turku, Finland in 1976 and received his PhD in physics from the University of Turku, Finland 1990. He has worked at the university almost all the time and is now an adjunct professor and the head of the microelectronics laboratory in department of information technology at the University of Turku. His research interests are in semiconductor manufacturing, processing, electrical characterization of semiconductors and silicon-based radiation detectors. He is also an author or co-author about 50 publications.

Publication IV

Hydrogen sensor of Pd decorated tubular TiO_2 film prepared by anodization with patterned electrodes on SiO_2/Si substrate, 2016, Sensors and Actuators B: Chemical, 222, 190-197.

Jongyun Moon, Hannu-Pekka Hedman, Marianna Kemell, Aulis Tuominen, Risto Punkkinen

Sensors and Actuators B 222 (2016) 190–197

Contents lists available at ScienceDirect

Sensors and Actuators B: Chemical

journal homepage: www.elsevier.com/locate/snb

Hydrogen sensor of Pd-decorated tubular TiO_2 layer prepared by anodization with patterned electrodes on SiO_2/Si substrate

Jongyun Moon[a,*], Hannu-Pekka Hedman[a], Marianna Kemell[b], Aulis Tuominen[c], Risto Punkkinen[a]

[a] Department of Information Technology, University of Turku, Turku FI-20014, Finland
[b] Department of Chemistry, University of Helsinki, P.O. Box 55, Helsinki FI-00014, Finland
[c] Department of Electrical Engineering and Automation, University of Vaasa, Vaasa FI-65101, Finland

ARTICLE INFO

Article history:
Received 22 December 2014
Received in revised form 27 June 2015
Accepted 12 August 2015
Available online 14 August 2015

Keywords:
Hydrogen sensor
Anodization
Nanostructures
Microelectronics

ABSTRACT

This study demonstrated a highly sensitive hydrogen sensor consisting of Pd-decorated TiO_2 tubular structures on SiO_2/Si substrate. Ti layer was deposited on a thermally oxidized Si substrate with patterned metal electrodes. TiO_2 nanotubes were prepared by an anodization of Ti layer in an organic electrolyte containing NH_4F 0.3 wt.% in ethylene glycol. Thin Pd layer was deposited on the detection area of the TiO_2 layer to enhance detection abilities. The formation of the TiO_2 layers on both the metal electrode and SiO_2 layers was investigated by FESEM and EDS. After annealing at 500 °C, the crystalline phase transformation from amorphous to anatase was confirmed by XRD. The hydrogen sensing properties of the sensor were investigated in synthetic air, nitrogen and humid air at 140–180 °C. The Pd deposition effectively improved the hydrogen sensing abilities of the sensor due to catalytic effect of Pd. The sensor showed promising hydrogen sensing characteristics, such as a high response, a wide detection range (1 ppm–1%), a fast reaction time and a good selectivity. This sensor fabrication process can offer feasibility for mass production of micro scaled sensors using anodically prepared TiO_2 sensors.

1. Introduction

The use of fossil fuels produces carbon dioxide (CO_2), the amount of which has increased in the atmosphere and caused environmental problems, such as global warming. Global energy resources are diminishing and becoming more expensive. Thus, substantial efforts have been made to utilize renewable energy resources [1] which can replace fossil fuels. For several decades, wind power [2], hydroelectric power [3] and photovoltaic technologies [4] have been favored as alternatives to fossil fuel. However, these technologies need further improvement of energy conversion efficiencies and have limitations with respect to storing or carrying the energy [5]. Hydrogen (H_2), on the other hand, shows great promise as an alternative fuel for our future energy needs. However, hydrogen is a potentially dangerous gas to use in industry because it is an invisible, odorless and flammable gas. Therefore, hydrogen sensors are crucially needed to detect any hydrogen leakage; as well as, precisely measure the hydrogen concentration in the hydrogen fuel cell system during all stages of hydrogen production, transportation and storage [6,7].

Many types of hydrogen sensors, such as, electrochemical [8], optical [9], catalytic [10,11], thermally conductive [12] and metal oxide semiconductor sensors [13,14], have been studied and commercialized. Metal oxide gas sensors have been widely used for hydrogen gas sensor applications because of their high sensitivity, fast response, long lifespan and feasibility to be miniaturized for use in the microelectronic devices. Especially, TiO_2 tubular structures prepared by anodization have shown significant hydrogen sensing properties. Most of anodic TiO_2 structures are prepared using metallic Ti as the base substrate [15,16]. This is due to the straightforward fabrication process and the easy modification of material's morphology by varying the experimental parameters, such as electrolyte concentration, pH, electrolyte temperature and applied voltage [17,18].

Gas sensors using an anodic TiO_2 layer which has a metal Ti basis can typically be constructed by placing two metal electrodes on the oxide layer to measure the resistance. Paulose et al. [19] reported remarkable hydrogen sensing properties of TiO_2 nanotube arrays prepared by an anodization of Ti foil in an electrolyte containing fluorine ion. In addition, such tubular TiO_2 arrays have also shown abilities to detect other gases, such as oxygen [20], ethanol

* Corresponding author. Tel.: +358 44 040 1555; fax: +358 2 333 8600.
E-mail address: jong.moon@utu.fi (J. Moon).

http://dx.doi.org/10.1016/j.snb.2015.08.054
0925-4005/

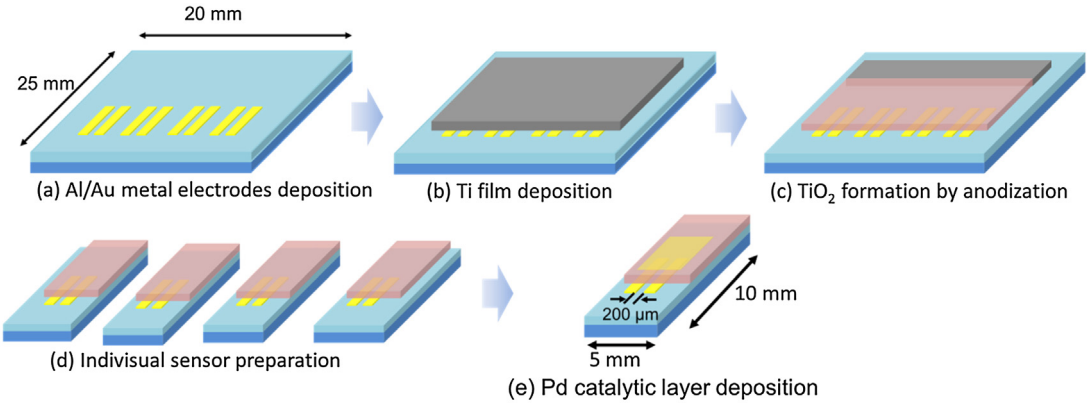

Fig. 1. Schematic of the sensor fabrication procedure.

and ammonia [21]. Yet anodic nanostructures formed on metallic Ti can be mechanically vulnerable; the top metal electrodes deposited on the oxide can diffuse into the TiO_2, which may cause an electrical short circuit. Besides, the oxide layer may get damaged during sensor manufacturing processes, such as wire bonding. More importantly the Ti layer underneath the oxide layer makes the device incompatible for use in microelectronic technology.

Thus, much effort has been recently contributed to developing gas sensors using anodic TiO_2 nanostructures on alternative substrates, which provide various advantages for microelectronic applications [22–24]. Several studies have reported the TiO_2 preparation on different base substrates, such as, conductive film (Indium tin oxide and Si) [25,26] and insulators (Al_2O_3, SiO_2 and glass) [22,27]. Essentially, the use of isolating substrates, such as SiO_2/Si, enables placement of metal electrodes under the anodic oxide layer [28]. For example, Kimura et al. [29] demonstrated a gas sensor using porous TiO_2 prepared by local anodization of Ti wire. This work showed that the reduction in sensor size could improve hydrogen detection properties. Using these TiO_2 nanotube sensors on isolating substrates, however, still would require further improvements considering the sensitivity, due to poorer hydrogen detection ability than sensors directly prepared from Ti foil [22]. Adding catalytic materials has commonly been used in modifying the sensing properties of metal oxide gas sensors. Particularly, noble metals, such as Pd [30], Pt [31] and Au [32], are favored as catalysts, due to their high hydrogen chemisorption. Hence, the gas sensing properties of anodic TiO_2 layer prepared on insulating substrates can be enhanced by loading catalytic materials.

In this present work, we report a hydrogen sensor consisting of tubular TiO_2 layer formed on SiO_2/Si with several pairs of electrodes under the TiO_2 layer. Metal electrodes (Al/Au) were patterned on the substrate followed by the deposition on a thin Ti layer which was then anodized to form tubular oxide structure. A thin Pd layer as a catalyst was deposited on the oxide layer to enhance hydrogen sensing property. Hydrogen sensing measurements were performed under synthetic air, N_2, ambient air and humid air. The Pd-decorated TiO_2 tubular layer showed excellent hydrogen sensing properties that detect from 1 ppm to 1% of hydrogen with fast response/recovery time.

2. Experimental

2.1. Sensor preparation

The sensor manufacturing process is described in Fig. 1. A thermally oxidized silicon slice (20 mm × 25 mm × 0.5 mm) with a 360 nm thick layer of SiO2 was degreased by ultrasonication in acetone, isopropanol and deionized (DI) water for 5 min. Metal electrodes with an interspacing distance of 200 nm were formed by depositing Al (10 nm) and Au (100 nm) layers onto the silicon slice through a mask with a DC magnetron sputter (BAL-TEC MED 020, Baltec Union, Balzers, Liechtenstein) in Ar at a pressure of 0.02 mbar. The slice was then thermally treated at 300 °C for 30 min in air to improve the adhesion of the metal electrodes to the substrate. A Ti layer (500 nm) was deposited on the slice through another mask (10 mm × 15 mm) in the same manner using a Ti target (purity 99.9%) at 150 °C.

2.2. Anodization process

TiO_2 nanotubular structures were prepared via an electrochemical anodization process using a two-electrode configuration with the Ti layer as an anode, and Pt foil (20 mm × 20 mm × 0.1 mm, purity 99.9%) as a cathode. The distance between the electrodes was 2 cm. The anodization was performed for 40 min at 5 °C in an organic electrolyte solution containing 0.3 wt.% of NH_4F in ethylene glycol. Electric potential of 60 V was applied gradually during anodization, with a ramp rate of 1 V/s. After this process, the anodized sample was rinsed with DI water and dried in an air stream. A thin Pd layer (ca. 2 nm, purity 99.9%) was deposited on the sensing area between metal electrodes using the DC magnetron sputter. The sample was then crystallized by annealing for 6 h at 500 °C in ambient air with a ramp rate of 1 °C/min in a furnace (Vulcan 3-130, Burlington, New Jersey, USA).

2.3. Material characteristics

The formation of the anodic TiO_2 structure was verified using a field emission scanning electron microscope (FESEM, Hitachi S—4800, Tokyo, Japan) equipped with an energy dispersive X-ray spectrometer (EDS, Oxford INCA 350, Abingdon, UK). EDS measurements were conducted at 10 keV to analyze the elemental composition of TiO_2 on the metal electrodes and SiO_2/Si substrate. The crystalline structure of the anodic TiO_2 layer was investigated by X-ray diffraction (XRD, X'Pert Pro MPD X-ray powder diffractometer Philips, Holland) using CuK_α radiation.

2.4. Gas detection measurements

An individual sensor unit was separated from the sample to fabricate a gas sensor. The sensor was then fixed on alumina substrate, and electrical contacts were made to the metal electrodes using Cu wires fixed with conducting Ag epoxy. The sensor was subsequently placed on an Al plate, which was equipped with a ceramic heater (15 mm × 15 mm; ULTRAMIC 600, Watlow Electric Manufacturing

Co., Chicago, IL, USA.) to control the operating temperature. This whole device was placed in an Al chamber (75 cm^3) covered with a Teflon plate. A precision multi-meter (Keithley 6487 Picoammeter Voltage Source, Keithley Instruments Inc., OH, USA) was used to record the resistance of the sensor with the applied DC voltage of 5 V. Carefully shielded coaxial cables and short Cu wires were used to reduce noise generated from the high resistance of the sensor, allowing the measurement of resistances beyond 1 TΩ.

During the measurements, the gas flow through the chamber was kept at 1 l/min using mass flow controllers. The gas mixtures were made by mixing high purity gases at specified flow rates that enabled to make the minimum hydrogen concentration of 10 ppm. The sensor temperature was stabilized at 180 °C which increased the gas temperature inside the chamber to 45 °C. The response of the sensor to hydrogen was defined as $S = (R_0 - R_{H_2})/R_{H_2}$, where R_0 is the resistance in the absence of hydrogen, and R_{H_2} is the resistance in the presence of hydrogen.

The sensor was tested in synthetic dry air with hydrogen concentrations ranging from 10 to 5050 ppm. In order to study the hydrogen sensing properties below 10 ppm, a series of measurements at different operating temperatures (140, 160 and 180 °C) in ambient air was performed in a glass chamber (56 l). Details of the gas measurements in this system are described in Supporting information S1.

The influence of the pre-adsorbed oxygen in the sensor was investigated by measuring the response to 10, 100 and 1000 ppm H_2 in N_2. To study the influence of humidity, the sensor was tested at constant hydrogen concentration (1000 ppm) in synthetic air at varied relative humidities (RH) between 0 and 20%. The RH of the gas was adjusted by feeding the carrier gas partially through the incubator (17.6 °C). The selectivity of the sensor was investigated with 100 ppm of acetone, ethanol, CO and CO_2 in synthetic air. Detailed information of the gases and liquids used in the experiments is described in Supporting information S2.

3. Results and discussion

3.1. Characterization of Pd decorated nanotubular TiO_2 layer

The morphology of the obtained anodic TiO_2 layer was investigated by FESEM as shown in Fig. 2. The results showed that the anodization process converted Ti layer into tubular TiO_2 structures with a thickness of approximately 450 nm (Fig. 2a), and the tops of the tubes are open and the bottoms are closed with thin oxide layer with a thickness of approximately 40 nm. The tubes have an average diameter of 40 nm (standard deviation 6 nm) and a tube wall thickness of 15 nm (Fig. 2b).

EDS measurements were conducted to analyze the elemental composition of TiO_2 on the metal electrodes and SiO_2/Si substrate. The spectra of the EDS results are seen in Fig. 3. The EDS results indicated the presence of elements: O, Au, Si, Pd and Ti on the metal electrodes, and O, Si, Pd and Ti on SiO_2/Si substrate. The XRD patterns of the TiO_2 layer in Fig. 4 were drawn to observe the change in crystallinity of the as-anodized and the annealed samples. The sample obtained after anodization indicated an amorphous structure as expected [33]. The sample annealed at 500 °C showed only anatase peak (1 0 1). This is in good agreement with other studies reported [22,29]. However, in the case of TiO_2 nanotubes prepared from Ti foil, a mixture of anatase and rutile can be obtained when annealed at 480 °C [34]. During this crystallization, rutile grows at the interface of TiO_2/Ti metal substrate where thermal oxidation takes place. While in the case of TiO_2 on SiO_2, the crystalline phase transformation of rutile was not observed due to the location of TiO_2 tubes being separately formed on the SiO_2 layer.

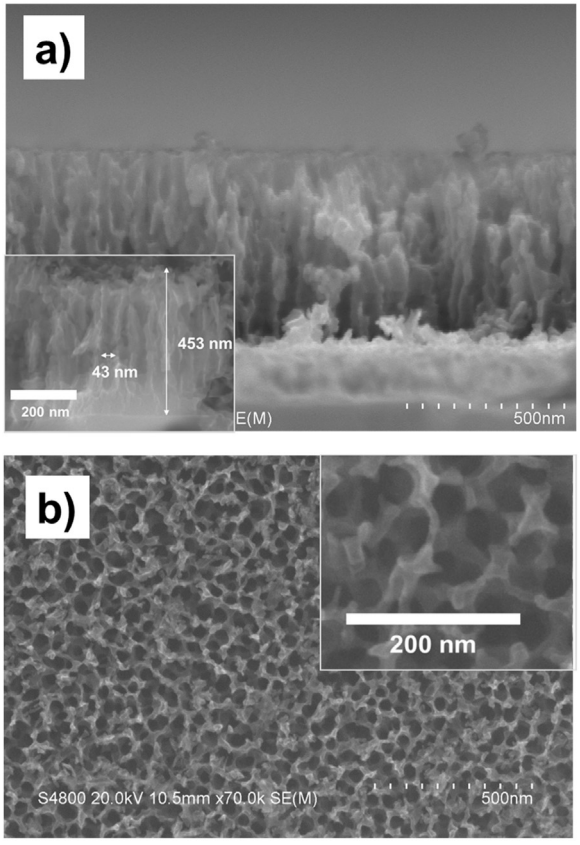

Fig. 2. FESEM images of the TiO_2 tubular structure on Si/SiO_2 substrate: (a) a cross-sectional image. The inset shows detached tubes from SiO_2 layer, (b) top view image. The inset shows top view at high magnification.

From the XRD patterns, the anatase (1 0 1) orientation degree can be determined by using the Lotgering orientation factor (LF), defined as [35],

$$\mathrm{LF} = \frac{P - P_0}{1 - P_0} \quad (1)$$

where P_0 or $P = \sum I(1\,0\,1)/\sum I(h\,k\,l)$ is the ratio of the intensity of $I(1\,0\,1)$ to the sum of all the intensities $I(h\,k\,l)$ in the scanned range of 2θ, for as-anodized and annealed TiO_2, respectively. Non oriented sample (P_0) leads to LF = 0 and oriented sample (P) increases from LF = 0 to LF = 1, making LF a method of measuring the degree of orientation as a quality factor. The LF obtained from the XRD patterns is 0.63, which is considered as good orientation.

3.2. Hydrogen detection properties

3.2.1. Hydrogen detection as a function of the presence of oxygen

The resistance variation of the sensor at 180 °C to hydrogen in dry synthetic air is shown in Fig. 5a. The response of the sensor to 10–5050 ppm H_2 varied from 1.25 to 7800 (Fig. 5b) and the resistance returned to its initial value after repeated test cycles. The response seems to obey the power law, $y = 0.102x^{1.3701}$, where x is hydrogen concentration (ppm), with good correlation ($R^2 = 0.9825$).

The response time of the sensor was defined as the time when the sensor reached 90% of the total response to hydrogen and the recovery time was defined as the time when the sensor returned to 90% of the total response as plotted in Fig. 5c. The sensor showed fast response and recovery times of less than 30 s and 10 s at 100–5050 ppm H_2, respectively. It should also be noted that the actual response time is in fact shorter, due to the delay time (ca.10 s) for changing the gas concentration in the chamber.

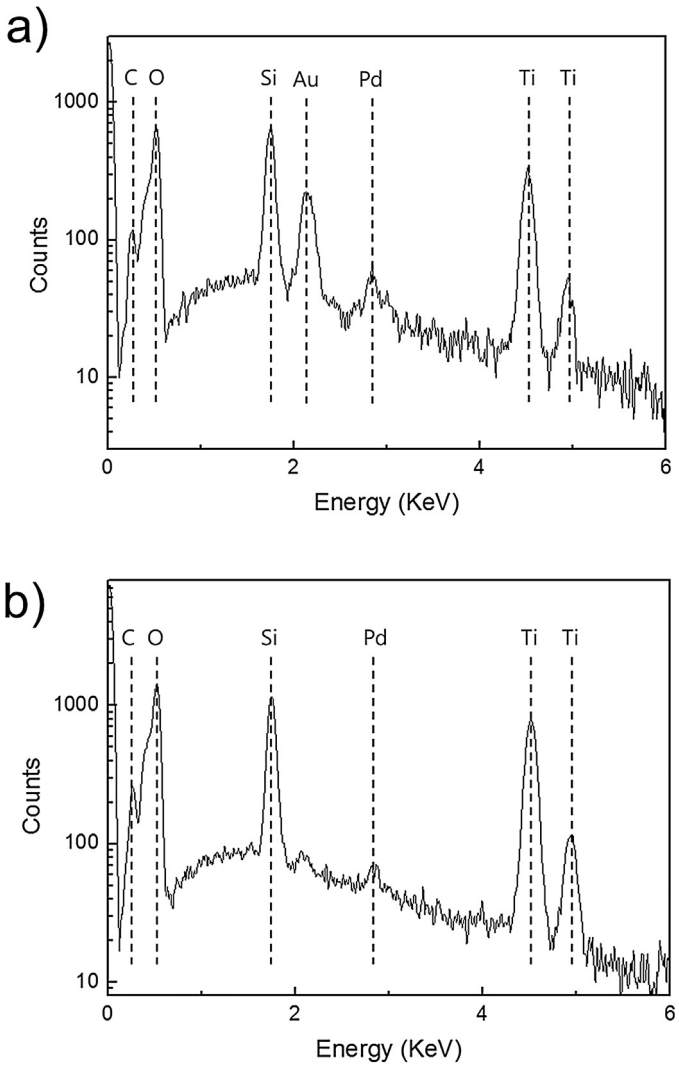

Fig. 3. EDS spectra of the TiO_2 layer on (a) metal electrode and (b) SiO_2 substrate.

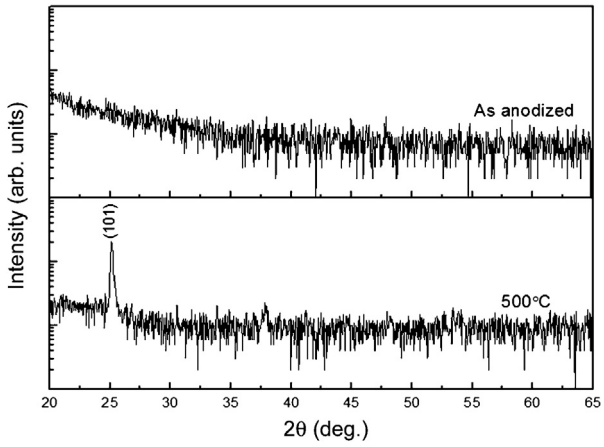

Fig. 4. XRD patterns of the TiO_2 film before and after the heat treatment at 500 °C for 6 h in ambient atmosphere.

Hydrogen sensing measurements conducted in ambient air (32% RH) are shown in Fig. 6. The resistance changes of the sensor when exposed to 1–50 ppm H_2 at different temperatures are shown in Fig. 6a. Our sensor seems to be capable of detecting hydrogen concentrations below 1 ppm. The results showed that increasing the

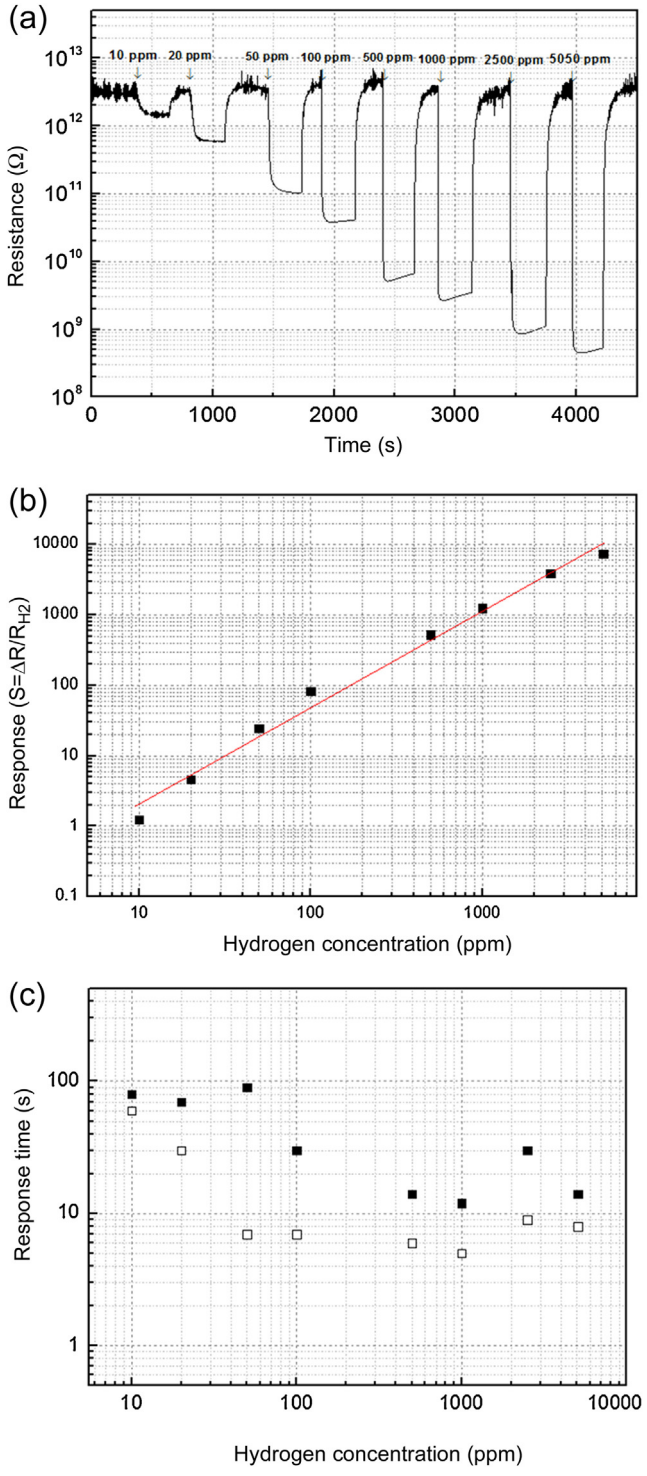

Fig. 5. Hydrogen sensing properties of Pd decorated TiO_2 sensor to 10–5050 ppm H_2 in synthetic air at 180 °C: (a) the resistance change; (b) the response (■); (c) the recovery (□) time.

operating temperature shortened the response (Fig. 6b) and recovery time (Fig. 6c) and decreased the resistance and noise level.

The variation in resistance of the sensor to different concentrations of hydrogen in N_2 is depicted in Fig. 7a. The sensor responses were 25, 6000 and 17,000 to 10, 100 and 1000 ppm H_2, respectively, which are higher responses than in air. The response times were 90, 40 and 15 s. However, slow recovery times were observed, with the resistance having still not reached its initial value after 50 min in

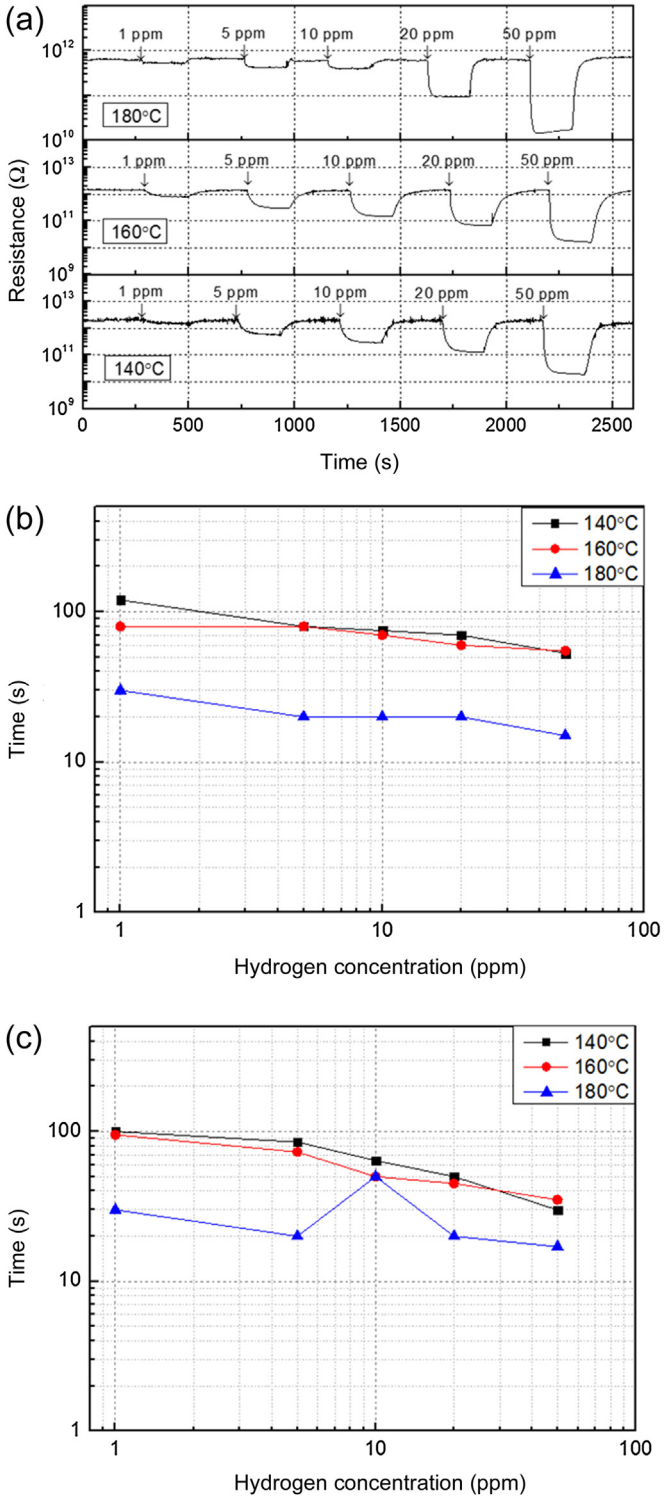

Fig. 6. Hydrogen sensing properties of Pd decorated TiO_2 sensor to 1–50 ppm H_2 in ambient air at different operating temperatures at 140–180 °C (RH 32%): (a) the resistance change; (b) the response time; (c) the recovery time.

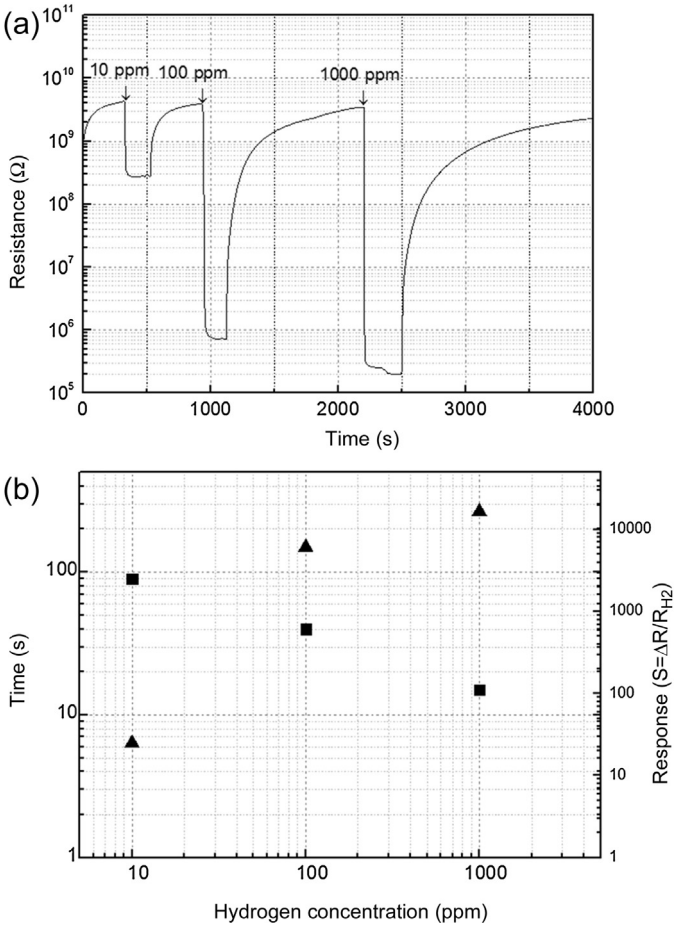

Fig. 7. Hydrogen sensing properties of Pd decorated TiO_2 sensor to 10–1000 ppm H_2 in N_2 at 180 °C: (a) the resistance change; (b) the response time (▲); response time (■).

N_2. Our sensor displays promising results comparing to previously reported sensors as shown in Table 1.

3.2.2. Hydrogen sensing mechanism

In the presence of oxygen, the behavior of TiO_2 sensors has been explained as hydrogen removing oxygen from the lattice or the removal of chemisorbed oxygen [42,43]. The chemisorbed oxygen is responsible for resistance change of TiO_2 in the presence of hydrogen. Several types of oxygen ions, such as O^{2-}, O^- and O_2^- can be formed on the oxide surface when electrons are captured from the conduction band of the oxide. This process forms a space charge region on the oxide surface, leading to high resistivity of the oxide [44]. This is the reason for the higher base resistance of the sensor in the air than N_2.

When the sensors operate in the absence of oxygen, different approaches for understanding the sensing behavior have to be considered. The base resistance of the sensor in N_2 (Fig. 7) was significantly lower (1/1000) than in air (Fig. 5). The high response in N_2 can be explained by the process of hydrogen dissociation [45]. When hydrogen molecules reach the oxide surface, they are ionized. The ionized hydrogen atoms release electrons, which decrease the resistivity of TiO_2. Thus, at this stage, the increase of hydrogen concentration increases the amount of electrons on the oxide surface, where the electrons are accumulated. When the donor level crosses the Fermi level, no further increase of electrons in the accumulation layer takes place. Therefore, the response to hydrogen in N_2 tends to be saturated as seen in Fig. 7b. This type of effect was also reported in other studies [19,46]. Afterwards, the decrease of the hydrogen concentration leads to the increase of the resistivity due to desorption of hydrogen molecules [47].

The morphological structures of the sensing material are crucial to the sensing properties. Xu et al. [48,49] reported the grain-size models which described the correlation between the grain-size and the gas sensor sensitivity. In ambient air, the high response

Table 1
Summary of H_2 gas sensors using TiO_2 nanostructures in the literature.

Structure	Synthesis method	Catalyst	Test H_2 concentration (ppm)	Operating temperature (°C)	References
Porous film on Ti	Anodization	Pt	500	250	[36]
Thin film	Thermal oxidation		10	300	[37]
Nanotube arrays on Ti	Anodization	Pd	20–1000	RT	[19]
Porous film on Ti	Anodization		1000	250	[38]
Nanotube arrays on glass	Anodization	Pd, Pt	10	290	[27]
Nanowire	Thermal evaporation	Pd	500	100	[39]
Nanotube arrays on polymer film	ALD		100–1000	100	[40]
Single nanotube	Anodization		1000	RT	[41]
Nanotubes on SiO_2/Si	Anodization	Pd	1–10,000	140–180	Present work

Table 2
Response comparison of the sensor to 100 ppm of CO, CO_2, ethanol, acetone and H_2.

Gas	Response
CO	–
CO_2	–
Ethanol	1.2
Acetone	–
H_2	91

to hydrogen is the result of desorption of hydrogen molecules [19]. This may occur at the tube walls and the tube necks connecting tubes of the crystallized TiO_2. According to the grain size correlation model, if half of the tube wall thickness is less than or comparable to space charge layer, the necks of tubes are responsible for the electric resistance of the TiO_2 layer and are expected high sensitivity.

The comparison of the sensor response to hydrogen with or without Pd layer is shown in Supporting information S3. It clearly showed that the Pd layer is responsible for significantly improved hydrogen sensing ability. The enhancement of the hydrogen sensing ability by adding noble catalysts has been explained by electronic and chemical concepts [50]. The electronic concept is based on an interaction of the Pd particles with TiO_2. When oxygen chemisorption takes place, the sputtered fine Pd particles form Schottky-barriers that resulted from the work function difference of TiO_2 and Pd [51–54]. When hydrogen is introduced on the oxide surface, the chemisorbed oxygen on Pd-decorated TiO_2 surface is removed through reaction with hydrogen, and then the barrier height becomes lower, which is responsible for resistance change. The chemical concept is so called "spill-over effect" [55,56]. Pd is an excellent adsorptive material to hydrogen, playing a role as hydrogen collector. The introduced hydrogen can be dissociated on and dissolved into the Pd. The dissociated hydrogen atoms can then move towards the interface between Pd and TiO_2, forming Pd hydride (2), which later reacts with the adsorbed ionic oxygen and injects electrons into the TiO_2 layer (3) [57].

$$Pd + \frac{x}{2}H^2 \rightarrow PdH_x \quad (2)$$

$$PdH_x + \frac{x}{4}O^{2-} \rightarrow Pd + \frac{x}{2}H_2O + \frac{x}{4}e^- \quad (3)$$

In air atmosphere, Pd particles were partially oxidized or condensed at 180 °C. The surface to volume ratio of Pd became smaller, which resulted in the decrease of the amount of hydrogen dissolved in Pd particles [39]. The partially oxidized Pd, on the other hand, can be reduced in N_2 at 180 °C, to metallic Pd. Thus, the surface to volume ratio of Pd was increased leading to the increase of the amount of hydrogen dissolved in the Pd particles. This resulted in higher responses of the sensor in N_2 than air, as seen in Fig. 7.

3.2.3. Selectivity

The response to 100 ppm of CO, CO_2, ethanol and acetone measured in dry air is summarized in Table 2. Our sensor showed negligible responses to these gases. These results are in contradiction with other results of TiO_2-based gas sensors [19,20,58,59]. For example, TiO_2 nanotubes prepared on SiO_2/Si substrate with a mixture of anatase and rutile have shown high response to acetone and ethanol at 400 °C [28]. TiO_2 nanohelix arrays prepared by oblique angle deposition were able to detect NO_2, CO and H_2 [60]. The different selectivity of our sensor compared to other TiO_2-based sensors can be caused by various distinctive features, such as the relatively low operating temperature (180 °C), the different crystalline structure and the Pd decoration. These selective sensing properties of anodic TiO_2 sensors are summarized in Table 3.

3.2.4. Influence of humidity

When the metal oxide sensor is operated in humid atmosphere, the absorbed water molecules on the oxide surface potentially lower the base resistance of the sensor [19]. In addition, water molecules may disturb chemisorption of oxygen species on the oxide surface, leading to a decreased active sensing area. Therefore, it is important to investigate how the sensor operates at different humidities.

The resistance variation of the sensor to 1000 ppm H_2 with different humidities (dry air, 5, 10 and 20% of RH) is shown in Fig. 8a. The base resistance of the sensor decreased rapidly when dry air was changed to humid air (5% RH). The humid atmosphere in the test chamber led to minor reduction of the response to 1000 ppm H_2, due to physisorption of H_2O molecules on chemisorbed OH^- radical layer at porous surface reducing the resistance of TiO_2 [63,64]. While the physisorption takes place,

Table 3
Summary of gas sensors using anodically prepared TiO_2 in the literature.

Structure	Synthesis Method	Catalyst	Annealing temp (°C)	Crystal structure	Target gas	Operating temp (°C)	References
Nanotubes on Ti	Anodization			Amorphous	Oxygen	50–300	[20]
Nanowire	Hydrothermal	Pd	450	Rutile, anatase	Isopropanol, ethanol, methanol	200	[30]
Nanotube on Ti	Anodization		500	Rutile, anatase	SF6	200–400	[61]
Nanotube on Ti	Anodization		400; 700	Rutile, anatase	NO_2	300–500	[62]
Nanotube on Pt patterned SiO_2/Si	Anodization		600	Rutile, anatase	Acetone, ethanol, NO_2	400	[28]
Nanotubes on Al/Au patterned SiO_2/Si	Anodization	Pd	500	Anatase	H_2	140–180	Present work

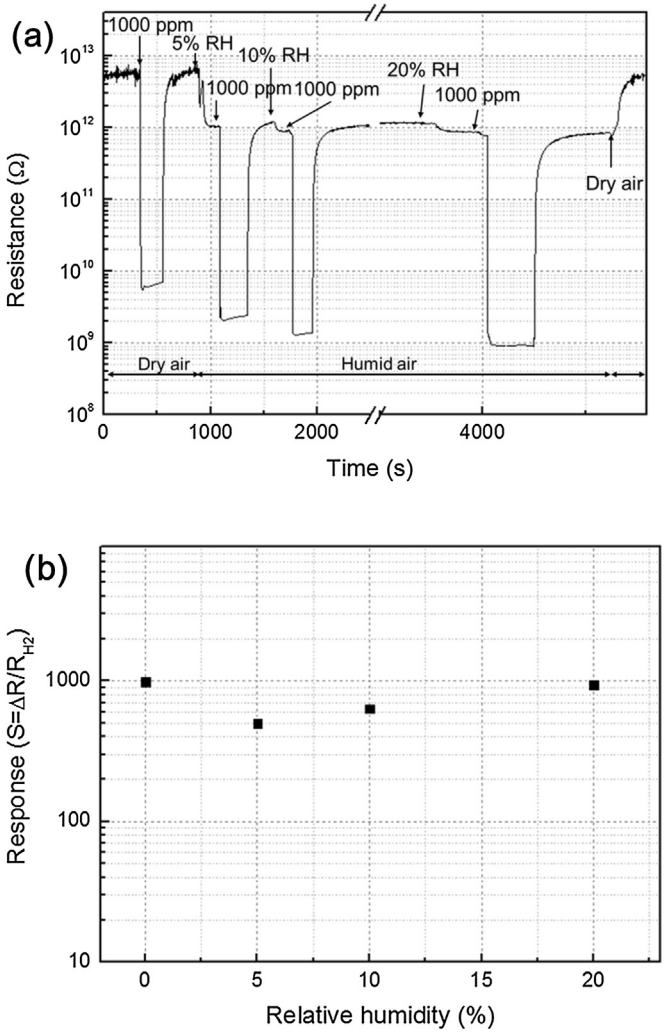

Fig. 8. Hydrogen sensing properties of Pd decorated TiO_2 sensor to 1000 ppm H_2 at 0–20% RH in synthetic air at 180 °C: (a) the resistance variation; (b) the response to 1000 ppm H_2.

the decreased response to hydrogen is due to the H_2O molecules adsorbed on the oxide surface hindering hydrogen chemisorption [64].

4. Conclusion

We demonstrated the hydrogen sensor consisting of Pd-decorated TiO_2 nanotubular structure. The TiO_2 tubular structures were successfully formed on SiO_2/Si substrate. Several pairs of metal electrodes were formed underneath the oxide layer. The thin Pd decorated TiO_2 layer showed an excellent response to hydrogen in different surrounding atmospheres including the presence or absence of oxygen and humid air. The obtained responses were 1.25–7800 to 10–5050 ppm H_2 in synthetic air and the sensor showed fast response and recovery times. In N_2 atmosphere, the response (25–17,000 to 10–1000 ppm H_2) was greater than in synthetic air, while the sensor showed slow recovery. The results indicated that the sensor is not only capable to detect below 1 ppm level of H_2 in ambient air, but also promising for the utilization of our sensor in various hydrogen applications. We expect to enhance the hydrogen detection properties by reducing the size of the sensor and the electrodes, and ultimately reaching the mass production process of micro-sized anodic TiO_2 sensors using this method.

Acknowledgements

J. Moon gratefully acknowledges Fortum Foundation (B2 grant number 12-118). Authors cordially thank Gasera Ltd. and Sensorex Oy for technical assistance in gas sensing measurements.

Appendix A. Supplementary data

Supplementary data associated with this article can be found, in the online version, at http://dx.doi.org/10.1016/j.snb.2015.08.054.

References

[1] M.Z. Jacobson, Review of solutions to global warming, air pollution, and energy security, Energy Environ. Sci. 2 (2009) 148–173.
[2] F. Díaz-González, A. Sumper, O. Gomis-Bellmunt, R. Villafáfila-Robles, A review of energy storage technologies for wind power applications, Renewable Sustainable Energy Rev. 16 (2012) 2154–2171.
[3] R. Raja Singh, T.R. Chelliah, P. Agarwal, Power electronics in hydro electric energy systems—a review, Renewable Sustainable Energy Rev. 32 (2014) 944–959.
[4] A. Shah, P. Torres, R. Tscharner, N. Wyrsch, H. Keppner, Photovoltaic technology: the case for thin-film solar cells, Science 285 (1999) 692–698.
[5] M. Lenzen, Current state of development of electricity-generating technologies: a literature review, Energies 3 (2010) 462–591.
[6] M. Ni, M.K.H. Leung, D.Y.C. Leung, K.K. Sumath, A review and recent developments in photocatalytic water-splitting using TiO_2 for hydrogen production, Renewable Sustainable Energy Rev. 11 (2007) 401–425.
[7] D.V. Bavykin, A.A. Lapkin, P.K. Plucinski, J.M. Friedrich, F.C. Walsh, Reversible storage of molecular hydrogen by sorption into multilayered TiO_2 Nanotubes, J. Phys. Chem. B 109 (2005) 19422–19427.
[8] G. Korotcenkov, S.D. Han, J.R. Stetter, Review of electrochemical hydrogen sensors, Chem. Rev. 109 (2009) 1402–1433.
[9] X. Bévenot, A. Trouillet, C. Veillas, H. Gagnaire, M. Clément, Surface plasmon resonance hydrogen sensor using an optical fibre, Meas. Sci. Technol. 13 (2002) 118–124.
[10] C.-H. Han, D.-W. Hong, S.-D. Han, J. Gwak, Singh K.C., Catalytic combustion type hydrogen gas sensor using TiO_2 and UV-LED, Sens. Actuators B 125 (2007) 224–228.
[11] E.-B. Lee, I.-S. Hwang, J.H. Cha, H.J. Lee, W.-B. Lee, J.J. Pak, J.-H. Lee, Ju B.-K., Micromachined catalytic combustible hydrogen gas sensor, Sens. Actuators B 153 (2011) 392–397.
[12] I. Simon, M. Arndt, Thermal and gas-sensing properties of a micromachined thermal conductivity sensor for the detection of hydrogen in automotive applications, Sens. Actuators A 97–98 (2002) 104–108.
[13] D. Dwivedi, R. Dwivedi, S.K. Srivastava, Sensing properties of palladium-gate MOS (Pd-MOS) hydrogen sensor-based on plasma grown silicon dioxide, Sens. Actuators B 71 (2000) 161–168.
[14] V. Aroutiounian, Metal oxide hydrogen, oxygen and carbon monoxide sensors for hydrogen setups and cells, Int. J. Hydrogen Energy 32 (2007) 1145–1158.
[15] G.K. Mor, O.K. Varghese, M. Paulose, K. Shankar, C.A. Grimes, A review on highly ordered, vertically oriented TiO_2 nanotube arrays: fabrication, material properties, and solar energy applications, Sol. Energy Mater. Sol. Cells 90 (2006) 2011–2075.
[16] P. Roy, S. Berger, P. Schmuki, TiO_2 nanotubes: synthesis and applications, Angew. Chem. Int. Ed. 50 (2011) 2904–2939.
[17] K. Shankar, G.K. Mor, H.P. Prakasam, S. Yoriya, M. Paulose, O.K. Varghese, C.A. Grimes, Highly-ordered TiO_2 nanotube arrays up to 220 μm in length: use in water photoelectrolysis, Nanotechnology 18 (2007) 065707.
[18] M. Paulose, H.E. Prakasam, O.K. Varghese, L. Peng, K.C. Popat, G.K. Mor, T.A. Desai, C.A. Grimes, TiO_2 nanotube arrays of 1000 μm length by anodization of titanium foil: phenol red diffusion, J. Phys. Chem. C 111 (2007) 14992–14997.
[19] M. Paulose, O.K. Varghese, G.K. Mor, C.A. Grimes, K.G. Ong, Unprecedented ultra-high hydrogen gas sensitivity in undoped titania nanotubes, Nanotechnology 17 (2006) 398–402.
[20] H.F. Lu, F. Li, G. Liu, Z.-G.D.-W. Wang, H.-W. Fang, G.-Q. Lu, Z.-H. Jiang, H.-M. Cheng, Amorphous TiO_2 nanotube arrays for low-temperature oxygen sensors, Nanotechnology 19 (2008) 405504.
[21] P.M. Perillo, D.F. Rodríguez, The gas sensing properties at room temperature of TiO_2 nanotubes by anodization, Sens. Actuators B 171–172 (2012) 639–643.
[22] J. Moon, P. Hedman, M. Kemell, A. Suominen, E. Mäkilä, H. Kim, A. Tuominen, R. Punkkinen, A study of monitoring hydrogen using mesoporous TiO_2 synthesized by anodization, Sens. Actuators B 189 (2013) 246–250.
[23] G.K. Mor, O.K. Varghese, M. Paulose, K.G. Ong, C.A. Grimes, Fabrication of hydrogen sensors with transparent titanium oxide nanotube-array thin films as sensing elements, Thin Solid Films 496 (2006) 42–48.
[24] J.M. Macak, H. Tsuchiya, S. Bauer, S. Fujimoto, P. Schmuki, On wafer TiO_2 nanotube-layer formation by anodization of Ti-films on Si, Chem. Phys. Lett. 428 (2006) 421–425.
[25] V. Galstyan, E. Comini, F. Guido, G. Sberveglieri, TiO_2 nanotubes: recent advances in synthesis and gas sensing properties, Sensors 13 (2013) 14813–14838.

[26] S.L. Lim, Y. Liu, J. Li, E.-T. Kang, C.K. Ong, Transparent titania nanotubes of micrometer length prepared by anodization of titanium thin film deposited on ITO, Appl. Surf. Sci. 257 (2011) 6612–6617.
[27] B. Berger, A. Ghicov, Y.-C. Nah, P. Schmuki, Transparent TiO_2 nanotube electrodes via thin layer anodization: fabrication and use in electrochromic devices, Langmuir 25 (2009) 4841–4844.
[28] S. Joo, I. Muto, N. Hara, hydrogen gas sensor using Pt and-Pd added anodic TiO_2 nanotube films, J. Electrochem. Soc. 157 (2010) J221–J226.
[29] D.H. Kim, Y.-S. Shim, H.G. Moon, H.J. Chang, D. Su, S.Y. Kim, J.-S. Kim, B.K. Ju, S.-J. Yoon, H.W. Jang, Highly ordered TiO2 nanotubes on patterned substrates: synthesis in place for ultrasensitive chemiresistors, J. Phys. Chem. C 117 (2013) 17824–17831.
[30] Y. Kimura, S. Kumura, R. Kojima, M. Bitoh, M. Abe, M. Niwano, Micro-scaled hydrogen gas sensors with patterned anodic titanium oxide nanotube film, Sens. Actuators B 177 (2013) 1156–1160.
[31] E. Şennik, U. Soysal, Z.Z. Öztürk, Pd loaded spider-web TiO_2 nanowires: fabrication, characterization and gas sensing properties, Sens. Actuators B 199 (2014) 424–432.
[32] Y.-J. Choi, I.-S. Hwang, J.-G. Park, K.-J. Choi, J.-H. Park, J.-H. Lee, Novel fabrication of an SnO_2 nanowire gas sensor with high sensitivity, Nanotechnology 19 (2008) 095508.
[33] N. Hongsith, C. Viriyaworasakul, P. Mangkomtong, N. Mangkorntong, S. Choopun, Ethanol sensor based on ZnO and Au-doped ZnO nanowires, Ceram. Int. 34 (2008) 823–826.
[34] J.M. Macak, H. Tsuchiya, P. Schmuki, High-aspect-ratio TiO2 nanotubes by anodization of titanium, Angew. Chem. Int. Ed. 44 (2005) 2100–2102.
[35] O.K. Varghese, D. Gong, M. Paulose, C.A. Grimes, E.C. Dickey, Crystallization and high-temperature structural stability of titanium oxide nanotube arrays, J. Mater. Res. 18 (2003) 156.
[36] F.K. Lotgering, Topotactical reactions with ferrimagnetic oxides having hexagonal crystal structures-I, J. Inorg. Nucl. Chem. 9 (1959) 113–123.
[37] G. Yamamoto, T. Yamashita, K. Matsuo, Y. Shimizu, Effects of polytetrafluoroethylene or polyimide coating on H_2 sensing properties of anodized TiO_2 films equipped with Pd–Pt electrodes, Sens. Actuators B 183 (2013) 253–264.
[38] Y.-K. Jun, H.-S. Kim, J.-H. Lee, S.-H. Hong, Sens. Actuators B 107 (2005) 264–270.
[39] T. Iwanaga, T. Hyodo, Y. Shimizu, M. Egashira, H_2 sensing properties and mechanism of anodically oxidized TiO_2 film contacted with Pd electrode, Sens. Actuators B 93 (2003) 519–525.
[40] D. Meng, T. Yamazaki, T. Kikuta, Preparation and gas sensing properties of undoped and Pd-doped TiO_2 nanowires, Sens. Actuators B 190 (2014) 838–843.
[41] J. Lee, D.H. Kim, S.-H. Hong, J.Y. Jho, A hydrogen gas sensor employing vertically aligned TiO2 nanotube arrays prepared by template-assisted method, Sens. Actuators B 160 (2011) 1494–1498.
[42] M. Enachi, O. Lupan, T. Braniste, A. Saruna, L. Chow, Y.K. Mishra, D. Gedamu, R. Adelung, I. Tiginyanu, Rapid Res. Lett. 9 (2015) 171–174.
[43] K.H. Kim, E.J. Ju, J.S. Choi, Electrical conductivity of hydrogen reduced titanium dioxide (rutile), J. Phys. Chem. Solids 45 (1984) 1265–1269.
[44] G.C. Mather, F.M.B. Marques, J.R. Frade, Detection mechanism of TiO_2 ceramic H_2 sensors, J. Eur. Ceram. Soc. 19 (1999) 887–889.
[45] G. Heiland, Homogeneous semiconducting gas sensors, Sens. Actuators 2 (1982) 343–361.
[46] L.D. Birkefeld, A.M. Azad, S.A. Akbar, Carbon monoxide and hydrogen detection by anatase modification of titanium dioxide, J. Am. Ceram. Soc. 75 (1992) 2964–2968.
[47] M. Hübner, R.G. Pavelko, N. Barsan, U. Weimar, Influence of oxygen backgrouds on hydrogen sensing with SnO_2 nanomaterials, Sens. Actuators B 154 (2011) 264–269.
[48] O.K. Varghese, O.K.D. Gong, M. Paulose, K.G. Ong, C.A. Grimes, Hydrogen sensing using titania nanotubes, Sens. Actuators B 93 (2003) 338–344.
[49] C. Xu, T. Jun, N. Miura, N. Yamazoe, Correlation between gas sensitivity and crystallite size in porous SnO_2-based sensors, Chem. Lett. 3 (1990) 441–444.
[50] C. Xu, J. Tamaki, N. Miura, N. Yamazoe, Grain size effects on gas sensitivity of porous SnO_2-based elements, Sens. Actuators B 3 (1991) 147–155.
[51] N. Yamazoe, New approaches for improving semiconductor gas sensors, Sens. Actuators B 5 (1991) 7–19.
[52] W. Huang, R. Zhai, X. Bao, Investigation of oxygen adsorption on Pd (100) with defects, Appl. Surf. Sci. 158 (2000) 287–291.
[53] Y. Shimizu, T. Hyodo, M. Egashira, H_2 sensing performance of anodically oxidized TiO_2 thin films equipped with Pd electrode, Sens. Actuators B 121 (2007) 219–230.
[54] K.D. Schierbaum, U.K. Kirner, J.F. Geiger, W. Göpel, Schottky-barrier and conductivity gas sensors based upon Pd/SnO_2 and Pt/TiO_2, Sens. Actuators B 4 (1991) 87–94.
[55] H. Kobayashi, K. Kishimoto, Y. Nakato, H. Tsubomura, Sens. Actuators B 13 (1993) 125–127.
[56] U. Roland, T. Braunschweig, F. Roessner, On the nature of split-over hydrogen, J. Mol. Catal. A: Chem. 127 (1997) 61–84.
[57] A. Kolmakov, D.O. Klenov, Y. Lilach, S. Stemmer, M. Moskovits, Enhanced gas sensing by individual SnO_2 nanowires and nanobelts functionalized with Pd catalyst particles, Nano Lett. 5 (2005) 667–673.
[58] C. Xiang, Z. She, Y. Zou, J. Cheng, H. Chu, S. Qiu, H. Zhang, L. Sun, F. Xu, A room-temperature hydrogen sensor based on Pd nanoparticles doped TiO2 nanotubes, Ceram. Int. 40 (2014) 16343–16348.
[59] C. Garzella, E. Comini, E. Tempesti, C. Frigeri, G. Sberveglieri, TiO_2 thin films by a novel sol–gel processing for gas sensor applications, Sens. Actuators B 68 (2000) 189–196.
[60] S. Hwang, H. Kwon, S. Chhajed, J.W. Byon, J.M. Baik, J. Im, H.W. Jang, S.J. Yoon, J.K. Kim, A near single crystalline TiO_2 nanohelix array: enhanced gas sensing performance and its application as a monolithically integrated electronic nose, Analyst 138 (2013) 443–450.
[61] X. Zhang, J. Zhang, Y. Jia, P. Xiao, J. Tang, TiO_2 nanotube array sensor for detecting the SF6 decomposition product SO_2, Sensors 12 (2012) 3302–3313.
[62] Y. Gönüllü, G.C.M. Rodriguez, B. Saruhan, M. Ürgenb, Improvement of gas sensing performance of TiO_2 towards NO_2 by nano-tubular structuring, Sens. Actuators B 169 (2012) 151–160.
[63] T. Morimoto, M. Nagao, F. Tokuda, Relation between the amounts of chemisorbed and physisorbed water on metal oxides, J. Phys. Chem. 73 (1969) 243–248.
[64] Q. Wang, Y.Z. Pan, S.T. Ren, P. Li, J.J. Li, Resistive and capacitive response of nitrogen-doped TiO2 nanotubes film humidity sensor, Nanotechnology 22 (2011) 025501.

Biographies

Jongyun Moon received his M Eng at Department of Safety Engineering from Hoseo University, Republic of Korea. Currently he is a PhD student in Department of Information at University of Turku, Finland. His research interests are laid on self-organized metal oxide materials, and semiconductor gas sensor application, and photovoltaic devices.

Hannu-Pekka Hedman studied physics and microelectronics in University of Turku, Finland where he graduated as MSc in 1993. He has worked as laboratory engineer and as research assistant in Microelectronics laboratory in Department of Information Technology (formerly in Department of Physics), University of Turku since 1993. His responsibilities have been to work in the clean room and process silicon wafers. Main product has been space radiation sensors. He has also measured electrical parameters of a wide range of semiconductor materials. His hobbies are electronics and computer programming.

Marianna Kemell received her PhD in inorganic chemistry in 2003 from the University of Helsinki, Finland, and her MSc in physical chemistry in 1997 from the University of Oulu, Finland. She currently holds a position as a senior lecturer of inorganic chemistry at the University of Helsinki. Her research interests include preparation of inorganic nanomaterials and thin films, especially by electrochemical methods and atomic layer deposition, and characterization by scanning electron microscopy and X-ray microanalysis. She has authored and co-authored more than 90 peer-reviewed papers.

Aulis Tuominen received his BSc from the Technical Institute of Helsinki, Finland in 1976 and his MSc from Tampere University of Technology, Finland in 1991 and his DSc in Tampere University of Technology in 1999, respectively. He has worked in several industry positions in companies such as Evox Oy, Reka Cable Factory and Nokia holding a number of positions. In the year he was nominated a professor of manufacturing technology at Tampere University of Technology, Pori branch. He was a professor of Electronics Product Development (Productization) at the University of Turku in 2004–2013. He is currently an adjunct professor at University of Vaasa. He is also an author or co-author about 150 publications. He holds five patents and several patents are applied.

Risto Punkkinen received his MSc degree in physics from the University of Turku, Finland in 1976 and received his PhD in physics from the University of Turku, Finland 1990. He has worked at the university almost all the time and is now an associated professor. He is the head of the Microelectronics laboratory at the University of Turku. His research interests are in semiconductor manufacturing, processing, electrical characterization of semiconductors and silicon-based radiation detectors. He is also an author or co-author about 50 publications.

Turku Centre for Computer Science
TUCS Dissertations

1. **Marjo Lipponen**, On Primitive Solutions of the Post Correspondence Problem
2. **Timo Käkölä**, Dual Information Systems in Hyperknowledge Organizations
3. **Ville Leppänen**, Studies on the Realization of PRAM
4. **Cunsheng Ding**, Cryptographic Counter Generators
5. **Sami Viitanen**, Some New Global Optimization Algorithms
6. **Tapio Salakoski**, Representative Classification of Protein Structures
7. **Thomas Långbacka**, An Interactive Environment Supporting the Development of Formally Correct Programs
8. **Thomas Finne**, A Decision Support System for Improving Information Security
9. **Valeria Mihalache**, Cooperation, Communication, Control. Investigations on Grammar Systems.
10. **Marina Waldén**, Formal Reasoning About Distributed Algorithms
11. **Tero Laihonen**, Estimates on the Covering Radius When the Dual Distance is Known
12. **Lucian Ilie**, Decision Problems on Orders of Words
13. **Jukkapekka Hekanaho**, An Evolutionary Approach to Concept Learning
14. **Jouni Järvinen**, Knowledge Representation and Rough Sets
15. **Tomi Pasanen**, In-Place Algorithms for Sorting Problems
16. **Mika Johnsson**, Operational and Tactical Level Optimization in Printed Circuit Board Assembly
17. **Mats Aspnäs**, Multiprocessor Architecture and Programming: The Hathi-2 System
18. **Anna Mikhajlova**, Ensuring Correctness of Object and Component Systems
19. **Vesa Torvinen**, Construction and Evaluation of the Labour Game Method
20. **Jorma Boberg**, Cluster Analysis. A Mathematical Approach with Applications to Protein Structures
21. **Leonid Mikhajlov**, Software Reuse Mechanisms and Techniques: Safety Versus Flexibility
22. **Timo Kaukoranta**, Iterative and Hierarchical Methods for Codebook Generation in Vector Quantization
23. **Gábor Magyar**, On Solution Approaches for Some Industrially Motivated Combinatorial Optimization Problems
24. **Linas Laibinis**, Mechanised Formal Reasoning About Modular Programs
25. **Shuhua Liu**, Improving Executive Support in Strategic Scanning with Software Agent Systems
26. **Jaakko Järvi**, New Techniques in Generic Programming – C++ is more Intentional than Intended
27. **Jan-Christian Lehtinen**, Reproducing Kernel Splines in the Analysis of Medical Data
28. **Martin Büchi**, Safe Language Mechanisms for Modularization and Concurrency
29. **Elena Troubitsyna**, Stepwise Development of Dependable Systems
30. **Janne Näppi**, Computer-Assisted Diagnosis of Breast Calcifications
31. **Jianming Liang**, Dynamic Chest Images Analysis
32. **Tiberiu Seceleanu**, Systematic Design of Synchronous Digital Circuits
33. **Tero Aittokallio**, Characterization and Modelling of the Cardiorespiratory System in Sleep-Disordered Breathing
34. **Ivan Porres**, Modeling and Analyzing Software Behavior in UML
35. **Mauno Rönkkö**, Stepwise Development of Hybrid Systems
36. **Jouni Smed**, Production Planning in Printed Circuit Board Assembly
37. **Vesa Halava**, The Post Correspondence Problem for Market Morphisms
38. **Ion Petre**, Commutation Problems on Sets of Words and Formal Power Series
39. **Vladimir Kvassov**, Information Technology and the Productivity of Managerial Work
40. **Frank Tétard**, Managers, Fragmentation of Working Time, and Information Systems

41. **Jan Manuch**, Defect Theorems and Infinite Words
42. **Kalle Ranto**, Z_4-Goethals Codes, Decoding and Designs
43. **Arto Lepistö**, On Relations Between Local and Global Periodicity
44. **Mika Hirvensalo**, Studies on Boolean Functions Related to Quantum Computing
45. **Pentti Virtanen**, Measuring and Improving Component-Based Software Development
46. **Adekunle Okunoye**, Knowledge Management and Global Diversity – A Framework to Support Organisations in Developing Countries
47. **Antonina Kloptchenko**, Text Mining Based on the Prototype Matching Method
48. **Juha Kivijärvi**, Optimization Methods for Clustering
49. **Rimvydas Rukšėnas**, Formal Development of Concurrent Components
50. **Dirk Nowotka**, Periodicity and Unbordered Factors of Words
51. **Attila Gyenesei**, Discovering Frequent Fuzzy Patterns in Relations of Quantitative Attributes
52. **Petteri Kaitovaara**, Packaging of IT Services – Conceptual and Empirical Studies
53. **Petri Rosendahl**, Niho Type Cross-Correlation Functions and Related Equations
54. **Péter Majlender**, A Normative Approach to Possibility Theory and Soft Decision Support
55. **Seppo Virtanen**, A Framework for Rapid Design and Evaluation of Protocol Processors
56. **Tomas Eklund**, The Self-Organizing Map in Financial Benchmarking
57. **Mikael Collan**, Giga-Investments: Modelling the Valuation of Very Large Industrial Real Investments
58. **Dag Björklund**, A Kernel Language for Unified Code Synthesis
59. **Shengnan Han**, Understanding User Adoption of Mobile Technology: Focusing on Physicians in Finland
60. **Irina Georgescu**, Rational Choice and Revealed Preference: A Fuzzy Approach
61. **Ping Yan**, Limit Cycles for Generalized Liénard-Type and Lotka-Volterra Systems
62. **Joonas Lehtinen**, Coding of Wavelet-Transformed Images
63. **Tommi Meskanen,** On the NTRU Cryptosystem
64. **Saeed Salehi**, Varieties of Tree Languages
65. **Jukka Arvo**, Efficient Algorithms for Hardware-Accelerated Shadow Computation
66. **Mika Hirvikorpi**, On the Tactical Level Production Planning in Flexible Manufacturing Systems
67. **Adrian Costea**, Computational Intelligence Methods for Quantitative Data Mining
68. **Cristina Seceleanu**, A Methodology for Constructing Correct Reactive Systems
69. **Luigia Petre**, Modeling with Action Systems
70. **Lu Yan**, Systematic Design of Ubiquitous Systems
71. **Mehran Gomari**, On the Generalization Ability of Bayesian Neural Networks
72. **Ville Harkke**, Knowledge Freedom for Medical Professionals – An Evaluation Study of a Mobile Information System for Physicians in Finland
73. **Marius Cosmin Codrea**, Pattern Analysis of Chlorophyll Fluorescence Signals
74. **Aiying Rong**, Cogeneration Planning Under the Deregulated Power Market and Emissions Trading Scheme
75. **Chihab BenMoussa**, Supporting the Sales Force through Mobile Information and Communication Technologies: Focusing on the Pharmaceutical Sales Force
76. **Jussi Salmi**, Improving Data Analysis in Proteomics
77. **Orieta Celiku**, Mechanized Reasoning for Dually-Nondeterministic and Probabilistic Programs
78. **Kaj-Mikael Björk**, Supply Chain Efficiency with Some Forest Industry Improvements
79. **Viorel Preoteasa**, Program Variables – The Core of Mechanical Reasoning about Imperative Programs
80. **Jonne Poikonen**, Absolute Value Extraction and Order Statistic Filtering for a Mixed-Mode Array Image Processor
81. **Luka Milovanov**, Agile Software Development in an Academic Environment
82. **Francisco Augusto Alcaraz Garcia**, Real Options, Default Risk and Soft Applications
83. **Kai K. Kimppa**, Problems with the Justification of Intellectual Property Rights in Relation to Software and Other Digitally Distributable Media
84. **Dragoş Truşcan**, Model Driven Development of Programmable Architectures
85. **Eugen Czeizler**, The Inverse Neighborhood Problem and Applications of Welch Sets in Automata Theory

86. **Sanna Ranto**, Identifying and Locating-Dominating Codes in Binary Hamming Spaces
87. **Tuomas Hakkarainen**, On the Computation of the Class Numbers of Real Abelian Fields
88. **Elena Czeizler**, Intricacies of Word Equations
89. **Marcus Alanen**, A Metamodeling Framework for Software Engineering
90. **Filip Ginter**, Towards Information Extraction in the Biomedical Domain: Methods and Resources
91. **Jarkko Paavola**, Signature Ensembles and Receiver Structures for Oversaturated Synchronous DS-CDMA Systems
92. **Arho Virkki**, The Human Respiratory System: Modelling, Analysis and Control
93. **Olli Luoma**, Efficient Methods for Storing and Querying XML Data with Relational Databases
94. **Dubravka Ilić**, Formal Reasoning about Dependability in Model-Driven Development
95. **Kim Solin**, Abstract Algebra of Program Refinement
96. **Tomi Westerlund**, Time Aware Modelling and Analysis of Systems-on-Chip
97. **Kalle Saari**, On the Frequency and Periodicity of Infinite Words
98. **Tomi Kärki**, Similarity Relations on Words: Relational Codes and Periods
99. **Markus M. Mäkelä**, Essays on Software Product Development: A Strategic Management Viewpoint
100. **Roope Vehkalahti**, Class Field Theoretic Methods in the Design of Lattice Signal Constellations
101. **Anne-Maria Ernvall-Hytönen**, On Short Exponential Sums Involving Fourier Coefficients of Holomorphic Cusp Forms
102. **Chang Li**, Parallelism and Complexity in Gene Assembly
103. **Tapio Pahikkala**, New Kernel Functions and Learning Methods for Text and Data Mining
104. **Denis Shestakov**, Search Interfaces on the Web: Querying and Characterizing
105. **Sampo Pyysalo**, A Dependency Parsing Approach to Biomedical Text Mining
106. **Anna Sell**, Mobile Digital Calendars in Knowledge Work
107. **Dorina Marghescu**, Evaluating Multidimensional Visualization Techniques in Data Mining Tasks
108. **Tero Säntti**, A Co-Processor Approach for Efficient Java Execution in Embedded Systems
109. **Kari Salonen**, Setup Optimization in High-Mix Surface Mount PCB Assembly
110. **Pontus Boström**, Formal Design and Verification of Systems Using Domain-Specific Languages
111. **Camilla J. Hollanti**, Order-Theoretic Mehtods for Space-Time Coding: Symmetric and Asymmetric Designs
112. **Heidi Himmanen**, On Transmission System Design for Wireless Broadcasting
113. **Sébastien Lafond**, Simulation of Embedded Systems for Energy Consumption Estimation
114. **Evgeni Tsivtsivadze**, Learning Preferences with Kernel-Based Methods
115. **Petri Salmela**, On Commutation and Conjugacy of Rational Languages and the Fixed Point Method
116. **Siamak Taati**, Conservation Laws in Cellular Automata
117. **Vladimir Rogojin**, Gene Assembly in Stichotrichous Ciliates: Elementary Operations, Parallelism and Computation
118. **Alexey Dudkov**, Chip and Signature Interleaving in DS CDMA Systems
119. **Janne Savela**, Role of Selected Spectral Attributes in the Perception of Synthetic Vowels
120. **Kristian Nybom**, Low-Density Parity-Check Codes for Wireless Datacast Networks
121. **Johanna Tuominen**, Formal Power Analysis of Systems-on-Chip
122. **Teijo Lehtonen**, On Fault Tolerance Methods for Networks-on-Chip
123. **Eeva Suvitie**, On Inner Products Involving Holomorphic Cusp Forms and Maass Forms
124. **Linda Mannila**, Teaching Mathematics and Programming – New Approaches with Empirical Evaluation
125. **Hanna Suominen**, Machine Learning and Clinical Text: Supporting Health Information Flow
126. **Tuomo Saarni**, Segmental Durations of Speech
127. **Johannes Eriksson**, Tool-Supported Invariant-Based Programming

128. **Tero Jokela**, Design and Analysis of Forward Error Control Coding and Signaling for Guaranteeing QoS in Wireless Broadcast Systems
129. **Ville Lukkarila**, On Undecidable Dynamical Properties of Reversible One-Dimensional Cellular Automata
130. **Qaisar Ahmad Malik**, Combining Model-Based Testing and Stepwise Formal Development
131. **Mikko-Jussi Laakso**, Promoting Programming Learning: Engagement, Automatic Assessment with Immediate Feedback in Visualizations
132. **Riikka Vuokko**, A Practice Perspective on Organizational Implementation of Information Technology
133. **Jeanette Heidenberg**, Towards Increased Productivity and Quality in Software Development Using Agile, Lean and Collaborative Approaches
134. **Yong Liu**, Solving the Puzzle of Mobile Learning Adoption
135. **Stina Ojala**, Towards an Integrative Information Society: Studies on Individuality in Speech and Sign
136. **Matteo Brunelli**, Some Advances in Mathematical Models for Preference Relations
137. **Ville Junnila**, On Identifying and Locating-Dominating Codes
138. **Andrzej Mizera**, Methods for Construction and Analysis of Computational Models in Systems Biology. Applications to the Modelling of the Heat Shock Response and the Self-Assembly of Intermediate Filaments.
139. **Csaba Ráduly-Baka**, Algorithmic Solutions for Combinatorial Problems in Resource Management of Manufacturing Environments
140. **Jari Kyngäs**, Solving Challenging Real-World Scheduling Problems
141. **Arho Suominen**, Notes on Emerging Technologies
142. **József Mezei**, A Quantitative View on Fuzzy Numbers
143. **Marta Olszewska**, On the Impact of Rigorous Approaches on the Quality of Development
144. **Antti Airola**, Kernel-Based Ranking: Methods for Learning and Performace Estimation
145. **Aleksi Saarela**, Word Equations and Related Topics: Independence, Decidability and Characterizations
146. **Lasse Bergroth**, Kahden merkkijonon pisimmän yhteisen alijonon ongelma ja sen ratkaiseminen
147. **Thomas Canhao Xu**, Hardware/Software Co-Design for Multicore Architectures
148. **Tuomas Mäkilä**, Software Development Process Modeling – Developers Perspective to Contemporary Modeling Techniques
149. **Shahrokh Nikou**, Opening the Black-Box of IT Artifacts: Looking into Mobile Service Characteristics and Individual Perception
150. **Alessandro Buoni**, Fraud Detection in the Banking Sector: A Multi-Agent Approach
151. **Mats Neovius**, Trustworthy Context Dependency in Ubiquitous Systems
152. **Fredrik Degerlund**, Scheduling of Guarded Command Based Models
153. **Amir-Mohammad Rahmani-Sane**, Exploration and Design of Power-Efficient Networked Many-Core Systems
154. **Ville Rantala**, On Dynamic Monitoring Methods for Networks-on-Chip
155. **Mikko Pelto**, On Identifying and Locating-Dominating Codes in the Infinite King Grid
156. **Anton Tarasyuk**, Formal Development and Quantitative Verification of Dependable Systems
157. **Muhammad Mohsin Saleemi**, Towards Combining Interactive Mobile TV and Smart Spaces: Architectures, Tools and Application Development
158. **Tommi J. M. Lehtinen**, Numbers and Languages
159. **Peter Sarlin**, Mapping Financial Stability
160. **Alexander Wei Yin**, On Energy Efficient Computing Platforms
161. **Mikołaj Olszewski**, Scaling Up Stepwise Feature Introduction to Construction of Large Software Systems
162. **Maryam Kamali**, Reusable Formal Architectures for Networked Systems
163. **Zhiyuan Yao**, Visual Customer Segmentation and Behavior Analysis – A SOM-Based Approach
164. **Timo Jolivet**, Combinatorics of Pisot Substitutions
165. **Rajeev Kumar Kanth**, Analysis and Life Cycle Assessment of Printed Antennas for Sustainable Wireless Systems
166. **Khalid Latif**, Design Space Exploration for MPSoC Architectures

167. **Bo Yang**, Towards Optimal Application Mapping for Energy-Efficient Many-Core Platforms
168. **Ali Hanzala Khan**, Consistency of UML Based Designs Using Ontology Reasoners
169. **Sonja Leskinen**, m-Equine: IS Support for the Horse Industry
170. **Fareed Ahmed Jokhio**, Video Transcoding in a Distributed Cloud Computing Environment
171. **Moazzam Fareed Niazi**, A Model-Based Development and Verification Framework for Distributed System-on-Chip Architecture
172. **Mari Huova**, Combinatorics on Words: New Aspects on Avoidability, Defect Effect, Equations and Palindromes
173. **Ville Timonen**, Scalable Algorithms for Height Field Illumination
174. **Henri Korvela**, Virtual Communities – A Virtual Treasure Trove for End-User Developers
175. **Kameswar Rao Vaddina**, Thermal-Aware Networked Many-Core Systems
176. **Janne Lahtiranta**, New and Emerging Challenges of the ICT-Mediated Health and Well-Being Services
177. **Irum Rauf**, Design and Validation of Stateful Composite RESTful Web Services
178. **Jari Björne**, Biomedical Event Extraction with Machine Learning
179. **Katri Haverinen**, Natural Language Processing Resources for Finnish: Corpus Development in the General and Clinical Domains
180. **Ville Salo**, Subshifts with Simple Cellular Automata
181. **Johan Ersfolk**, Scheduling Dynamic Dataflow Graphs
182. **Hongyan Liu**, On Advancing Business Intelligence in the Electricity Retail Market
183. **Adnan Ashraf**, Cost-Efficient Virtual Machine Management: Provisioning, Admission Control, and Consolidation
184. **Muhammad Nazrul Islam**, Design and Evaluation of Web Interface Signs to Improve Web Usability: A Semiotic Framework
185. **Johannes Tuikkala**, Algorithmic Techniques in Gene Expression Processing: From Imputation to Visualization
186. **Natalia Díaz Rodríguez**, Semantic and Fuzzy Modelling for Human Behaviour Recognition in Smart Spaces. A Case Study on Ambient Assisted Living
187. **Mikko Pänkäälä**, Potential and Challenges of Analog Reconfigurable Computation in Modern and Future CMOS
188. **Sami Hyrynsalmi**, Letters from the War of Ecosystems – An Analysis of Independent Software Vendors in Mobile Application Marketplaces
189. **Seppo Pulkkinen**, Efficient Optimization Algorithms for Nonlinear Data Analysis
190. **Sami Pyöttiälä**, Optimization and Measuring Techniques for Collect-and-Place Machines in Printed Circuit Board Industry
191. **Syed Mohammad Asad Hassan Jafri**, Virtual Runtime Application Partitions for Resource Management in Massively Parallel Architectures
192. **Toni Ernvall**, On Distributed Storage Codes
193. **Yuliya Prokhorova**, Rigorous Development of Safety-Critical Systems
194. **Olli Lahdenoja**, Local Binary Patterns in Focal-Plane Processing – Analysis and Applications
195. **Annika H. Holmbom**, Visual Analytics for Behavioral and Niche Market Segmentation
196. **Sergey Ostroumov**, Agent-Based Management System for Many-Core Platforms: Rigorous Design and Efficient Implementation
197. **Espen Suenson**, How Computer Programmers Work – Understanding Software Development in Practise
198. **Tuomas Poikela**, Readout Architectures for Hybrid Pixel Detector Readout Chips
199. **Bogdan Iancu**, Quantitative Refinement of Reaction-Based Biomodels
200. **Ilkka Törmä**, Structural and Computational Existence Results for Multidimensional Subshifts
201. **Sebastian Okser**, Scalable Feature Selection Applications for Genome-Wide Association Studies of Complex Diseases
202. **Fredrik Abbors**, Model-Based Testing of Software Systems: Functionality and Performance
203. **Inna Pereverzeva**, Formal Development of Resilient Distributed Systems
204. **Mikhail Barash**, Defining Contexts in Context-Free Grammars
205. **Sepinoud Azimi**, Computational Models for and from Biology: Simple Gene Assembly and Reaction Systems
206. **Petter Sandvik**, Formal Modelling for Digital Media Distribution

207. **Jongyun Moon**, Hydrogen Sensor Application of Anodic Titanium Oxide Nanostructures

Turku
Centre *for*
Computer
Science

http://www. tucs.fi

tucs@abo.fi

University of Turku
Faculty of Mathematics and Natural Sciences
- Department of Information Technology
- Department of Mathematics and Statistics

Turku School of Economics
- Institute of Information Systems Science

Åbo Akademi University
Faculty of Science and Engineering
- Computer Engineering
- Computer Science

Faculty of Social Sciences, Business and Economics
- Information Systems

ISBN 978-952-12-3358-6
ISSN 1239-1883

Jongyun Moon

Hydrogen Sensor Application of Anodic Titanium Oxide Nanostructures